3-2007

Three Innovative Concepts for Short Span Steel Bridges

Aaron Jon Yakel
University of Nebraska - Lincoln

Atorod Azizinamini
University of Nebraska - Lincoln, aazizinamini1@unl.edu

Mohammadreza Farimani

Nazzanin Mossahebi

NDOR Research Project Number SPR-PL-1 (038) P539

FINAL REPORT

Three Innovative Concepts for Short Span Steel Bridges

Aaron Yakel
Mohammadreza Farimani
Nazanin Mossahebi
Atorod Azizinamini

National Bridge Research Organization (NaBRO)
(http://www.NaBRO.unl.edu)
Department of Civil Engineering
College of Engineering and Technology

W150 Nebraska Hall
Lincoln, Nebraska 68588-0531
Telephone (402) 472-5106
FAX (402) 472-6658

Sponsored By

Nebraska Department of Roads

March, 2007

University of Nebraska Lincoln

Table of Contents

List of Figures

List of Tables

Acknowledgement

Funding for this investigation was provided by the Nebraska Department of Roads. The authors would like to express their appreciation for this support. The authors would also like to express their thanks to Mr. Lyman Freemon and Sam Fallaha of the Bridge Division at the Nebraska Department of Roads (NDOR), and Curtis Smith of Capital Contractors for their assistance.

The authors would also like to thank the Tubular Products Division of the United States Steel Corporation for donation of the steel tube.

The opinions expressed in this report are those of the authors and do not necessarily represent the opinions of the sponsors.

Abstract

Three innovative bridge concepts were proposed in response to a series of design challenges. Two of the concepts were aimed at quick construction with the elimination of costly elements such as intermediate stiffeners and cross frames, while the third concept attempted to improve the performance of a composite girder deck in the negative moment region. The designs were investigated using a combination of theory, finite element analysis and experimentation. The first design concept was the inversion of a conventional box girder and the second was a steel tube filled with reinforced concrete. The third concept was known as the self-stressing girder, which was similar to a conventional composite steel I-girder, only the girder was shimmed upward over the pier prior to deck hardening. After hardening, the shim was removed to induce compression in the deck slab.

Executive Summary

Three innovative bridge concepts were investigated using a combination of theory, finite element analysis, and experimentation. These sytems were an inverted box girder, a concrete-filled tube girder, and a self stressing girder.

The inverted box girder was simply a conventional box girder that had been inverted. Since it could not be assumed that the AASHTO LRFD Bridge Design Specifications for box girders would apply directly to the proposed design, the provisions of the code were evaluated for their applicablity to the inverted box girder. Using the AASHTO provisions for conventional box girders, several inverted box girder bridges were designed, which were then analyzed with three-dimensional finite element analysis to assess their behavior under loading. Based on the results of the analyses, the advantages and disadvantages of the system were summarized. The AASHTO provisions were shown to be applicable to the inverted box, being conservative in some areas.

An experimental investigation was carried out to comprehend the behavior of a bridge girder consisting of a steel tube filled with reinforced concrete and made composite with an overlying concrete deck. The investigation consisted of designing and constructing a test specimen and loading it to

collapse. The experimental investigation provided information to assess various erection scenarios using such a system in bridge construction.

A moment curvature analysis was used to predict the ultimate capacity of the system. This approach was able to predict the observed test behavior with good accuracy. The test specimen showed good ductility and maintained its strength up to the end of the test.

The self-stressing girder was a design aimed at improving the performance of the deck slab in the negative region of a continuous bridge configuration. This was achieved by lowering the middle span of a two-span bridge model after the hardening of the deck slab. An experimental investigation was performed to evaluate the behavior of the system under dead load and ultimate loading. During ultimate loading, the time-dependent behavior of the system was observed and analyzed. The system proved to be a viable substitute to post-tensioning of the deck, delaying the cracking of the concrete. Although the lowering of a support in a full-scale bridge seems to be a difficult task at first, analysis of superstructure weights can prove otherwise. The lowering of a support in a common 130' simple-span bridge would require a capacity of approximately 100 tons. This equates to approximately 20-25 tons per girder, likely the lifting point. Relatively small, economical rams can easily be obtained with capacities ranging from 20-150 tons.

Chapter

1 Introduction

1.1 Project Desciption and Objective

The concepts presented herein use the advantages that steel and concrete offer as materials and have the potential to be used in bridge construction. The systems offer the potential to be constructed quickly and eliminate the need for costly elements such as intermediate transverse stiffeners and cross-frames. This report presents three such alternatives. The alternatives have been investigated using a combination of theory, finite element analysis and experimentation.

1.2 Problem Identification

There currently exists a large number of deficient bridges in the U.S. This problem coupled with increases in labor costs has spurred the search for innovative bridge configurations that are cost effective, easy to construct and durable.

1.3 Concepts

The proposed concepts are presented here. These designs include an inverted box girder, a tube girder, and a self-stressing system.

1.3.1 Inverted Box

The inverted box girder system is shown in Figure 1-1. This system uses an inverted steel box section as the main load-carrrying member. The top flange and webs are either welded together or consist of a plate bent into a U shape. The bottom flanges are then welded to the bottom of the webs for flexural capacity. Shear studs, attached to the top flange, provide the means for developing composite action between the box section and the slab deck.

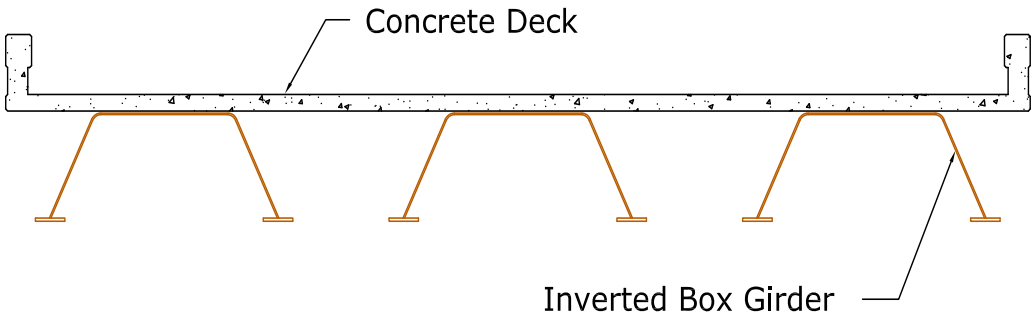

Figure 1-1: Inverted Box Girder Configuration

The inverted steel box section provides a configuration that eliminates some of the problems that are encountered with regular plate or steel box sections. The following are some advantages that the inverted box system provides:

1. Ease of construction
2. Elimination of cross frames
3. Applicability to various span ranges
4. Desirable alternative for county type bridges, where access to heavy equipment is limited
5. Inspection and maintenance are made easier

The focus of this investigative project was to comprehend the basic behavior of inverted steel box girders and identify the AASHTO requirements that are in need of modifications or further development.

1.3.2 Tube Girder

Figure 1-2 shows the proposed tube girder system. This system consists of a concrete-filled steel tube with longitudinal reinforcing bars placed in the bottom of the tube. The reinforcing bars increase the flexural capacity of the concrete filled tube girder. Shear studs are welded to the top of the tube prior to casting the slab deck. The shear studs provide composite action between the concrete-filled tube and the slab deck. The concrete-filled tube carries the weight of the wet slab during construction.

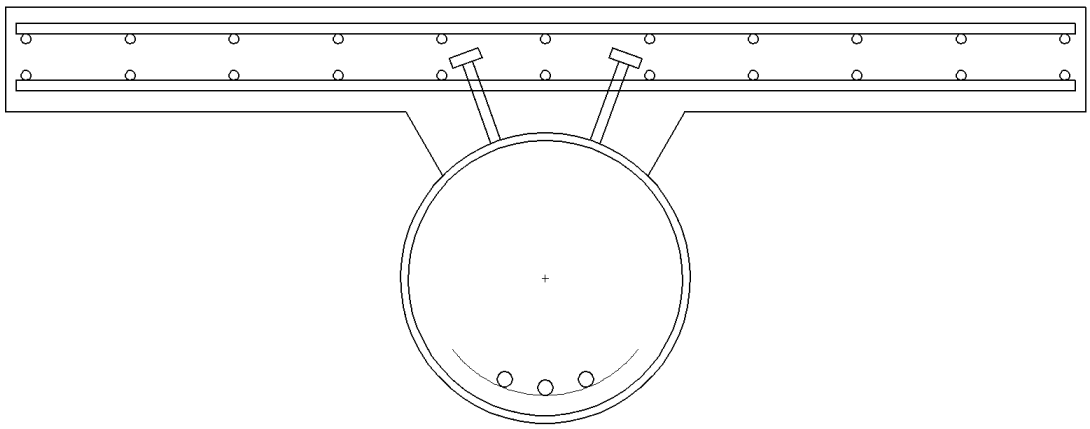

Figure 1-2: Tube Girder Configuration

The tube girder system provides similar advantages to those of the inverted box system. The following are some advantages that the tube girder system provides:

1. Ease of construction
2. Elimination of cross frames and stiffeners
3. Applicable to various span ranges
4. Inspection and maintenance are made easy

The focus of this investigation is to address the questions and concerns that need to be resolved before this new bridge system could be utilized in practice. The investigation carried out provides information to partially answer questions related to design and construction of bridges using the proposed concrete-filled tube girder. These answers were obtained through the design, construction and testing of a specimen in the structural laboratory of the University of Nebraska-Lincoln.

1.3.3 Self-Stressing Girder

The self-stressing girder system is for use on multi-span continuous structures with composite concrete decks. Although steel girders are used thorughout the discussion, the concept could be adapted to accomodate addional supporting member types as well.

In general, the location of maximum negative bending moment in a continuous structure is over the interior supports. This moment produces tensile stresses in the concrete deck and compressive stress in the bottom flanges of the girders. The tensile stress in the deck leads to cracking which can allow intrusion of moisture and road salt, causing corrosion and degredation of the reinforcement and supporting girders. Continued maintainence is required to forestall the decay, however, replacement of the deck is eventually required.

From a design perspective, an efficient design minimizes section transitions and splices. Oftentimes, in a continuous structure the region over the interior support requires a signifcantly larger section than is required throughout the remainder of the structure. To accomodate this, a transition to a larger section over the interior support is required or an oversized section can be used throughout. The self-stressing concept reduces the demand in the negative region which can then be satisfied by a smaller and more economical sectin. Additionally, the need for transitions can be reduced or eliminated.

Chapter

2 Inverted Box

An analytical investigation was carried out to comprehend the behavior of a bridge consisting of inverted box girders. The AASHTO Bridge Design Specifications were reviewed for the applicability to the inverted box girder design. Based on the AASHTO provisions, several bridges were designed for further studies. A three-dimensional refined finite element analysis was used to evaluate the behavior of the system. Based on the finite element results, the advantages and disadvantages of the system are addressed.

2.1 Description of Proposed System

The basic concept and configuration of the inverted box system were presented in Chapter 2. This section gives a more detailed description of the inverted box system.

In this proposed system, each girder consists of an inverted box section. The webs and flanges can have the same plate thickness or the flanges can be welded to the bottom of the webs. The inverted box portion of the bridge could be fabricated in the shop or made by bending a flat plate into a u-shape. A bent plate inverted box girder is shown in Figure 2-1. It is feasible for a different sector of the industry, such as utility pole manufacturers, to make the u-shaped portion of the inverted box. A fabrication shop could then weld the flanges to the u-shape.

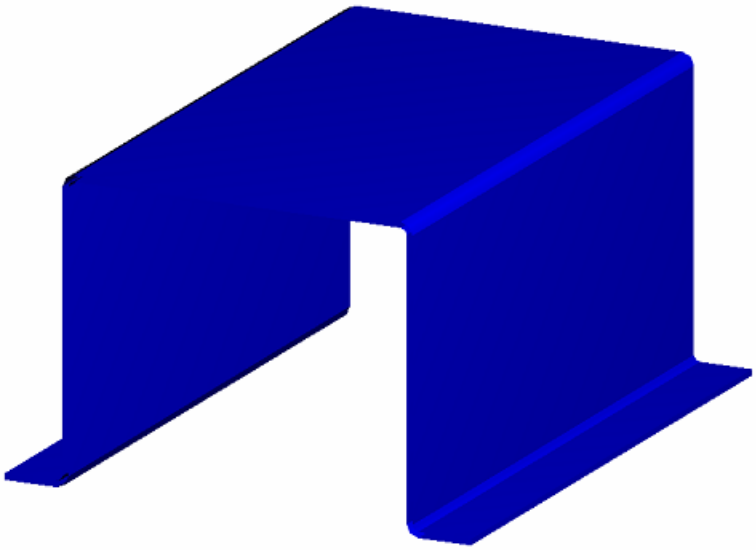

Figure 2-1: Bent Plate Inverted Box Girder

The knee braces at the exterior girders, shown in Figure 2-2, will have two functions. They will provide support for overhang, thereby eliminating the need for temporary knee braces that support the overhang during construction. They will also partially prevent the flanges from movement in the horizontal direction under gravity loads.

.

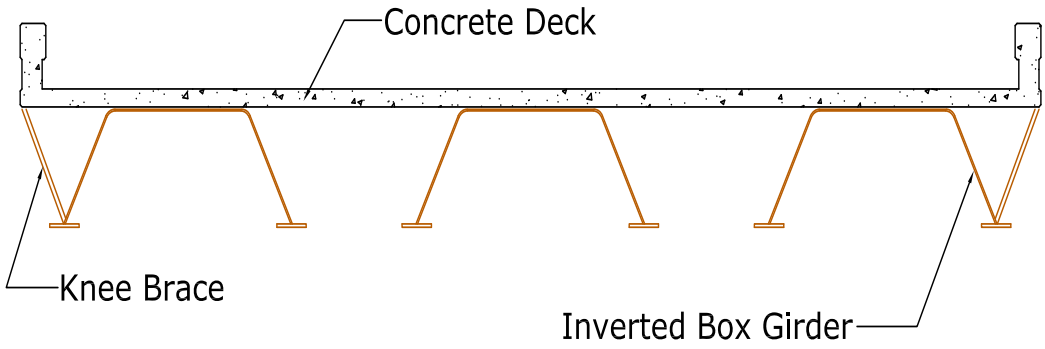

Figure 2-2: Knee Bracing

Upon the application of the vertical traffic or construction loads, there will be a tendency for the flanges to "kick out" or bend in the horizontal direction. Providing initial curvature in the horizontal plane for the flanges could solve this problem. This initial horizontal curvature will result in initial compressive force in the flanges, due to dead loads. This, in turn, will increase the live load capacity of the girder.

The wide top flanges of the inverted box girder could need to be stiffened. This could be achieved in a variety of ways, such as welding T sections to the top of the girder. These stiffeners could also act as a mechanism for transferring the shear forces between the girder and concrete deck. The wide top flanges of the inverted box girder also provide a convenient platform for the construction workers.

The shape of the inverted box girder provides a stable configuration during construction. This will drastically reduce the need for cross frames, which are costly and responsible for fatigue cracking in steel plate girders. The stability also allows for easy transportation.

A problem with the regular steel box section is the need for inspecting the inside of the box. As a result, small box sections are not a feasible configuration because workers cannot easily fit inside the box for inspection and maintenance. The inverted steel box girder eliminates this problem. Furthermore, it could be adapted to bridges of any span length.

2.2 Design Examples

In order to determine the applicability of the inverted box girder system, several designs were considered. A two-span (139 ft. each) normal box girder was designed for a previous project which provided a basis of comparison for the inverted box system. Details of the design for the same bridge with inverted box girders are presented. The design summary for a single-105 ft span bridge is also given for comparison.

2.2.1 2-139-ft Span Bridge

A two-span conventional box girder bridge, with each span measuring 139 ft, was designed and built according to AASHTO LRFD Bridge Design Specifications [1]. The bridge was constructed on Highway 2 over Interstate 80 in Nebraska [7]. For comparison, a design of this bridge with inverted box girders is presented in the following section. The same girder spacing, girder plate dimensions and slab dimensions are used for each design. The conventional box girders are simply inverted for the new design, shown in Figure 2-3. The dimensions of each individual inverted box are shown in Figure 2-4. An angle is added to the top flange for the inverted box girder to account for buckling under construction loads.

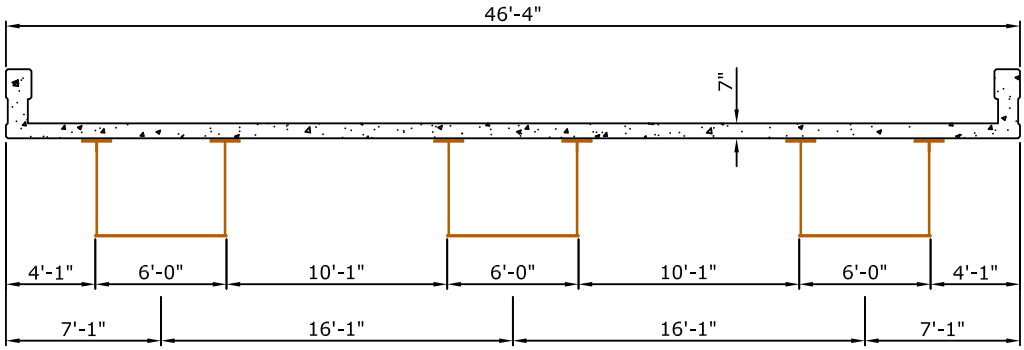

Conventional Box Girder Design

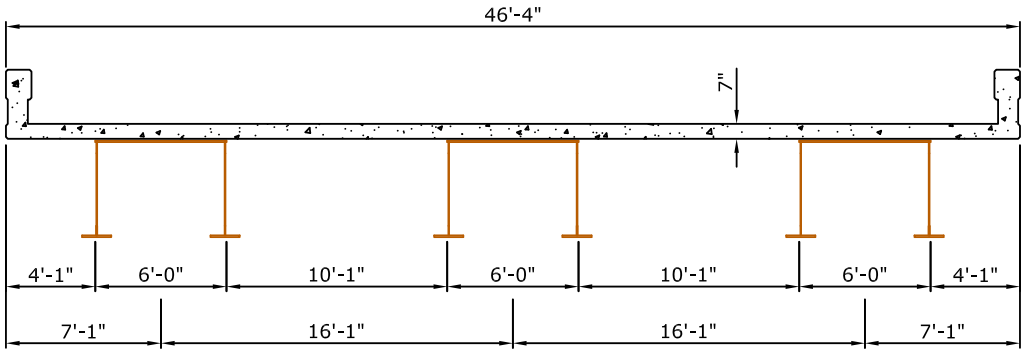

Inverted Box Girder Design

Figure 2-3: Bridge Cross-Sections for 2-139' Span Bridge

2.2.1.1 Section Properties

The slab effective width was determined according to AASHTO recommendations for short and long term effects. The procedure for calculating the effective width came from AASHTO Article 4.6.2.6, the same approach that was employed for the conventional bridge system. In addition, the section area, neutral axis depth, moment of inertia, and the section modulus were computed at the tenth points based on the elastic properties of the section.

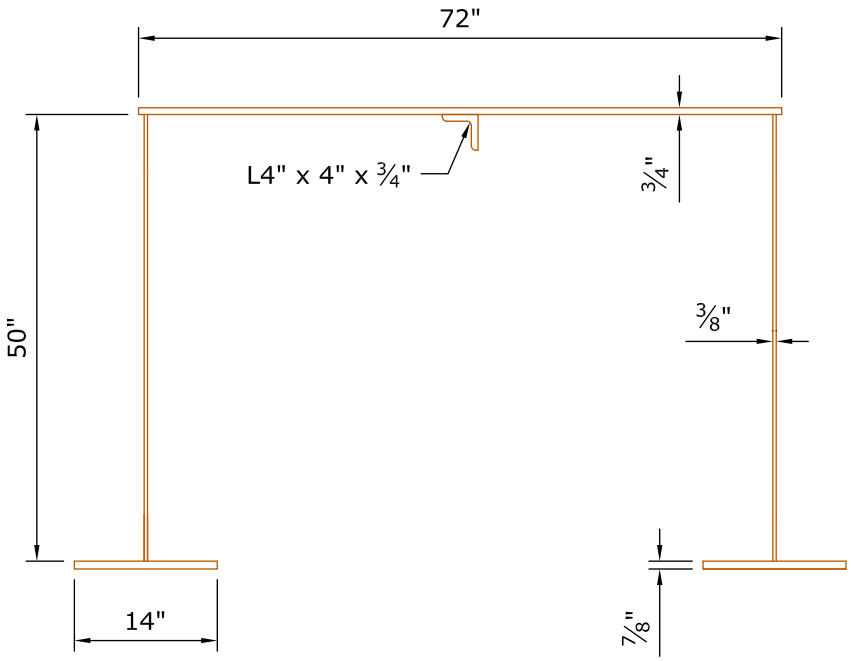

Figure 2-4: Dimensions of Inverted Box for 2-139' Span Bridge

2.2.1.2 LOADING

The system was designed such that it acted as a simple span for the dead loads applied before casting the concrete and continuous for all loads applied after the concrete was cast [13]. This included the superimposed dead loads. The dead load consisted of slab concrete weight, steel girder self-weight, formwork, and initial superimposed load. The live load distribution factor was calculated according to Article 4.6.2.2.2 of AASHTO. The live load was assigned according to AASHTO HL-93 design vehicular live load.

2.2.1.3 ANALYSIS

A two-dimensional bridge analysis under dead loads and live loads was conducted using QConBridge software. In all analyses carried out, the live

loads were applied to girders acting as continuous. The live load distribution factor was computed based on the normal box section properties.

2.2.1.4 Review of AASHTO Provisions

A review of the AASHTO (2002) bridge code was needed to identify sections that could be adopted for designing the inverted box system. The provisions of Article 6.11 apply to flexure of straight steel single or multiple closed-box or tub sections symmetrical about the vertical axis in the plane of the web in simple or continuous bridges of spans up to 350 ft. Thus, Article 6.11 is limited to bridges with the conventional box girder sections. However, these provisions can be used for designing the inverted box with some considerations. In summary, design of the proposed system is not completely covered by existing AASHTO LRFD Bridge Design Specifications.

Cross-Section Proportion Limits (6.11.2)

Web and flange proportions were checked according to the Article 6.11.2.1 and 6.11.2.2. The web is vertical as shown in Figure 2-4 and satisfies the requirement of Article 6.11.2.1.1 for the inclination angle. The depth of web to the thickness is also less than 150. The bottom flange of the box was checked for the flange proportion limits described in Article 6.11.2.3.

Constructibility Requirements (6.11.3)

The web plate was checked for the bend-buckling resistance according to Article 6.10.1.9. The web thickness as shown in Figure 2-4 was 3/8 inch. The web depth to thickness ratio satisfied this requirement.

The top flange of the box girder in positive flexure is required to resist the compressive stress. During the pouring of the concrete slab, the top flange is not composite. The thin top flange plate is prone to local buckling in positive flexure. The flexural resistance of the top flange in compression was evaluated using the Article 6.11.8.2.2 for unstiffened flanges. Based on the dimensions shown in Figure 2-4, the governing equation for the compres-

sive strength is equation three of Article 6.11.8.2.2. This indicates that the top flange slenderness lies in the elastic buckling region. The limiting flange slenderness for the top flange to yield before buckling is 19, which requires a flange thickness of 1.0 inch. Obviously, using this thickness for the top flange makes the section less economical compared to the conventional box girder. The flange thickness was selected to be ¾ inch and a longitudinal stiffener was assumed to have been welded to the top flange to prevent local buckling. The dimensions of the inverted box girder were exactly the same as the conventional box girder except that the section was rotated 180º and there is an extra longitudinal angle on the top flange.

OTHER LIMIT STATES

The Service Limit State II (Article 6.11.4), Fatigue Limit State (6.11.5) and Strength Limit State (6.11.6) were checked for the dimensions required from the constructibility sections. The designed section satisfied each requirement. Reviewing these limit states revealed that the weakness of the inverted box girder was buckling of the top flange under non-composite loads in positive flexure. This may explain part of the discrepancy between buckling stress computed from AASHTO and Finite Element Analysis, which is presented later.

2.2.2 105-FT SPAN BRIDGE

A second bridge with a single-105 ft span was designed to check the feasibility of the inverted box system in the medium span range. The bridge cross section is shown in Figure 2-5. The roadway width was 34'-8" with three girder lines spaced at 11'-9". The slab overhang on each side was 3'-8". The deck thickness was 7 ½" plus an additional ½" integral wearing surface. The dimensions of each individual inverted box girder are shown in Figure 2-6. A single plate is used to construct a uniform web and top flange configuration. This allows for the web and top flange to be formed by bending a plate, which eliminates welding. The bottom flanges are then welded

to the webs to create the inverted box section. The entire section is assumed to have a yield strength of 50 ksi.

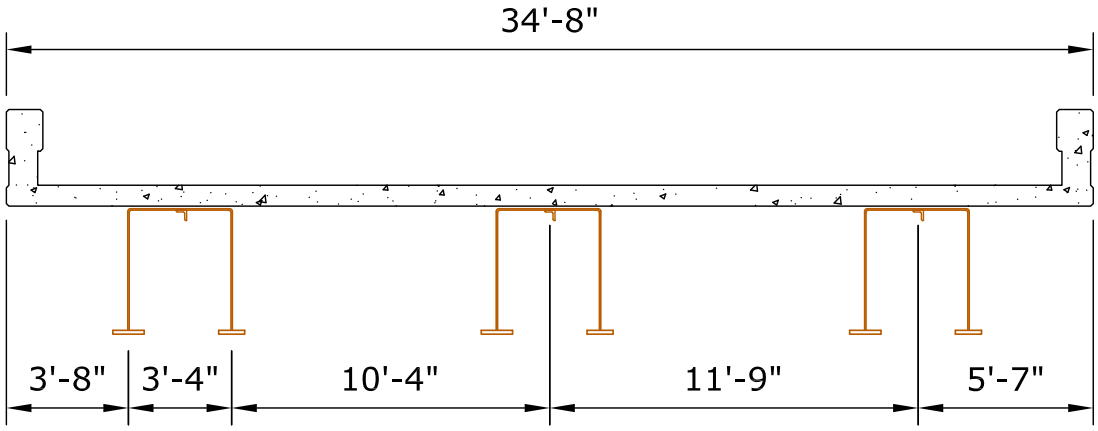

Figure 2-5: Bridge Cross-Section for 105' Span Bridge

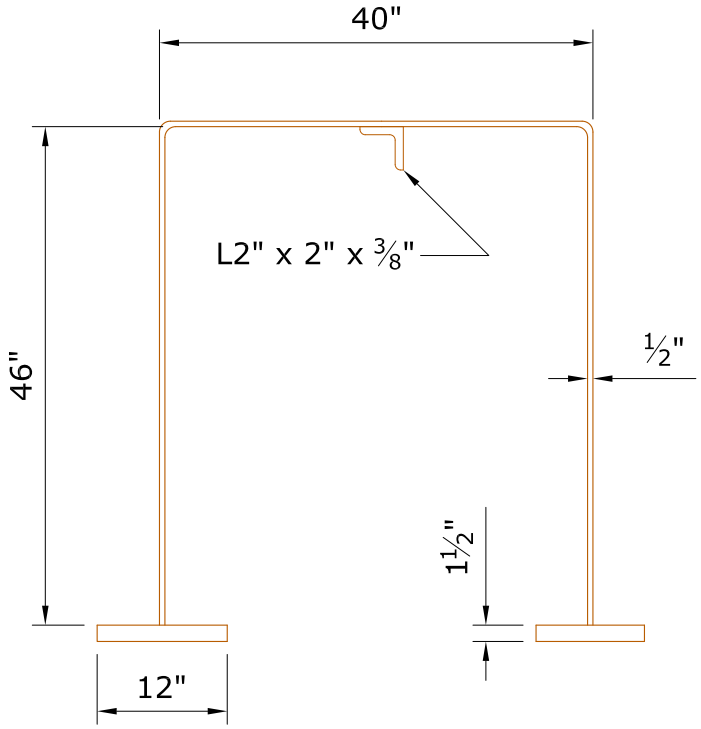

Figure 2-6: Dimensions of Box Girder for 105' Span Bridge

The bridge was designed as described in Section 2.2.1. Similar to the sections for the 139-ft span bridge, this section was also weak at the top flange in the positive flexure region. The strength of the section was not adequate to carry the construction loads of wet concrete and the girder self-weight. The thin top flange easily buckles under the compressive forces. A continuous longitudinal stiffener was attached to the top flange as shown in Figure 2-5 to prevent the elastic buckling and increase the buckling strength of the flange. The thickness of the bottom flange was governed by Strength Limit State I requirements.

The bridge was also checked for the case of two spans. It is assumed that the girders are simple for dead loads and continuous for live loads. In this case, the bottom flange thickness was reduced to 1-3/8", since the live load positive moment was decreased.

2.3 Finite Element Analysis

The two 139-ft span bridge designed in Section 3.2.1 was analyzed using the detailed three-dimensional finite element analysis approach. The ANSYS finite element analysis program was used for the analysis. A sensitivity analysis was done for the development of the finite element models. Material and geometrical nonlinearities were included in the numerical models. Results of these analyses will be used to further comprehend the basic behavior of steel inverted box bridge systems. In addition, the results are compared to the current AASHTO design equations.

2.3.1 Model Development

The basic numerical model for the finite element analyses was developed using ANSYS 5.7. The flanges, web, and stiffeners were all modeled using the SHELL181 element, a shell element suitable for analyzing thin to moderately thick shell structures. It is a four-noded element with six degrees of freedom at each node and is well suited for linear, large rotation, and/

or large strain nonlinear applications. All elements have an aspect ratio close to one. The cross frames, spacers, and braces were modeled using BEAM188 (ANSYS element Library) [5], which is suitable for analyzing slender to moderately thick beams. This element has large deformation and plasticity capabilities.

Since the shell elements used for the analyses were flat elements, there was a slight deviation from actual physical models arising from flange to web connectivity. With flat elements, the thickness of each element is not realized in the geometry of the model, thus a difference in cross section can be seen between the finite element model and an actual physical model for the same geometry of interest. In the current analyses, the web depth was increased to the distance between the centers of the flanges.

For the numerical analyses, the Bilinear Isotropic Hardening option within the ANSYS program was used to model the material behavior. This option is like the multilinear isotropic hardening option, except that a bilinear curve is used. A value of 29000 ksi was used for slope of the elastic portion of the material strain-stress curve and five percent strain hardening was considered after the yielding limit. The yield strength of the steel plates was input as 100 ksi which was based on the High Performance Steel material specifications used in the N2 over I-80 bridge.

The solution method used for all analyses was the Newton-Raphson technique. Before each solution, the Newton-Raphson method evaluates the out-of-balance load vector, which is the difference between the restoring forces (the loads corresponding to the element stresses) and the applied loads. The program then performs a linear solution, using the out-of-balance loads, and checks for convergence. If convergence criteria are not satisfied, the out-of-balance load vector is re-evaluated, the stiffness matrix is updated, and a new solution is obtained. This iterative procedure continues

until the problem converges. If convergence cannot be achieved, then the program attempts to solve with a smaller load increment.

To check the numerical accuracy of the mesh, two models were created using different mesh sizes. For the first model, the maximum mesh size of the shell elements was limited to 20 inches, while the mesh size was limited to 10 inches in the second model. Since the finer mesh produced a buckling coefficient that deviated from that of the original mesh, the finer mesh was selected for the rest of the analyses. This was done to obtain more accurate results in the range of nonlinear analysis.

Load was applied to the model in the form of pressure on the top flange to simulate the weight of concrete slab, steel girder, and formwork (DC1). The size of the load increment applied to the model was determined based upon the AASHTO predicted capacity. By multiplying the predicted capacity by 2.5, a target load was obtained. The target load was then divided into a number of sub-steps to obtain the size of the increment.

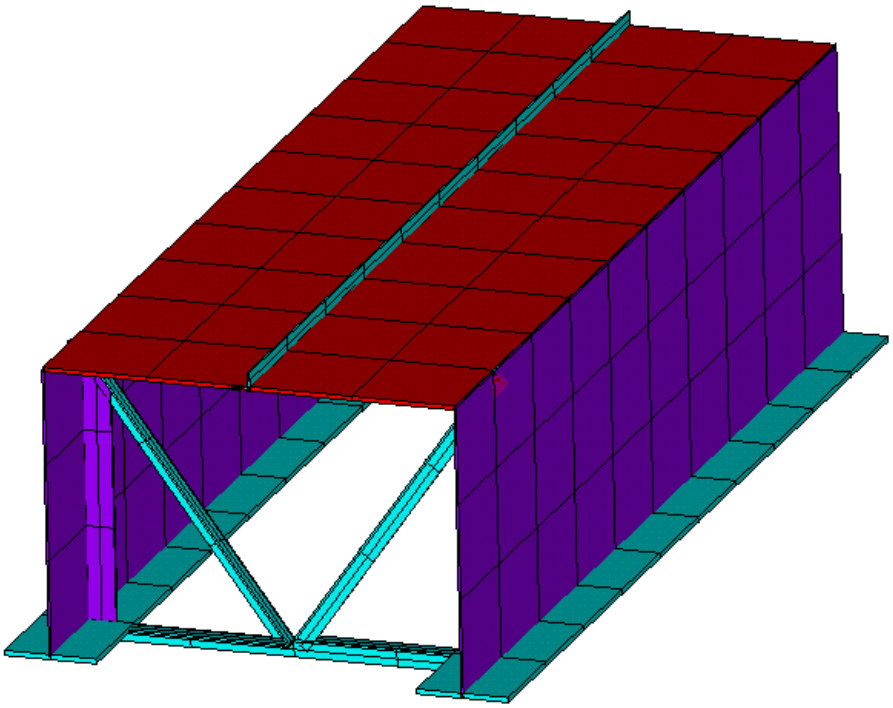

Figure 2-7: Finite Element Model

A variation from flatness was introduced into the model in order to initiate out-of-plane deformations. The model was analyzed with initial imperfections based on the Euler buckling mode shape. The mode shape was obtained by running an elastic buckling analysis in ANSYS. The maximum value of out-of-flatness was input as D/120, which is the permitted initial out-of-flatness in the ANSI/AASHTO/AWS D1.5-96 Bridge Welding Code [3], where D is the depth of the web, or flange width.

2.3.2 FINITE ELEMENT RESULTS

DEFLECTION CHECK

The maximum vertical deflection was 12.10 inches under the dead loads (DC1) from a linear 3-D finite element analysis of a single inverted box. The elastic deflection of a simply supported beam under distributed load is given by

$$\Delta = \frac{5wl^4}{384EI} \tag{2-1}$$

Where

Δ = deflection (in)
w = distributed dead load (k/in)
l = span length (in)
E = elastic modulus (ksi)
I = moment of inertia (in^4)

For the current example, the numerical values were substituted into Equation 2-1.

$$\Delta = \frac{5(0.161 \text{ k/in})(1{,}668 \text{ in})^4}{384(29{,}000 \text{ ksi})(57{,}977 \text{ in}^4)} = 9.6 \text{ in} \tag{2-2}$$

Part of the difference between the elastic calculation and that of the finite element analysis is due to shear deformation, which is not included in the elastic calculation.

The elastic calculation results in a maximum factored compressive stress (1.25xDC1) of 24.1 ksi at the top flange. The three-dimensional linear finite element analysis yields a stress magnitude of 23.5 ksi at the junction of the top flange and the web at midspan under the same load. It is noted that in finite element analysis, the compressive stress at the two web plates at the top flange is more than 23.5 ksi. This is due to bending of the top flange which cannot be computed by simple hand calculations.

BUCKLED SHAPE

Elastic buckling analysis of a single inverted box girder was conducted using the Block Laczos method [5]. A distributed pressure was applied on the flanges to simulate the dead load effect. For the first analysis, the inverted box was unstiffend, in which longitudinal stiffeners were neglected. For the second analysis, the inverted box was stiffend with longitudinal stiffeners at the top flange. Three modes of buckling were extracted for the stiffened box, as shown in Figure 2-8. The inflection points of the buckled waves were at the locations of cross frames or spacers. The ratio of each buckling load to the applied dead load for the unstiffened and stiffened box girder is given in Table 2-1.

The constructibility check for flexural resistance of the compression flange according to AASHTO revealed that the top flange with one longitudinal stiffener is prone to elastic buckling. The elastic buckling resistance of the flange is given by Equation 6.11.8.2.2-3 of AASHTO [2]. The stress obtained from this equation is also given in Table 2-1. It can be seen that the AASHTO prediction of the elastic buckling capacity is conservative compared to finite element analysis. The difference occurs because the AASHTO equation does not consider the interaction of the web plate, stiffeners, and cross-frames on the buckling resistance of the top flange.

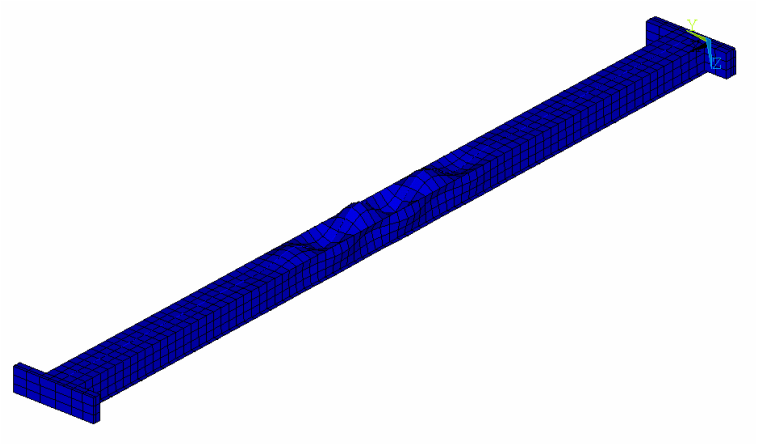

1st Mode

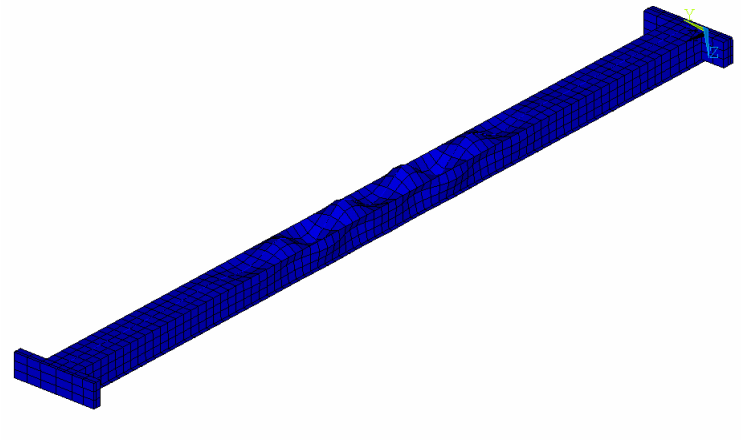

2nd Mode

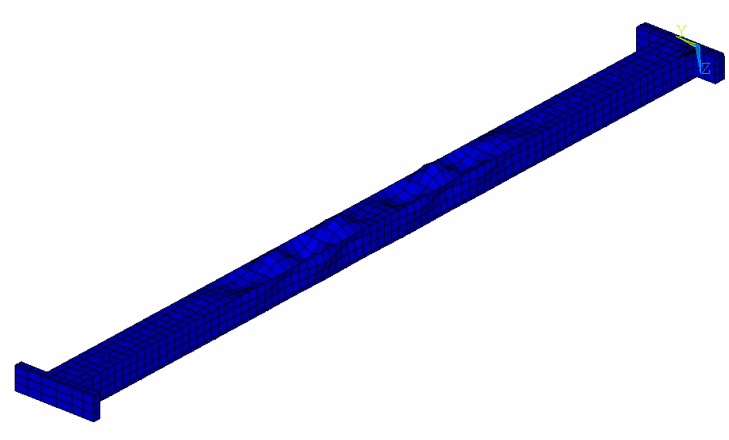

3rd Mode

Figure 2-8: Elastic Buckling Analysis

Unstiffened

Buckling Mode	Buckling load/dead load(DC1)	Buckling stress (ksi)	
FEA	FEA	FEA	AASHTO
1	0.64	16.42	11.32
2	0.66	16.94	
3	0.67	17.19	

Stiffened

Buckling Mode	Buckling load/dead load (DC1)	Buckling stress (ksi)	
FEA	FEA	FEA	AASHTO
1	1.42	35.65	26.30
2	1.49	37.41	
3	1.58	39.67	

Table 2-1: Elastic Buckling of a Single Inverted Box Girder

ULTIMATE STRENGTH

The ultimate capacity of the inverted box girder was computed using finite element analysis for the unstiffened and stiffened box girder.

The nonlinear finite element analysis of the unstiffened box girder showed that the ultimate strength was 2.05 times the applied dead load (DC1). The plastic strain contours of the box are shown in Figure 2-9. The maximum plastic strain was at the junction of the top flange and the web at midspan.

The nonlinear finite element analysis of the stiffened box girder showed that the ultimate strength was 2.35 times the applied dead load (DC1). In this case, yielding was seen in a wider area than the previous case, as shown in Figure 2-10.

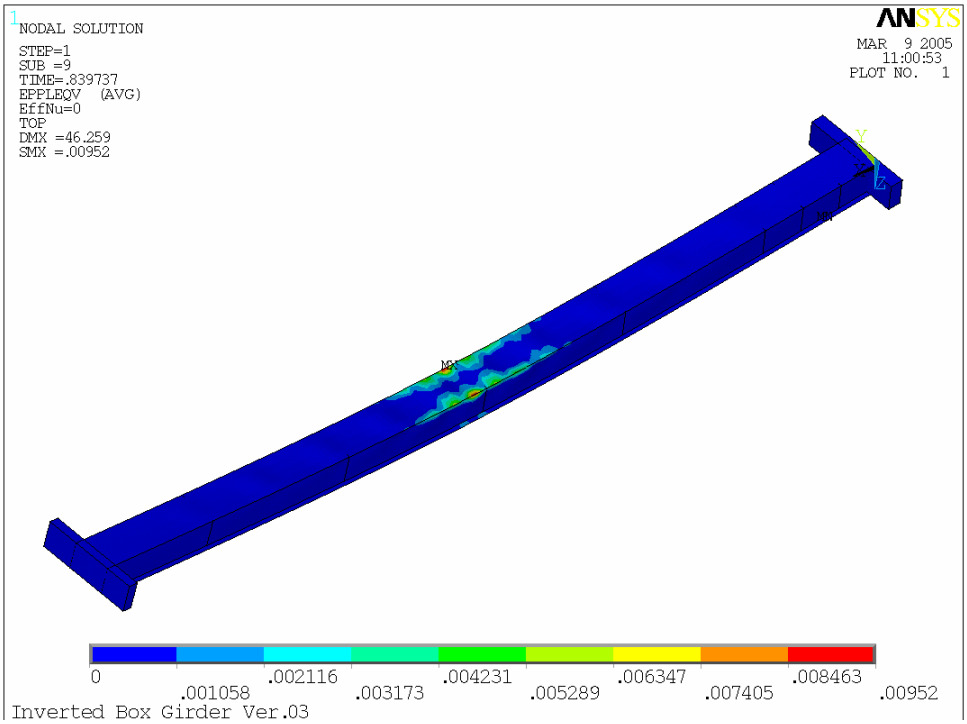

Figure 2-9: Von-Mises Plastic Strain for Unstiffened Box Girder

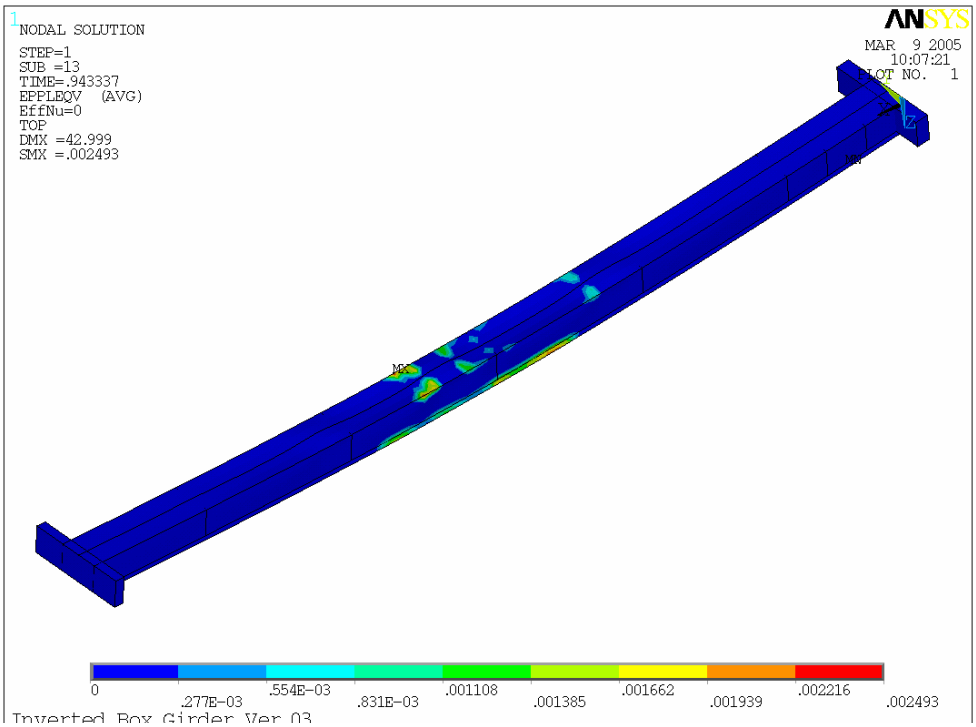

Figure 2-10: Von-Mises Plastic Strain for Stiffened Box Girder

The ultimate capacity for each case was calculated using AASHTO equations and finite element analysis. The ratio of the ultimate strength to the applied dead load (DC1) is summarized for each approach in Table 3-2. The AASHTO equations limit the capacity of the box to the elastic buckling strength of the top flange while finite element analysis shows that the there is substantial post-buckling strength.

	Capacity/ Applied Dead load (DC1)	
	AASHTO	FEA
Unstiffened	0.59	2.05
Stiffened	1.36	2.35

Table 2-2: Ultimate Capacity

2.4 CONCLUSIONS

The bridge system presented in this paper would likely be best suited for shorter spans of less than 100 ft for vehicular traffic. An additional economic analysis is required to determine the optimum applicable span range. In addition, the numerical study and parametric design of the new concept show that:

1. AASHTO-LRFD equations for normal box girder bridges can be used for design of inverted box girders.
2. AASHTO-LRFD prediction of buckling and ultimate capacity of a box section based on the compression flange is conservative.
3. Using a uniform thickness the web plate or top flange is not economical for longer span lengths.
4. A longitudinal stiffener is necessary to prevent top flange buckling under construction loads.

2.4.1 RECOMMENDATIONS FOR FUTURE RESEARCH

Based on the analysis and design checks carried out in this report, the following issues are suggested to further investigations:

1. The AASHTO equations for the elastic buckling and ultimate capacity of the box girder flange should be modified to include the post-buckling strength of box section.
2. Utilizing corrugated plates to eliminate the longitudinal stiffeners and reduce the steel girder weight is a possibility.
3. Combination of a normal box section and an inverted section for the length of the bridge is recommended for further study.

Chapter

3 Tube Girder

An experimental investigation was carried out to observe the behavior of a concrete-filled tube girder. Literature was reviewed for the applicability of the tube girder design. Based on these provisions, a 1/4-scale specimen was designed and tested. A numerical analysis was used to evaluate the behavior of the system. Based on the test results, the advantages and disadvantages of the system were addressed.

3.1 Description of the Proposed System

The system consists of a steel tube filled with concrete. To increase flexural strength, longitudinal reinforcing bars are placed in the bottom of the tube before it is filled with concrete. Figure 3-1 shows the proposed system.

Shear studs were welded to the top of the tube prior to casting the deck slab. The shear studs provided composite action between the concrete-

filled tube and the deck slab. The concrete-filled tube carried the weight of the wet slab.

Preliminary calculations indicated that placing the steel tube on the supports prior to filling it with concrete may not be feasible. This approach would result in high stresses in the tube walls due to the weight of wet concrete, thereby dictating the required tube thickness. Several strategies have been devised to address this situation.

1. The tube could be filled with concrete while resting on the ground and placed over the supports after the concrete hardens.
2. Lightweight concrete can be used to lower the weight of the section.
3. A void can be left in the concrete to reduce the volume of concrete required.

The third strategy can be explained as follows: when the composite system, including the deck, is at the ultimate load level, taken to be the plastic moment capacity, the neutral axis is located near the top of the tube. In this condition, the concrete inside the tube is not effective since it is under tension. Therefore, the concrete in this region can be omitted without affecting the ultimate capacity of the system. To accomplish this, prior to filling the steel tube with concrete, a second, smaller tube is positioned inside the main tube. The void created by the smaller tube reduces the weight of the girder.

3.2 Experimental Investigation

A tube girder specimen was constructed and tested to collapse. The following is a summary of the experimental investigation and results obtained.

3.2.1 Specimen Design

Section 6.12 of the AASHTO LRFD Bridge Design Specification provides limited design provisions that could be used for the design of the proposed bridge system [1]. However, these provisions are limited to concrete-filled tubes without a composite slab. Further, the design provisions listed in section 6.12 are overly conservative [9, 11]. In summary, design of the proposed system is not completely covered by existing AASHTO LRFD Bridge Design Specifications.

An attempt was made to develop criteria for selecting the test specimen cross-section. Ultimately, it was envisioned that the tube girder design would take the place of the traditional I-beam design made composite with the concrete slab and shear studs. With this in mind, the following procedure was used to determine the specimen cross-section in terms of pipe diameter, amount of reinforcement in the pipe and the concrete slab dimensions.

The American Iron and Steel Institute (AISI) and HDR Engineering have produced a document, Four LRFD Design Examples of Steel Highway Bridges [14]. The first three design examples in this document use composite steel beams. For these examples, the ratios of the plastic moment capacities of the composite section over the plastic moment capacities of the bare steel beams were calculated. For these calculations, the positive moment region was selected, where concrete is in compression and the bottom flange in tension. The ratios obtained were approximately 2.0.

The cross section of the test specimen was sized such that the ratio of the plastic moment capacity of the complete cross section over the plastic moment capacity of the pipe section, including the concrete and reinforcing bars was approximately 2.4. The availability of the steel pipe section was the primary reason for not being able to obtain a value closer to 2.0. For the suggested system, the plastic moment capacity was obtained using

the moment curvature analysis approach, which is described in Section 4.4.1.

3.2.2 Description of the Test Specimen

As shown in Figure 3-1, the test specimen was a simple span beam. Also shown in Figure 3-1 are the cross section dimensions of the specimen. The specimen consisted of a 29 ft and 3.5 inches long (8.929 m) ASTM A714-99 Class 4 Grade VII steel tube with a 14 inch (355.6 mm) outside diameter and a 0.375-inch (9.52 mm) wall thickness. To reduce weight, a piece of 6 inch (152.4 mm) SCHED 40 PVC pipe was placed inside the tube. The center of the PVC pipe was offset upwards from the center of the steel pipe by one inch. To increase the tensile capacity of the girder, three #6 Grade 60 reinforcing bars were placed at the bottom of the tube, as shown in Figure 3-1. The thickness of the cover concrete between the reinforcing bars and the steel tube was 1 inch (25.4 mm).

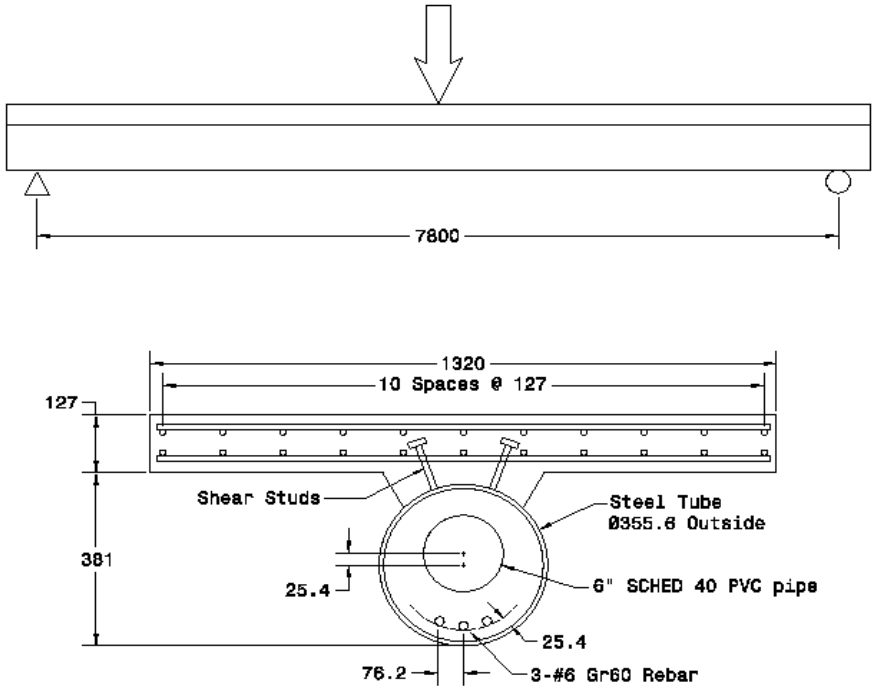

Figure 3-1: Longitudinal and Cross Section of Specimen

The width and thickness of the concrete slab were 52 inch (1320.8 mm) and 5 inches (127 mm), respectively. The longitudinal and transverse reinforcement in each face of the slab consisted of #4 bars spaced at 5 inches (127 mm) on center.

A haunch provided a transition from the deck to the steel tube as shown in Figure 3-1. Shear studs are also shown on the top of the steel tube. Two rows of shear studs spaced at 4-3/4 inches (120 mm) were welded on the top of the steel tube with a 5.5 inch (139.7 mm) pitch along the member to provide composite action between the tube and concrete slab. The pitch of shear studs was calculated using the AASHTO LRFD provisions [1].

3.2.3 Material Properties

Material testing was performed to determine the actual material properties. Tension tests were performed in accordance with ASTM standard A-370 specifications on the steel tube and #6 reinforcing bars [6]. Figure 3-2 shows the results of these tests.

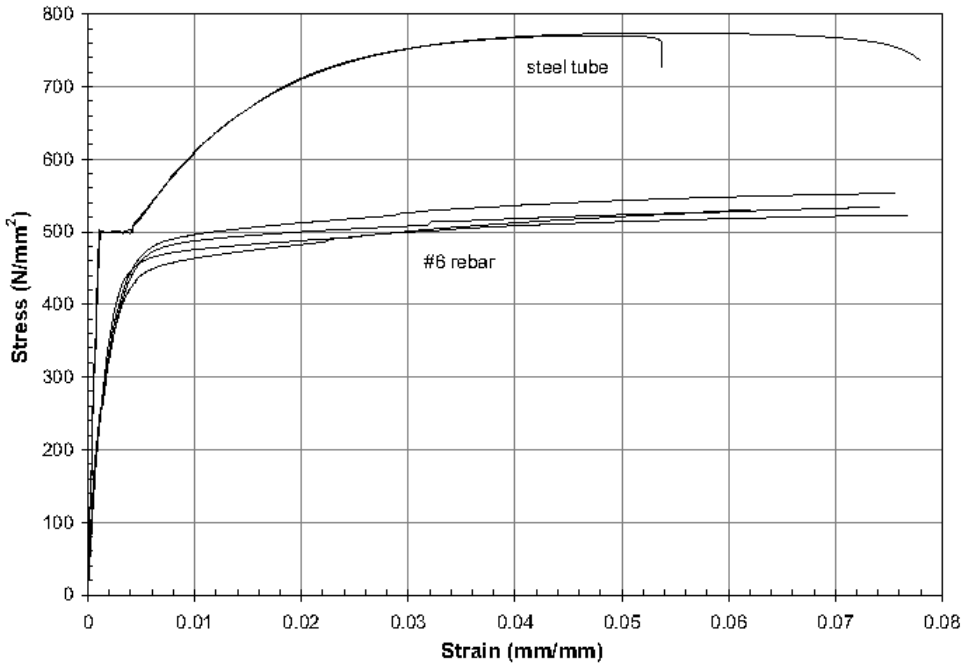

Figure 3-2: Tension Tests Results

Concrete for both inside the tube and the deck slab was provided by a local ready-mix supplier. The 28-day compressive strength of the concrete inside the tube was 6350 psi (43.8 N/mm2) , as determined by material testing. Super plasticizer was added to obtain an eight inch (203.2 mm) slump to facilitate the pumping of the concrete into the tube. The measured 28-day compressive strength of the deck slab concrete was 5388 psi (37.1 N/mm2) .

3.2.4 Construction Sequence of the Test Specimen

Construction of the specimen proceeded as follows:

1. The core, which consisted of the PVC pipe and three No. 6 deformed bars, was pre-fabricated. Small steel bars were bent in a semi-circular shape and the longitudinal reinforcement was tied to these bars. Spacing chairs were placed below the reinforcement and above the PVC pipe. This ensured the proper clearance and prevented the PVC pipe from floating during pumping the concrete inside the steel tube.
2. The core assembly was then inserted into the steel tube, as shown in Figure 3-3, and the steel tube was placed within the deck formwork.
3. Steel plates were welded on either end to seal the girder. A fitting which connected to the concrete pump was affixed to one end. A hole was placed near the top of the plate on the other end to vent the displaced air as the tube was filled.
4. The tube was filled by pumping concrete into the steel tube. The tube was lying flat on the floor during the filling process. Figure 3-4 shows the specimen while concrete was being pumped into the tube.
5. A few days after pumping the concrete into the pipe, the slab deck was cast while the specimen was resting on the floor.
6. After the slab deck had cured for one week, the entire specimen was lifted and placed onto the supports.

Figure 3-3: Assembly of core into steel tube

Figure 3-4: Concrete being pumped into the tube

3.2.5 INSTRUMENTATION PLAN

During the test, strains and deflections at various locations along the specimen were measured. Strains were monitored in both concrete and steel. Strains were measured using both resistive foil and vibrating wire strain gauges. Deflections were measured using potentiometers.

Figure 3-5 shows the instrumentation plan. This figure shows the locations where local strains were measured using resistive foil strain gages glued to the steel and concrete surfaces. These gages were designated SG. Figure 3-5 also shows locations where concrete strains were measured using vibrating wire embedment gages. These gages were designated EG. In the discussions to follow, results of the experimental investigation are partly summarized by reporting the strains at the gage locations indicated in Figure 3-5.

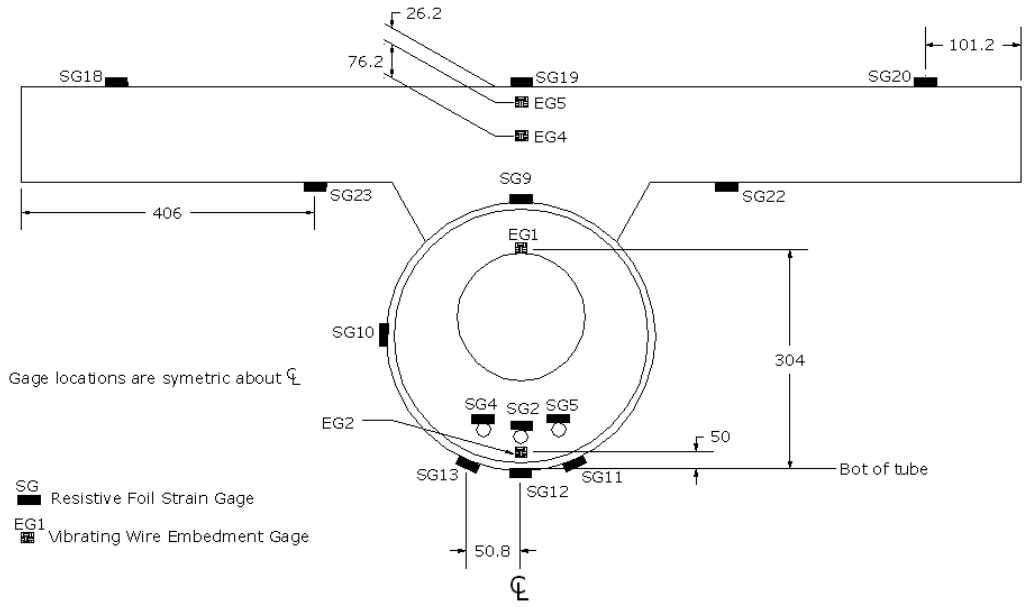

Figure 3-5: Gage Locations

The vertical deflection of the test specimen was measured using string potentiometers located at midspan and 30 inches (762 mm) to either side of midspan. Spring potentiometers were attached to the end of the speci-

men to monitor possible slippage of the concrete with respect to the pipe end. All the instruments were attached to a data-acquisition system controlled by a personal computer.

3.2.6 Test Setup and Testing Procedure

Figure 3-6 shows the test specimen and loading fixtures prior to testing. The test specimen was simply supported at both ends. Roller-type supports were used at both ends, which allowed the ends to freely rotate and translate in the horizontal direction. The end support was a U-shaped concrete block cast to fit the steel tube. Loading of the specimen was achieved using a spreader beam placed on top of the slab at mid-span. Two hydraulic jacks, as shown in Figure 3-6, were used to load the specimen. The specimen was loaded incrementally until collapse. Initially, each load increment was approximately 5 kips (22.24 kN). After the load deflection curve exhibited a plateau region, the loading of the specimen proceded by incrementing the displacement.

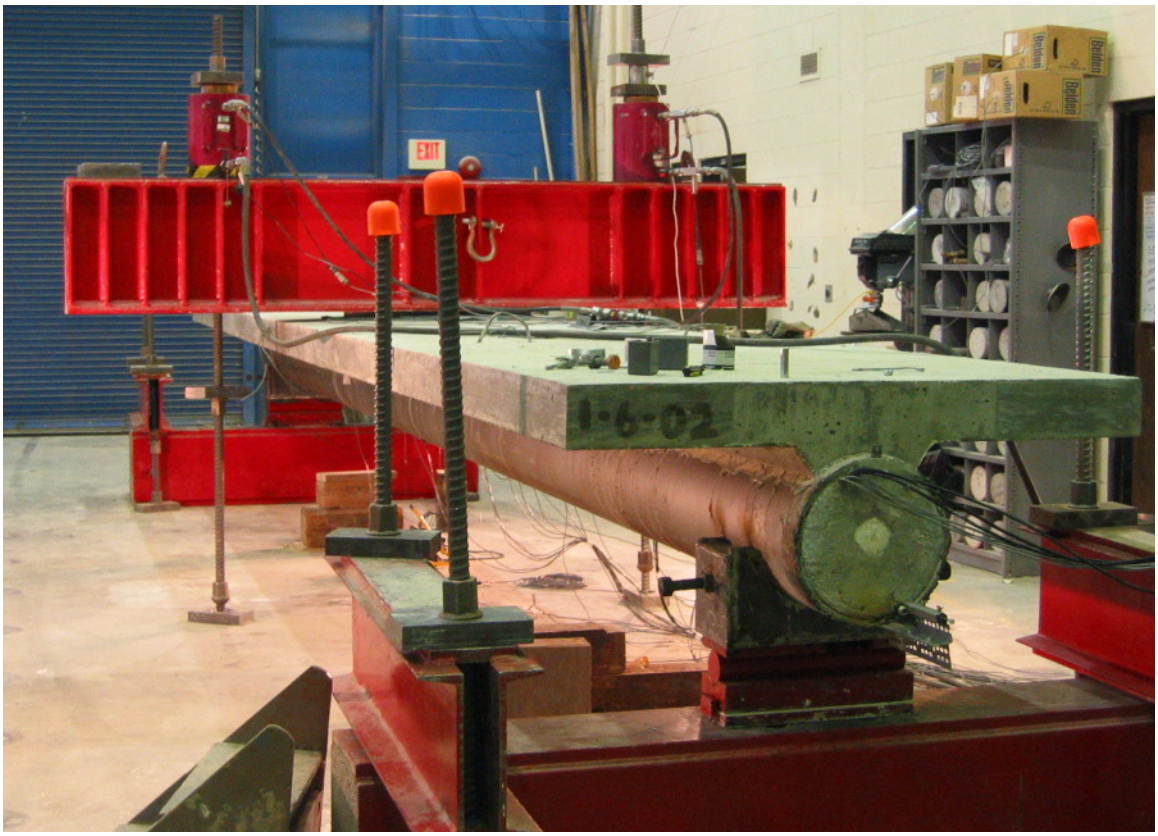

Figure 3-6: Specimen and loading fixtures before testing

3.3 Experimental Results

The following section provides general observations made throughout the testing and the numerical results obtained.

3.3.1 Load-Deflection Data

Figure 3-7 shows the observed load deflection curve. The specimen exhibited a good level of ductility before failure. As seen in Figure 3-7, the load deflection response of the system was nearly linear until a deflection of 1.85 inch (47 mm) , which corresponded to an applied load of 139.7 kips (621.38 kN). Analysis had indicated that the bottom of the steel tube would yield at this load level. Yielding of the steel at the bottom of the tube was confirmed by results obtained from strain gages.

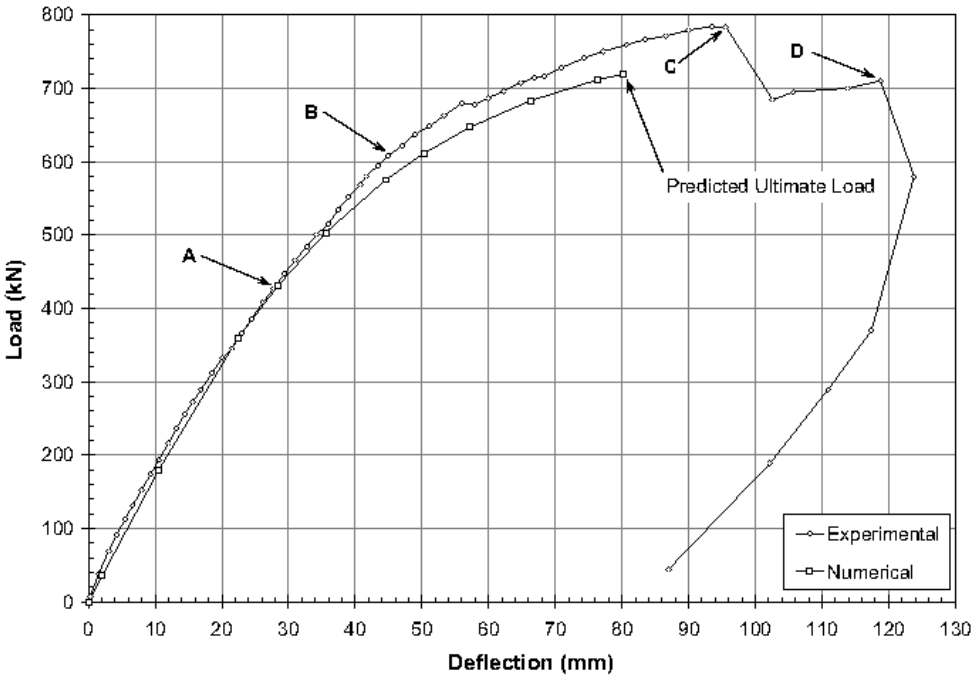

Figure 3-7: Load-deflection curve

There were very few observable events prior to reaching the ultimate load. When the load reached 160 kips (711.68 kN) some flexural cracks were observed in the very bottom of the concrete slab, indicating the neutral axis was indeed within the slab.

The maximum applied load was reached at approximately 3.76 inch (95.5 mm) of vertical deflection, corresponding to a load of 176.13 kips (783.4 kN). As indicated in Figure 3-7, after the specimen reached its ultimate flexural capacity (176.13 kips load at 3.76 inch of deflection) there was a drop in applied load which coincided with localized crushing of the concrete deck. This drop in flexural capacity was likely attributable to the crushing of the deck slab. However, after this event the specimen was able to absorb additional deflection at a reduced load level.

The maximum deflection was 4.87 inch (123.7 mm), which occurred after additional crushing of the concrete slab and a second drop in applied load,

down to 130.3 kips (579.6 kN). The reduced load level corresponds, approximately, to the flexural capacity of the reinforced concrete-filled steel tube in absence of the deck. The system was unloaded at this point. Previous research indicates that concrete filled tube members have excellent ductility and can sustain their flexural capacity at very high ductility levels [10, 11]. This could provide an explanation for the test specimen being able to sustain a load after crushing of the deck slab.

3.3.2 Strain Data

Figures 3-8 through 3-11 show the strain profiles at midspan corresponding to points A, B, C, and D in Figure 3-7. The ordinate value indicates the distance from the bottom of the steel tube and the abscissa value indicates the strain at that location.

Figure 3-8, corresponding to Point A in Figure 3-7, shows that at low load levels the strain profile at midspan was highly linear. Note that the strain in the concrete embedment gage at the top of the tube, denoted by an arrow, was in tension, which indicates the concrete core was acting composite with the rest of the system. Further indication of the composite action was given by the strain in the rebar at the bottom of the tube.

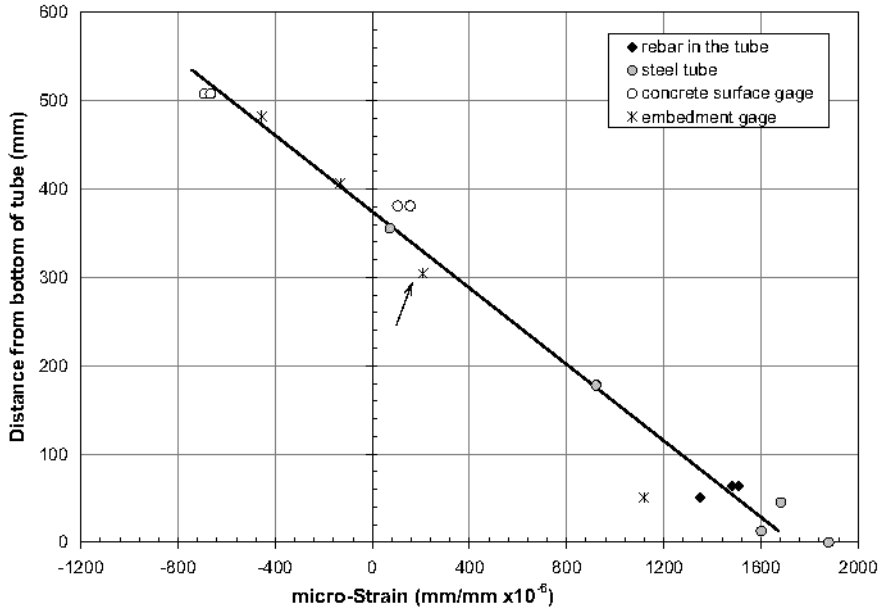

Figure 3-8: Strain Profile Corresponding to Point A in Figure 3-7

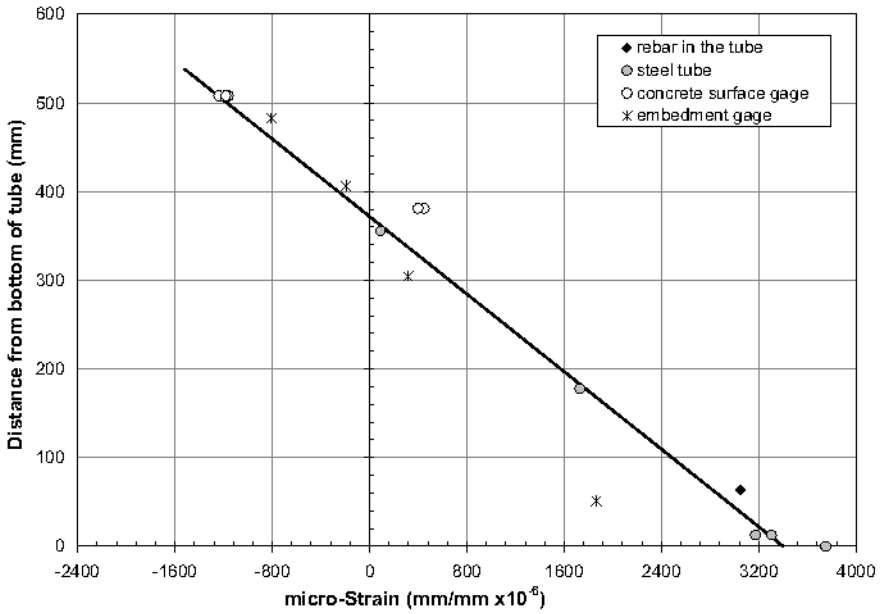

Figure 3-9: Strain Profile Corresponding to Point B in Figure 3-7

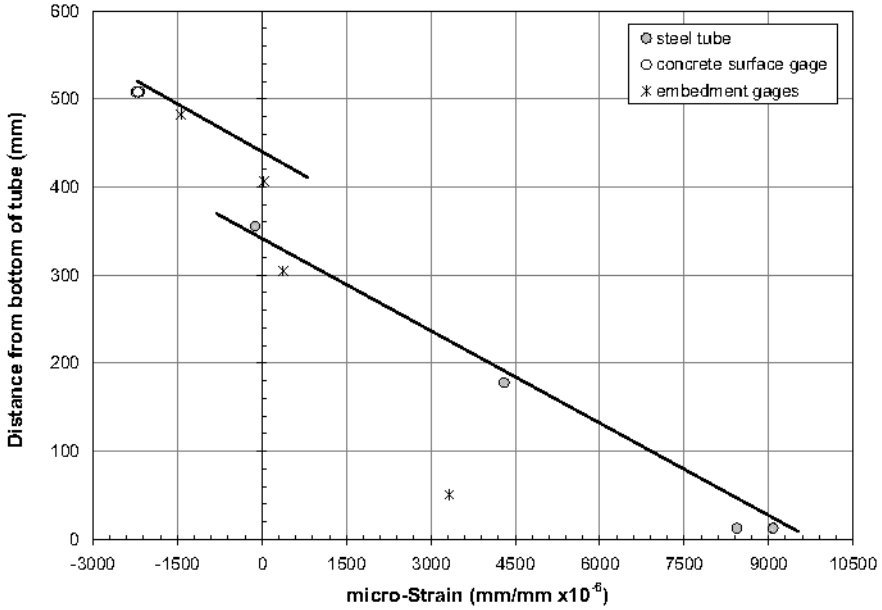

Figure 3-10: Strain Profile Corresponding to Point C in Figure 3-7

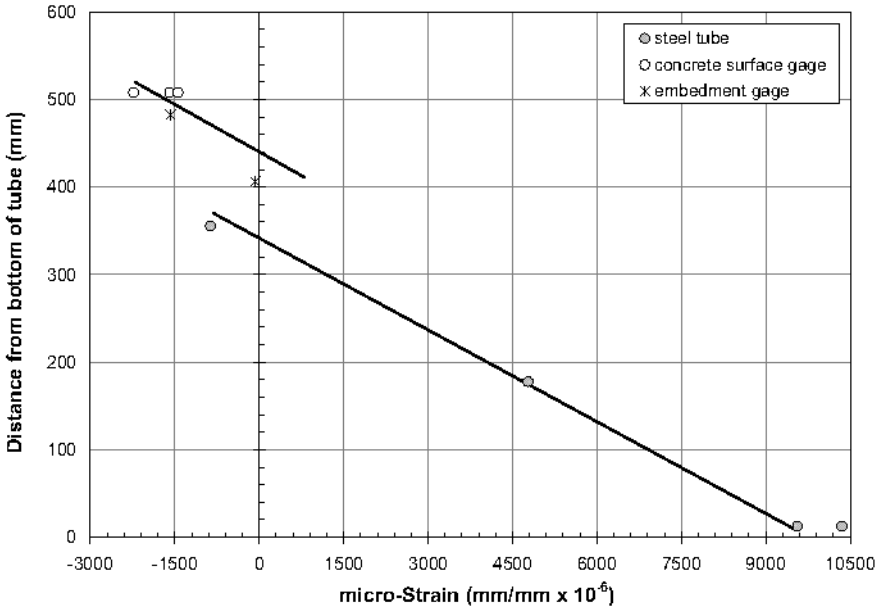

Figure 3-11: Strain Profile Corresponding to Point D in Figure 3-7

The load at point B was 81% of the ultimate value. As shown in Figure 3-9, the strain in the rebar indicated that the concrete core was still acting compositely with the system. Just beyond this point the final strain gage on the rebar failed and the degree of composite action could no longer be confirmed. Note that the strain readings from the embedment gages in the tube were lower than indicated by a line passing through the steel and deck gages. This was due to the short gage length of the embedment gage within concrete under tension.

Point C in Figure 3-7 indicates the ultimate load just prior to crushing of the concrete deck. Figure 3-10 indicates that there was discontinuity in the strain profile at the top of the tube. This discontinuity could have been due to slip between the steel tube and the concrete deck caused by the bending of, and local crushing around, the shear studs. Apart from this discontinuity, the strain distribution through the specimen was linear at the ultimate load condition, which validates one of the assumptions used in performing a moment curvature analysis as described in Section 3.4.1. As can be seen in Figure 3-10, the strain at the embedment gage located towards the top of the tube remained in tension, indicating at least some degree of composite action at the ultimate load condition.

Figure 3-11 shows the midspan strain profile just prior to the second drop in strength and is marked Point D in Figure 3-7. Again, one can see the slip discontinuity, in an otherwise linear distribution, at the top of the tube.

3.3.3 Specimen Dissection

Consolidation of the concrete inside the steel tube was a concern during the construction of the specimen. To investigate the condition of the concrete core, the steel tube was removed after the ultimate load test. Figure 3-12 shows the specimen after removal of the steel tube.

Except for some small voids in the sidewall of the concrete core, shown in Figure 3-13, no significant defects in the concrete were observed. Incorpo-

rating the use of self consolidating concrete would help to eliminate these voids.

Figure 3-12: Steel Tube Removed From Girder

Figure 3-13: Voids in Girder Concrete Viewed After Removal of Steel Tube

3.4 NUMERICAL ANALYSIS

Moment curvature analysis was used to predict the response of the system. Details of the moment curvature procedure are given in the following section. The conjugate beam method was used to determine the deflections from the results of the moment curvature analysis.

3.4.1 MOMENT CURVATURE ANALYSIS

Prior to construction of the test specimen, a numerical analysis was performed to estimate the flexural capacity of the system. Prior experience with concrete filled tube systems indicated that the moment curvature analysis was a suitable numerical technique to estimate, within a reasonable level of accuracy, the flexural capacity of concrete-filled steel tube members [10, 11]. The purpose of the analysis was to obtain an approximation for the expected behavior, not to perform an exhaustive complex analysis. As such, slippage between the steel tube and concrete deck was not considered in the analysis.

A computer program was developed to perform moment curvature analysis for composite sections. The following provides a brief description of the program and its main assumptions.

The moment-curvature analysis was performed according to the following steps:

1. Divide the entire girder cross section into a number of layers; the amount of a particular material on each layer is determined from the section.
2. Select a curvature for which the moment will be calculated, ϕ.
3. Assume a value for the strain at the top of the slab, ε_{max}
4. Calculate depth to the neutral axis, $y_n = \varepsilon_{max} / \phi$.
5. Calculate the strain at each layer of the cross section assuming a linear strain distribution

6. Calculate the stress at each layer based on the appropriate constitutive relationship for each material.
7. Integrate the stresses over the cross section to obtain net force on section.
8. If equilibrium is not satisfied assume a new strain at the top of the slab.
9. Iterate step 4 through 9 until net force on section is zero.
10. Calculate the moment from stresses; this results in one point on the moment curvature curve
11. Select next curvature value and repeat steps 3-10

3.4.1.1 MATERIAL MODELS

The Comite Europeen du Beton (CEB) constitutive model was used for the concrete portions of the section [19]. The stress-strain curve is represented by Equation 6. The value for concrete crushing stress was obtained from compression cylinder tests.

$$f_c = \frac{0.85 f_c'(a - 206,000\varepsilon_c)\varepsilon_c}{1 + b\varepsilon_c} \tag{3-1}$$

Where

$a = 39,000(0.85f'_c + 7.0)^{-0.95}$,

$b = 65,600(0.85f'_c + 10.0)^{-1.085} - 850$,

f_c = Stress in Concrete (MPa),

ε_c = Strain in Concrete (mm/mm), and

f'_c = Concrete Crushing Stress (MPa).

At the ultimate load level, a majority of the concrete in the steel tube will be in tension. Since the effects of confinement is most pronounced when concrete is in compression, the concrete inside the tube is conservatively assumed to be unconfined.

The material models for the steel tube and reinforcing bars were input as multi-linear stress/strain curves as obtained from the material test results.

3.4.2 RESULTS

The numerical analysis was used to investigate the effects that varying degrees of composite action between the concrete core and tube would have on the capacity of the system. Figures 3-14 and 3-15 show the results of these analyses. Figure 3-14 plots the predicted moment versus curvature for four conditions. The case referred to as core non-composite assumes that the slab and tube act compositely while the core is independent. Figure 3-15 shows the location of the neutral axis for each of the cases with respect to the features of the cross section. It can be seen in Figure 3-15 that the majority of the system capacity comes from the steel tube acting compositely with the deck slab. When the reinforced concrete core acts in parallel with the previous system there is a slight increase in strength. The strength from a fully composite system is only marginally greater than the parallel system.

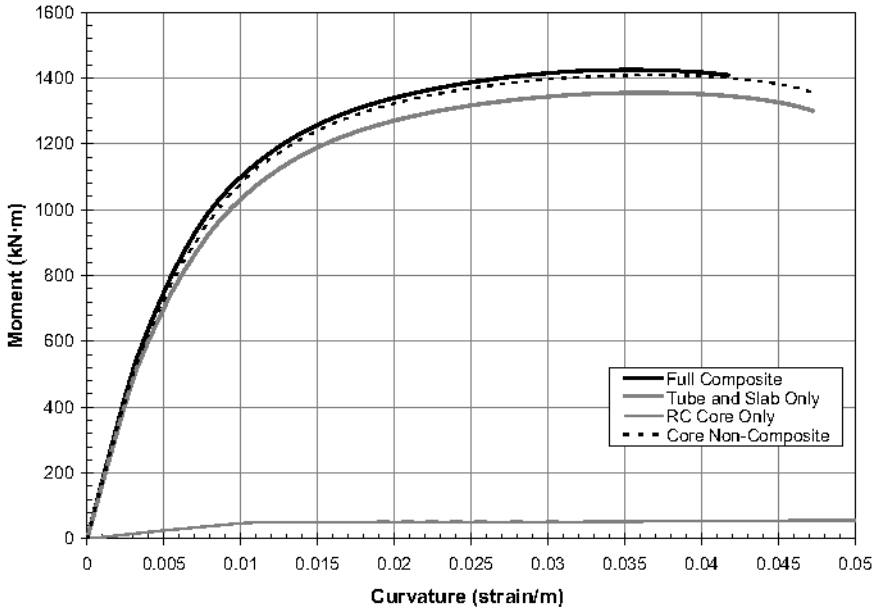

Figure 3-14: Numerical Moment-Curvature Prediction for Four Indicated Cases

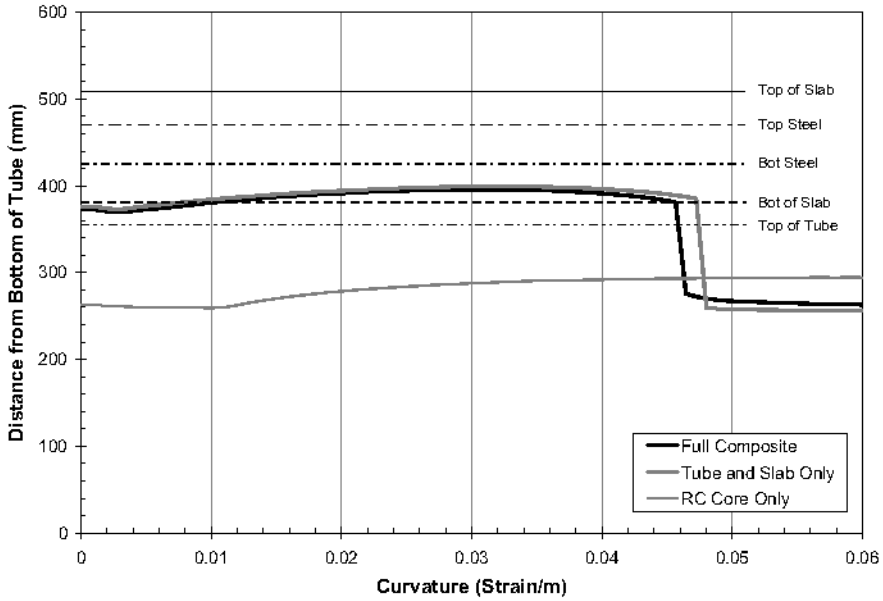

Figure 3-15: Numerical Prediction of the Location of the Neutral Axis for the Four Indicated Cases

Figure 3-7 shows the predicted load-deflection curve assuming complete composite action compared with the experimental results. As previously mentioned, analysis of the strain data suggested that complete composite action was developed until a load of 143.2 kips (637.1 kN) was obtained, after which, lack of data made such a determination no longer possible. Further indication that composite action was developed between the steel tube and concrete core was that zero relative deformation between the tube and core at the beam ends was observed throughout the entire test. Figure 3-7 shows that the numerical analysis does well in predicting the load-deflection response, although the predicted ultimate load is lower than the experimental value.

3.5 CONCLUSIONS

The concrete-filled tube exhibited good behavior up to the ultimate load level. The system exhibited good local and global stability. Filling the tube with concrete prevents local buckling of the steel while the closed shape of the tube provides torsional stability.

The mode of failure of the specimen was yielding of the steel tube followed by yielding of the reinforcement inside the steel tube and finally crushing of the deck slab. This mechanism provided a ductile failure similar in behavior to that of a conventional I-shaped girder.

The strain distribution within the specimen remained linear at all stages of loading. This facilitates the use of moment curvature analysis to predict the specimen behavior.

Moment curvature analysis showed a good prediction for the capacity of the system and can be used to evaluate the capacity of the section for a specific design.

Although there was not a practical way to vibrate the concrete inside the tube, no noticeable defects in the concrete within the steel tube were observed.

The bridge system presented in this paper would likely be best suited for shorter spans of less than 100 ft for vehicular traffic. An additional economic analysis is required to determine the optimum applicable span range. The system would also work well for pedestrian use, presenting a light and interesting appearance. Replacing the steel reinforcement with post-tensioning strand is one alternative which would extend the range of applicability of the system. The confinement provided by the steel tube would be of great value to this alternative.

The testing carried out was intended to determine the ultimate capacity of the system and investigate the failure mode. Additional testing to develop design criteria and the exploration of other limit states, such as fatigue, would be required prior to implementation.

Chapter

4 Self Stressing

Steel girder bridges often utilize continuity over the pier to reduce interior forces on the spans. In continuous spans, high negative moment can lead to cracking over the pier region. To alleviate this problem, a "self-stressing" system was developed, in which the center support is lowered after the slab has been poured and cured. An experimental investigation was performed to observe the behavior of this system. Time dependent effects and behavior of the system under the ultimate load were observed and analyzed. Based on the test results, the advantages and disadvantages of the system were addressed.

4.1 System Description

The system consisted of a continuous I-shape steel girder (W14x22) over two equal spans of 15'. A concrete slab was poured to act compositely with the steel girder. The center support was shimmed upward 0.3" above the elevation of the outer supports before the pouring of the concrete. In order to scale the effects of a larger section, additional weight was added to simulate the dead weight of a larger section. After the deck was poured and allowed to cure, the shim was released to create compression in the concrete. The creep in the deck was monitored for 100 days. Finally, an ultimate load test was performed by applying point loads in the middle of each span. Figure 4-1 shows the proposed system in the longitudinal direction.

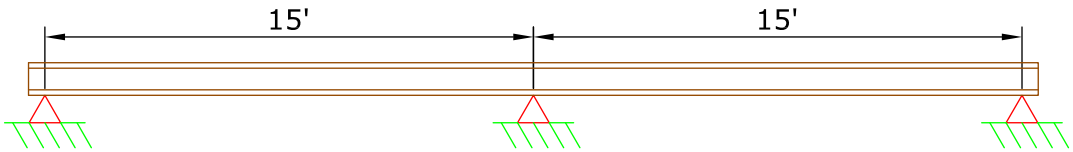

Figure 4-1: Specimen in Longitudinal Direction

The test specimen represents a ¼ scale model of a prototype structure. Since the simulation largely depends on self-weight gravity loading in order to maintain similitude, the density of the materials would need to be increased. This need can be demonstrated considering a simply supported beam with rectangular cross-section of width b and height h. The length of the beam is L and the unit weight is γ. The stress at the bottom of the beam at midspan can be found to be ¾ g L^2 / h. If the geometric parameters (L and h) are scaled by a factor α, the resulting stress is (α ¾ g L^2 / h), i.e. the stress has been scaled as well. In order to obtain the same stress levels, as is desired, the unit weight would need to be factored by $1/\alpha$. A similar result can be obtained for the actual structure.

Since it was impossible to alter the unit weight of the materials, ballast was added to the structure to obtain the desired correct stresses. These stresses were obtained from analysis of the full-sized prototype structure. A series of point ballasts were applied as a substitute for the more correct uniform ballast. The magnitude of the point loads were chosen to achieve the same stresses as would have been obtained from a uniform ballast.

Once the appropriate ballast loading had been calculated, the analysis of the structure was completed. Due to the lowering of the center support after the casting and hardening of the deck, the analysis of the specimen required an additional step in comparison with standard continuous girder bridges. To simulate the effect of the lowering action, an additional load effect had to be added to the specimen. This additional effect was quantified by using the effect of a downward point load at the center of a 30' span that would deflect the beam a distance downward equal to the shim distance.

The bottom flange stresses resulting from the different parts of the analysis can be seen in Figure 4-2. The first curve to observe is labeled continuous. This curve represents the stresses resulting from the self-weight of the beam (ballasted) considered continuous of the supports. The second curve to consider is labeled SS Point. As the shim is removed, the reaction at the center support is reduced. As the reaction is upwards, this reduction is equivalent to a downward point load. The effect on the stresses is therefore that which would result from the equivalent downward point load. This is labeled SS Point. Figure 4-2 shows the calculated stress in the bottom flange along the length of the beam. The final curve is the summation of the original continuous stresses and the point load stresses. Two curves are shown for this, the first being an idealized curve with continuous ballast (labelled final), and the second showing the results using the actual

point load ballasts. It is apparent that the ballast point loads were an effective substitute for a distributed ballast load.

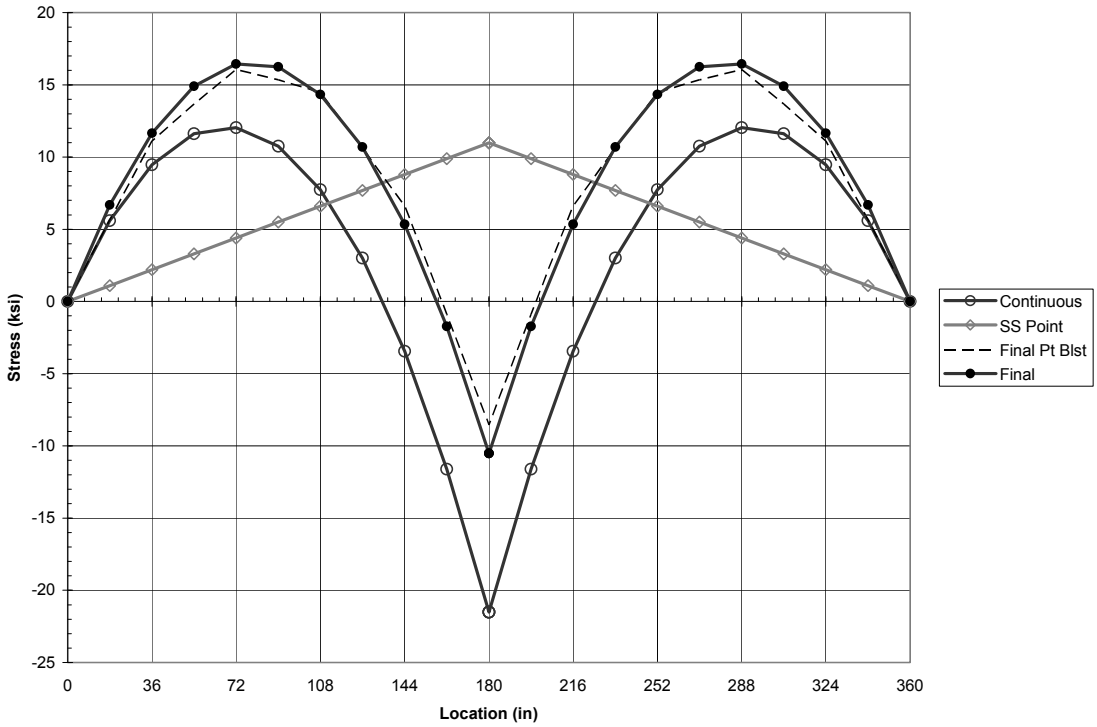

Figure 4-2: Results of structural analysis of the specimen, showing bottom flange stress

4.2 Test Specimen

The test specimen was built at the University of Nebraska-Lincoln Structures Laboratory in August 2005. Supports for the girder consisted of a 6' long W21x68 beam bolted to another concrete beam. The supports were post-tensioned to the strong floor to restrict movement. Lateral bracing was supplied at each support and at the loading points.

4.2.1 Construction Details

The composite section consisted of 4.5" thick, 30" wide concrete deck placed atop a continuous W22x14 steel girder. A constant haunch of 0.25" was also poured between the deck and gider. The longitudinal and transverse deck reinforcement consisted of #4 bars in the top and #3 bars in the

bottom, each at 12” spacing. Additional #5 bars were placed over the center support between the #3 bars in the top of the slab. Figure 4-3 shows the cross section of the specimen.

Two rows of shear studs were welded to the top flange to create composite action between the concrete deck and steel girder. The shear studs were spaced according to AASHTO LRFD provisions [1]. The total specimen can be seen in Figure 4-4.

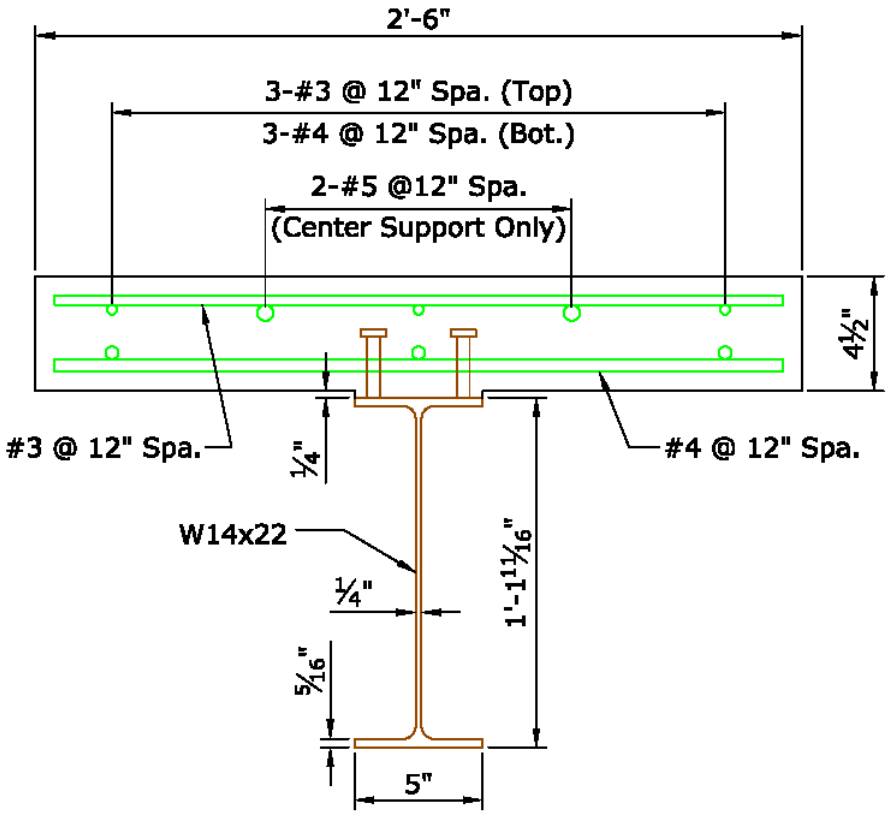

Figure 4-3: Specimen Cross Section

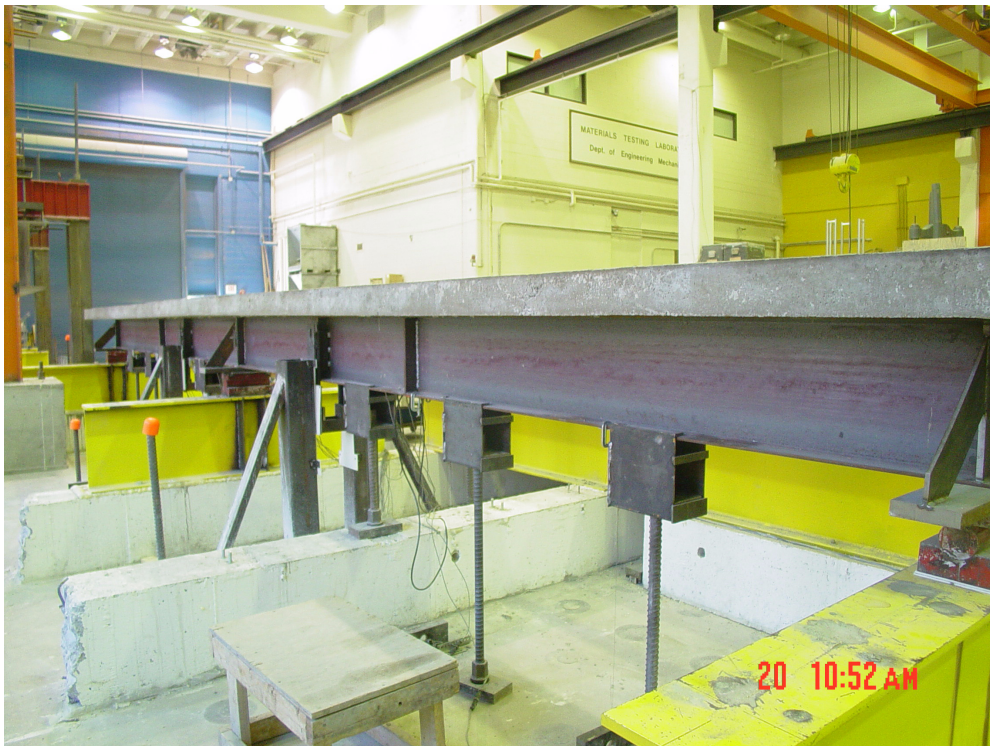

Figure 4-4: The Constructed Specimen

4.2.2 Material Properties

Concrete for the deck was specified to be 4000 psi and was supplied by a local ready-mix company. Four 6” x 12” conrete test cylinders were made according to ASTM C39-96 [6] procedures and cured in a similar fashion as the deck. The cylinders were tested at 14 and 28 days in which the average compressive strength was found to be 4580 psi and 5230 psi, respectively.

Steel samples were taken from the girder at locations of small strain. Coupons were tested according to ASTM E8-00b procedures. The average yield strength was 47.6 ksi and the average ultimate strength was 64 ksi. A plot of the testing data for a samples taken from the girder web is shown in

Figure 4-5 and the results from sample taken from the flange are shown in Figure 4-6..

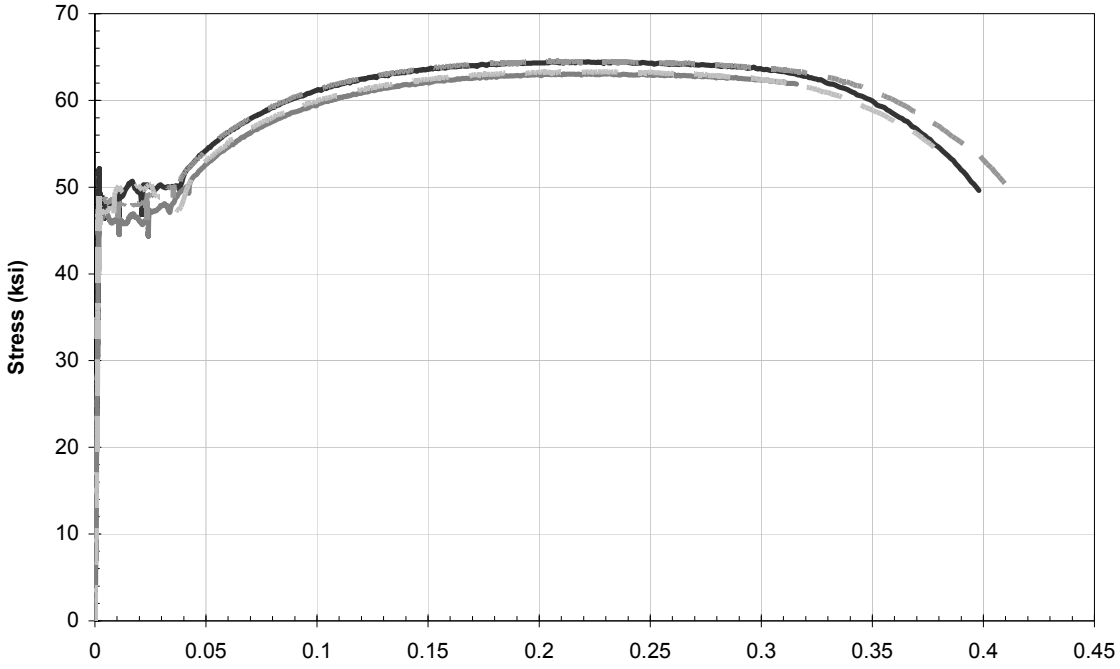

Figure 4-5: Stress-Strain plot for the samples taken from the girder web

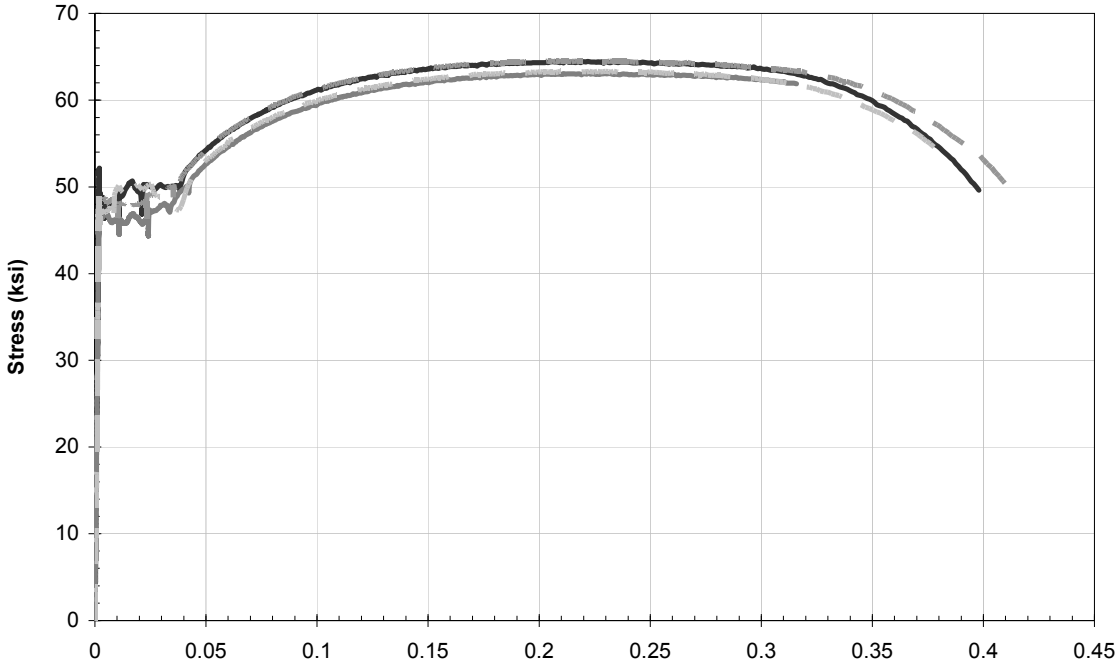

Figure 4-6: Stress-Strain plot for the samples taken from the girder flange

4.3 INSRUMENTATION

In order to measure strains and deflections at the various load stages, instrumentation was provided at several locations along the specimen.

Three different types of gages were used to measure strain on top of the deck, inside the deck and on the steel surface. The three types of strain gages used were spot-weldable vibrating wire gages, vibrating wire embedment gages and bondable electric strain gages.

The strain gages were arranged in two types of cross sections. Figure 4-7 shows the gage configuration for each type of section. The Type A Section consisted of 5 electric gages, 2 vibrating wire gages and 1 embedment gage. Electric gages were bonded to the bottom and top flanges as well as the middle of the web. Vibrating wire gages were located in the center of the top and bottom flanges. The embedment gage was located at 4" from the centerline of the girder. The Type B Section contained five electric gages only, in the same postions as those in the Type A Section.

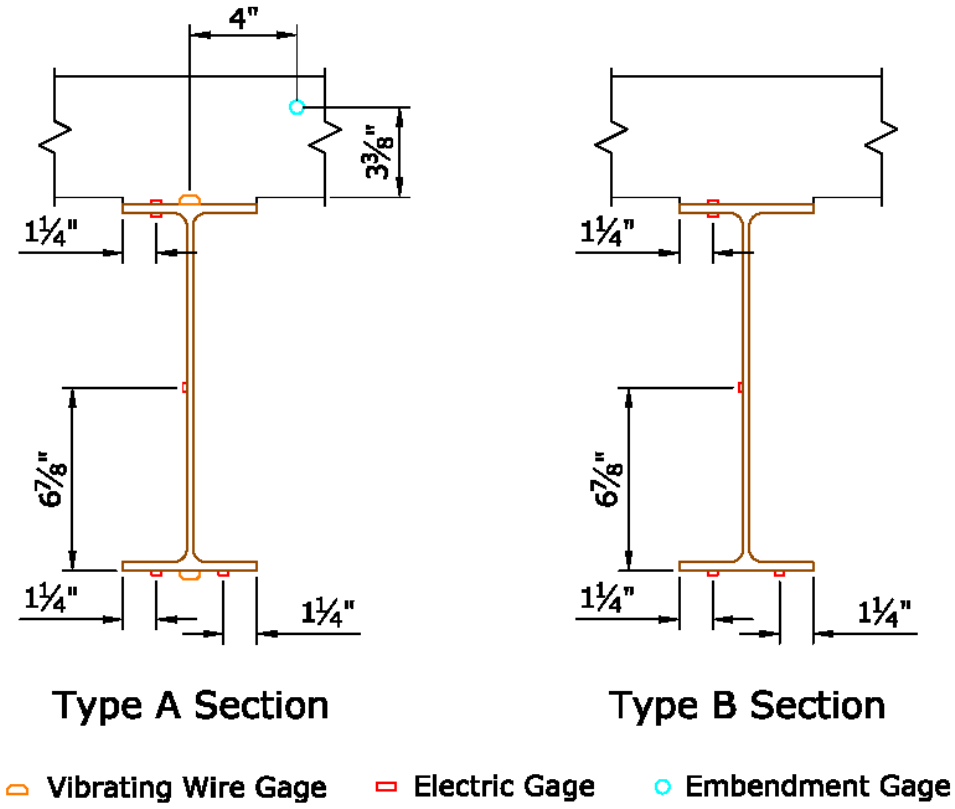

Figure 4-7: Strain Gage Configurations

The Type A Section was located at each midspan and just outside the center support. The Type B Section was located 2’ outside the center support of each span. Figure 4-8 shows the longitudinal locations of Type A and B Sections. The sections were labeled as shown in the figure. Figure 4-9 shows an electric gage, a vibrating wire gage and an embedment gage located at a Type A section.

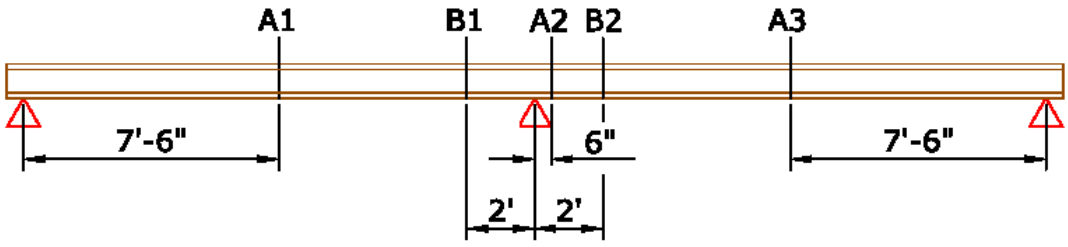

Figure 4-8: Gauge Sections

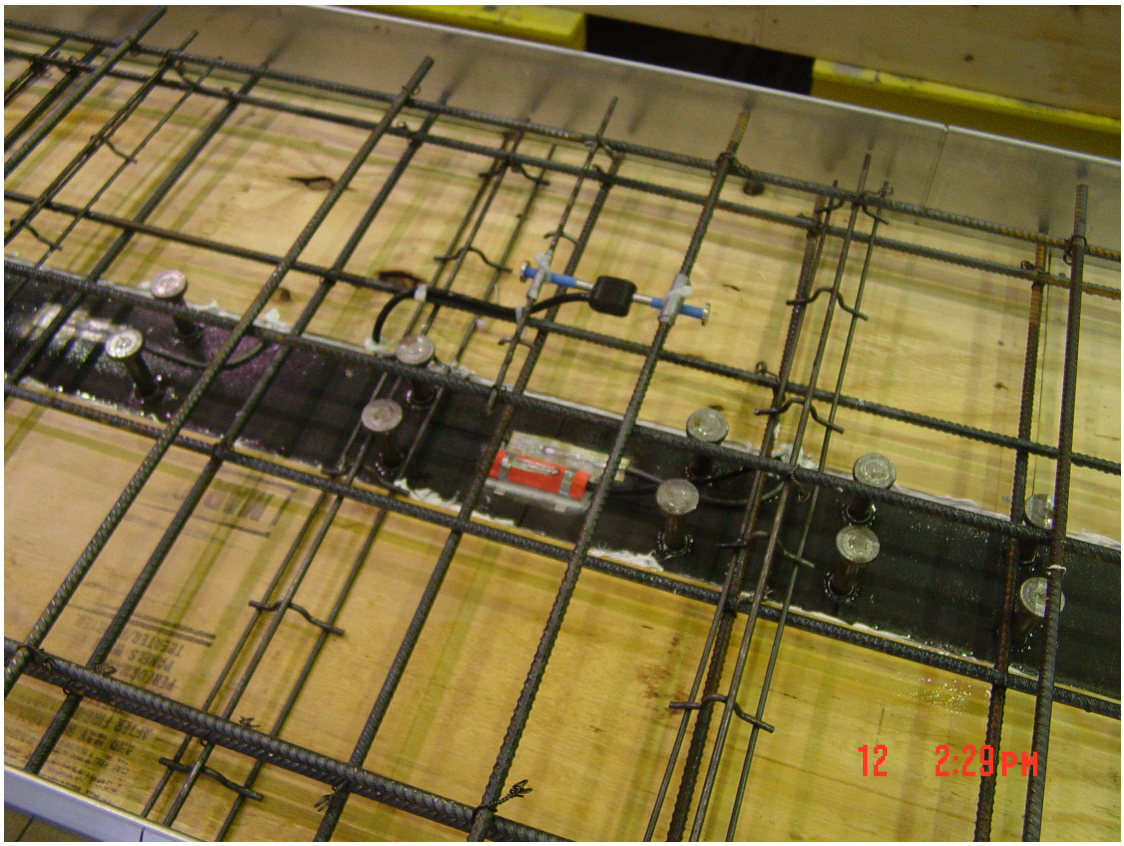

Figure 4-9: Gages Located at a Type A Section

Bondable electric strain gages were also located on the top of the slab at several locations. Gages were placed near each midspan, outside the pier on each span and over the center support. The placement of the bondable concrete gages is shown in Figure 4-10.

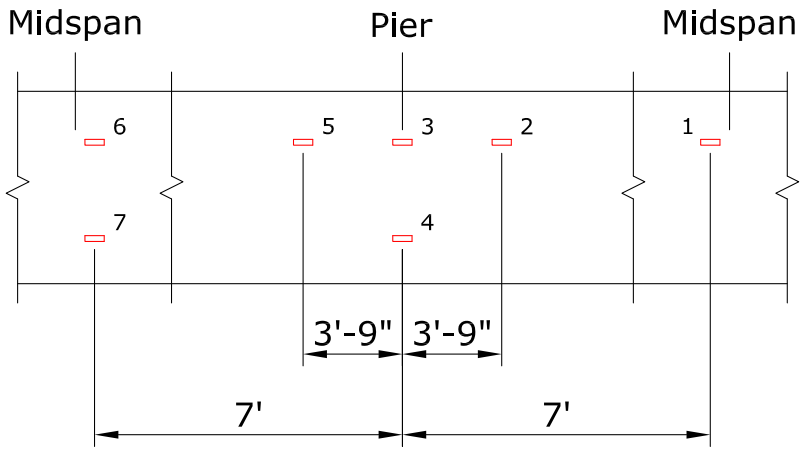

Figure 4-10: Concrete Gages

Deflections were measured with string potentiometers (pots) at the quarter points of each span as indicated in Figure 4-11. The six pots were labeled as shown in the figure.

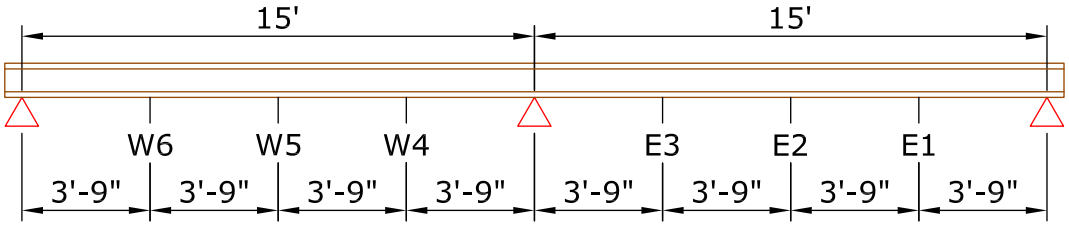

Figure 4-11: Pot Locations

4.4 Loading Sequence and Results

Load was applied to the specimen in four distinct phases at four different times. The total experiment progressed as follows:

-Ballast load applied at points along the length of each span.

-Deck cast along the entire length of the specimen.

-Following the hardening of the slab, the center support was lowered to the elevation of the exterior supports.

-Ultimate load test performed 100 days after support lowering

Details of the application of these loads and the resulting specimen responses are given below.

4.4.1 PHASE I LOADING

The first loading phase was the ballast load, which was added to the system to scale the effects of the dead weight to simulate a larger section. The ballast was designed such that the resulting stress in the steel (due to non-composite dead loads) was the same as it would have been in a full-scale specimen. Ideally, a uniform ballast would have been used. As this was not technically feasible, a series of point loads was specified such that the resulting bending moment diagram matched as closely as possible to what would have been obtained with a uniform load.

The ballast load consisted of point loads every three feet along each span, as indicated in Figure 4-12. This came to a total of 36.5 kips. The result of applying the ballast load provided a tensile stress in the top of the flange over the pier of 13.9 ksi.

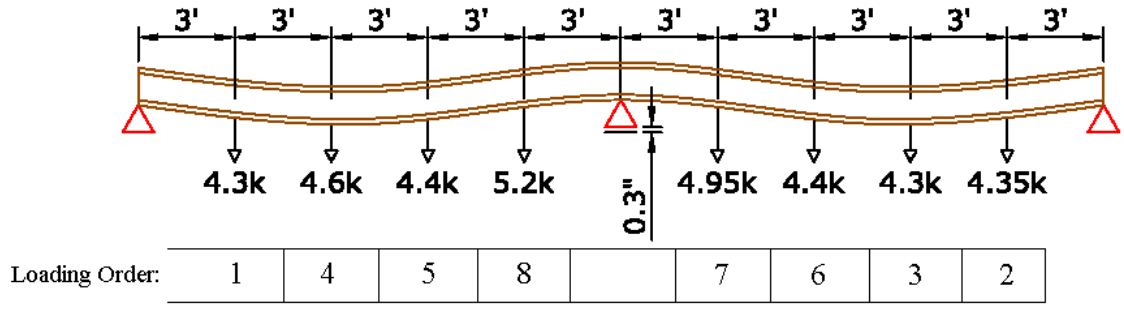

Figure 4-12: Ballast Load

Figures 4-13 through 4-17 show the development of strain throughout the ballast loading of the specimen. Each figure shows the data from strain gages at a particular section of the beam. The location of the sections can be found in Figure 4-8. Each set of data in each figure is associated with a particular gage. The location of the gage on the section is denoted by a set

of abbreviations. Those abbreviations refer to Top of Top Flange, Bottom of Top Flange, Web, South side of Bottom of Bottom Flange, and North side of Bottom of Bottom Flange.

Figures 4-18 and 4-19 show the effect that each of the ballast loads had on the strains of the top and bottom flange, respectively. The eight concentrated loads were applied in the order indicated at the bottom of Figure 4-12. Each set of data in Figures 4-18 and 4-19 shows the strain along the span due to the indicated concentrated load. Figures 4-20 and 4-21 show the stresses corresponding to the ballast-load strains for the top and bottom flange, respectively. Deflections were also measured during the ballast-loading portion of the test. Figure 4-22 shows the deflection at the quarter points as the ballast load was applied.

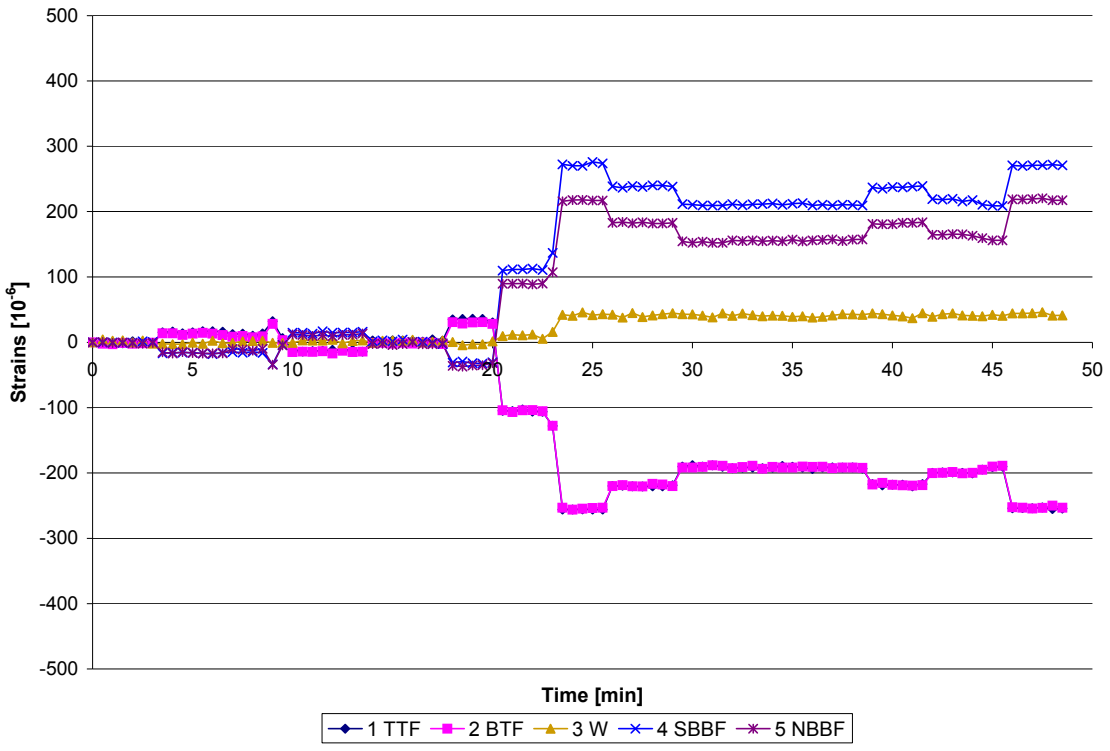

Figure 4-13: Development of strains in steel girder during ballast loading - Section A3

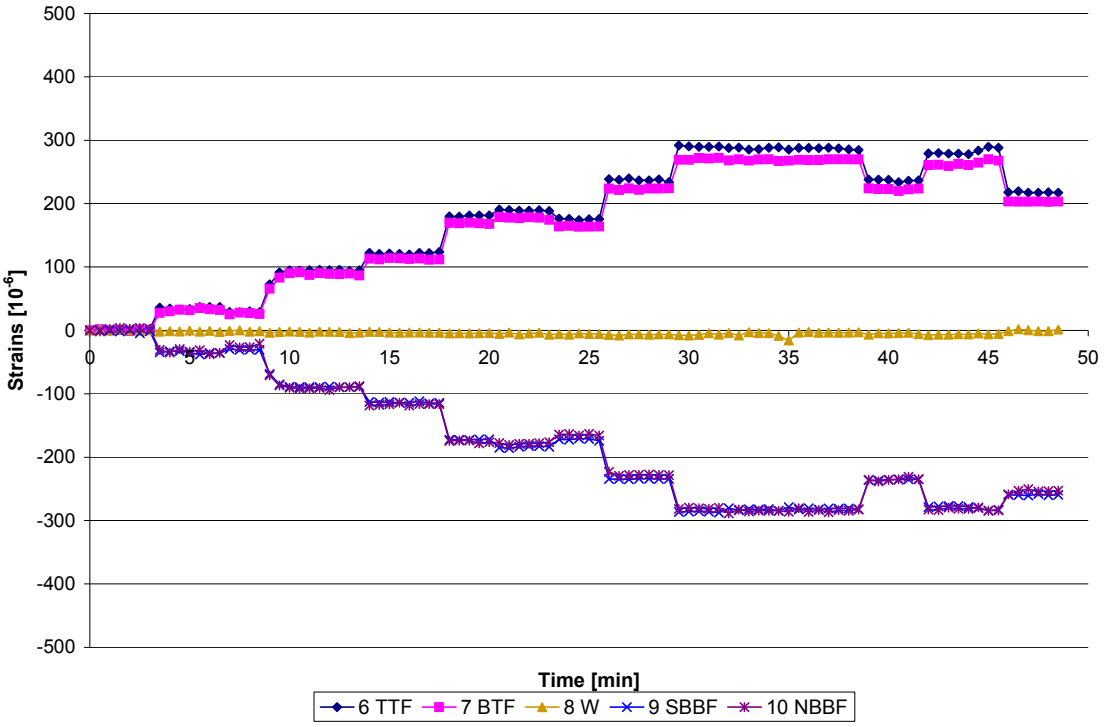

Figure 4-14: Development of strains in steel girder during ballast loading - Section B2

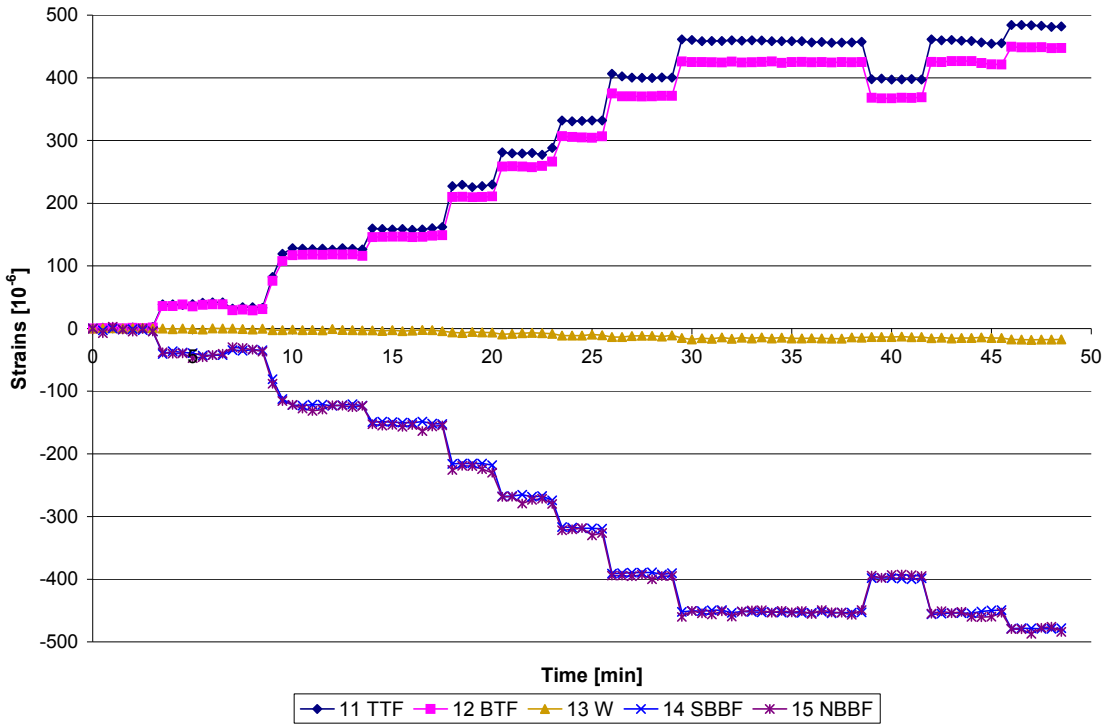

Figure 4-15: Development of strains in steel girder during ballast loading - Section A2

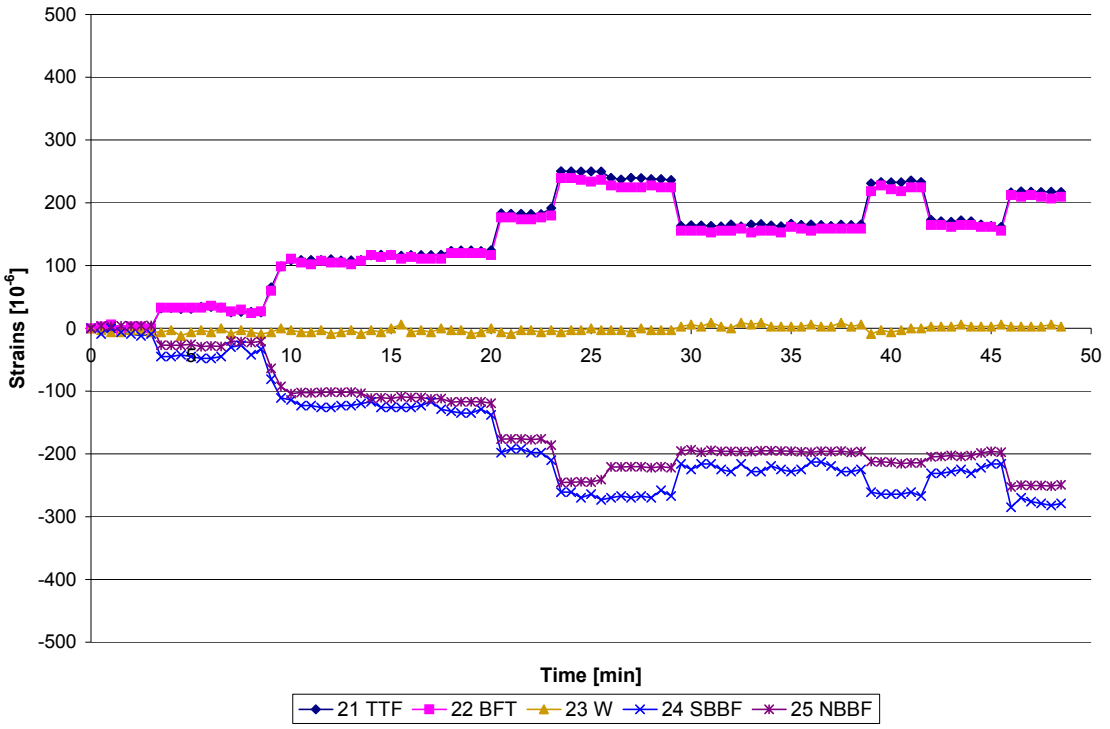

Figure 4-16: Development of strains in steel girder during ballast loading - Section B1

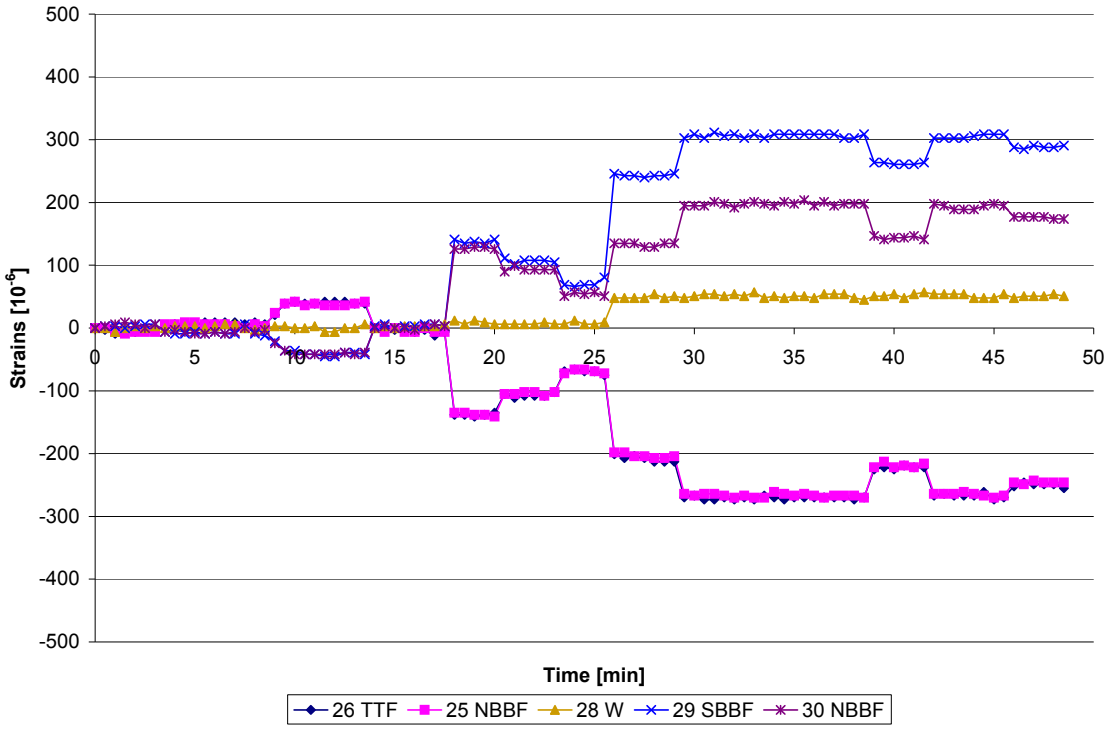

Figure 4-17: Development of strains in steel girder during ballast loading - Section A1

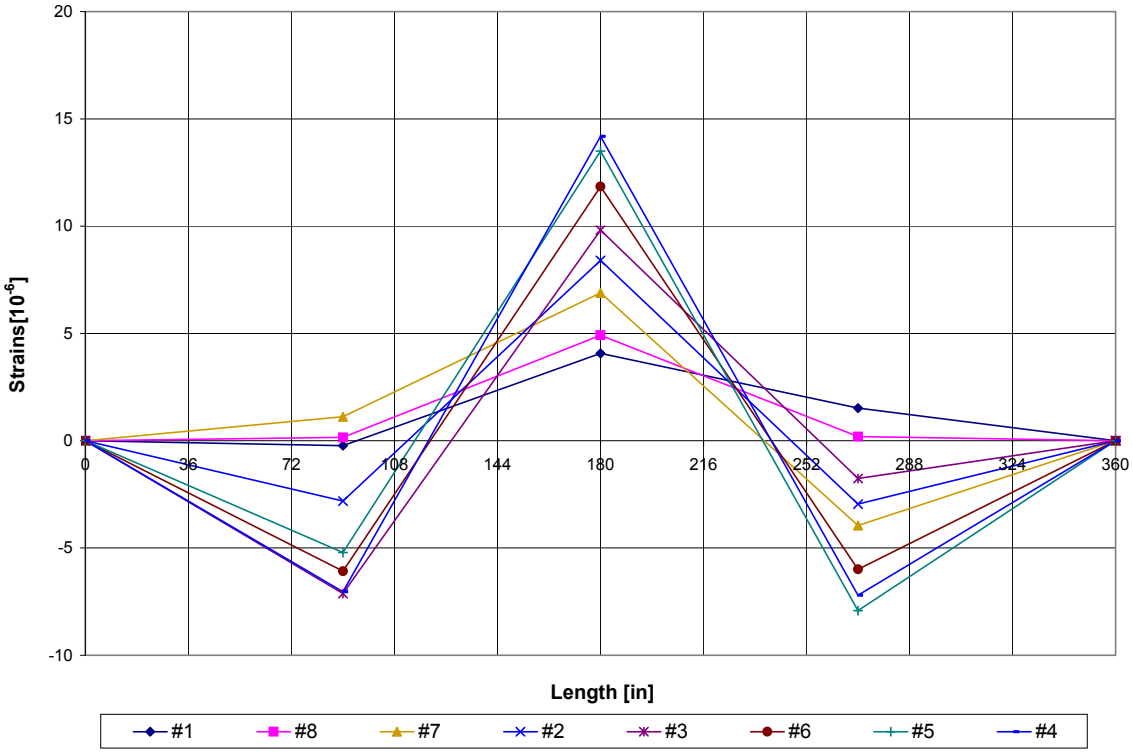

Figure 4-18: Strain along the length of the top flange of the steel girder during the ballast loading

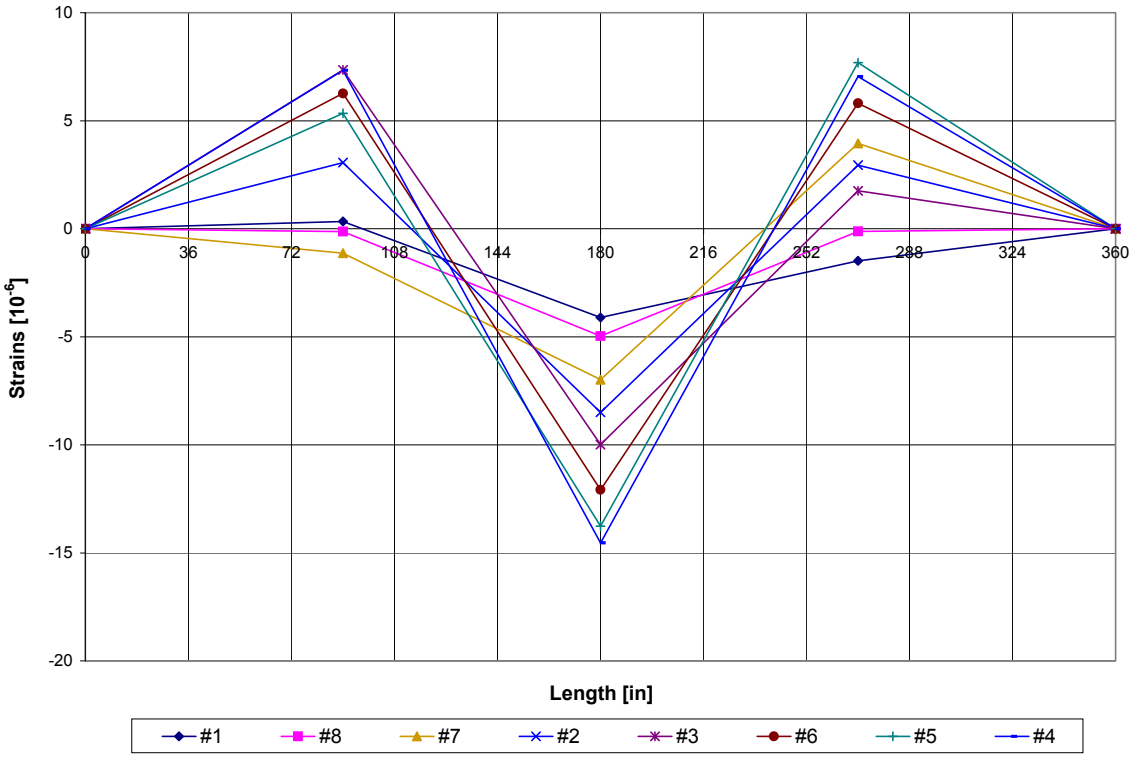

Figure 4-19: Strain along the length of the bottom flange of the steel girder during the ballast loading

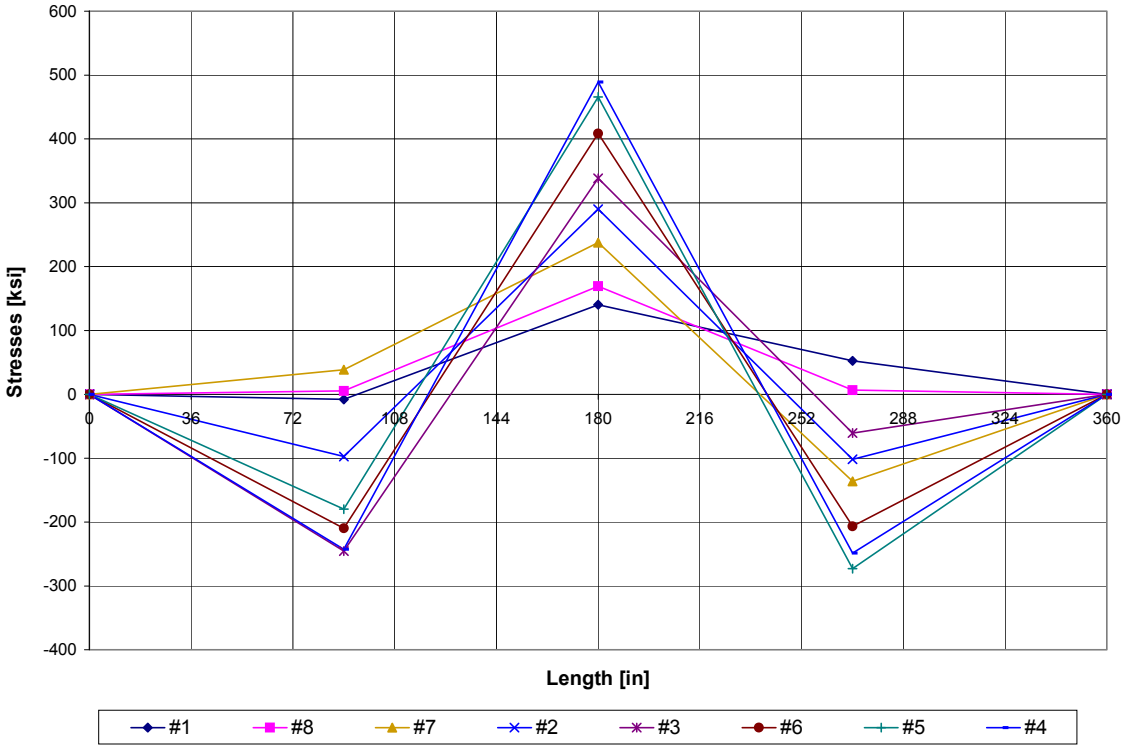

Figure 4-20: Stress along the length of the top flange of the steel girder during the ballast loading

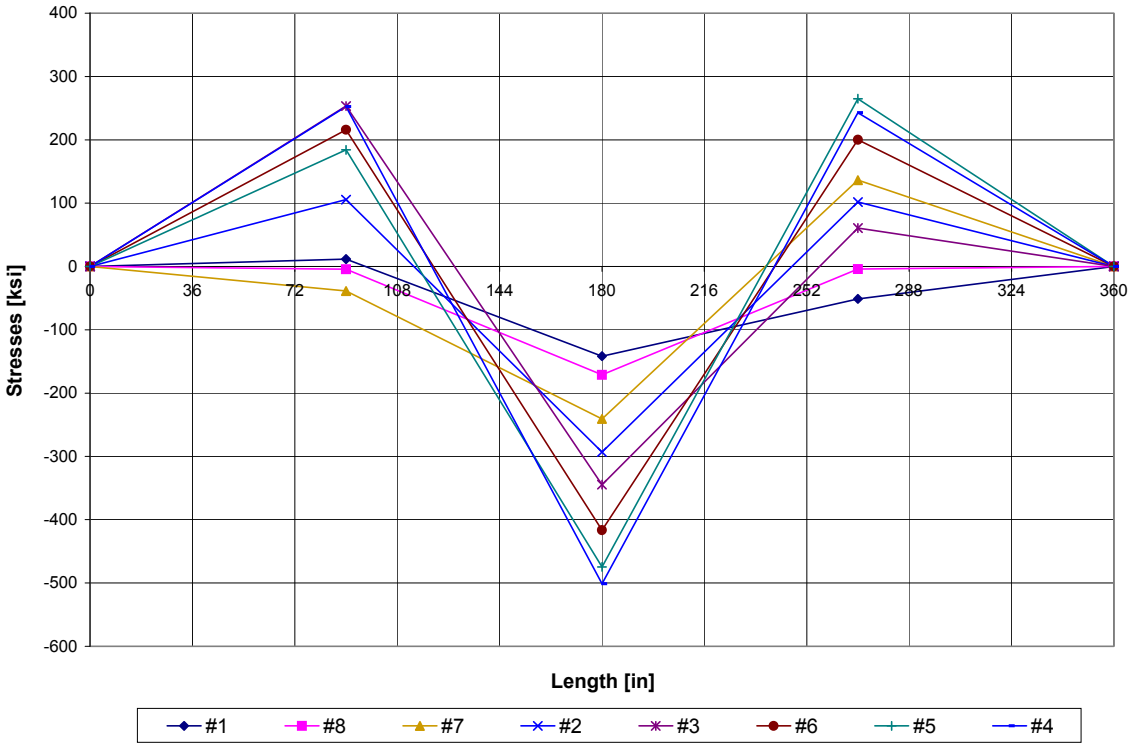

Figure 4-21: Stress along the length of the bottom flange of the steel girder during the ballast loading

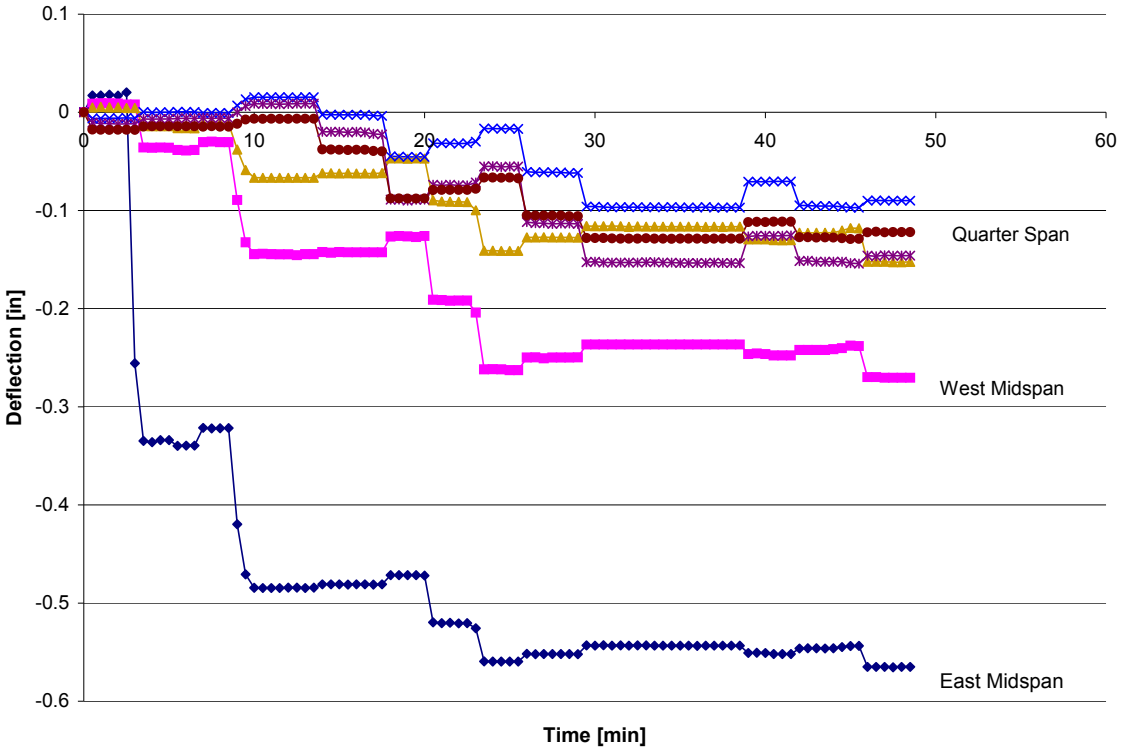

Figure 4-22: Deflection of the steel girder during balast loading

4.4.2 PHASE II LOADING

The next loading phase was the application of the wet slab. At the time of the deck pour, the center support was still displaced upward by 0.3”. The result of applying the slab load provided additional tensile stress in the top of the flange at the pier of 1.36 ksi. Figure 4-23 shows load due to the wet slab.

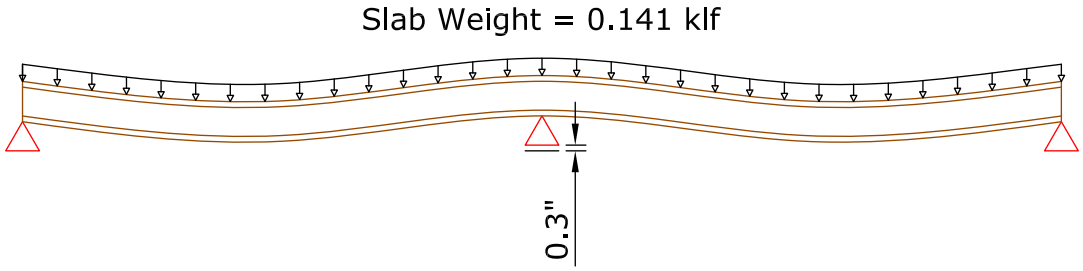

Figure 4-23: Wet Slab Load

Using the same gages as for the ballast loading, strains at each instrumented section were recorded. This data can be found in Figures 4-24

through 4-28. The location of the sections can be found again in Figure 4-8. The deflection at the middle of the west span during the casting of the deck was also recorded. These values can be found in Figure 4-29.

For the eight days following the casting of the slab, readings were completed to find the stress in the girder flanges due to the concentrated ballast loads and the distributed deck load. For these readings, the embedment gages were also used to find the strain in the concrete. Figure 4-30 shows how the stress varied along the length of the girder flanges. The stress along the length of the deck slab can be found in Figure 4-31.

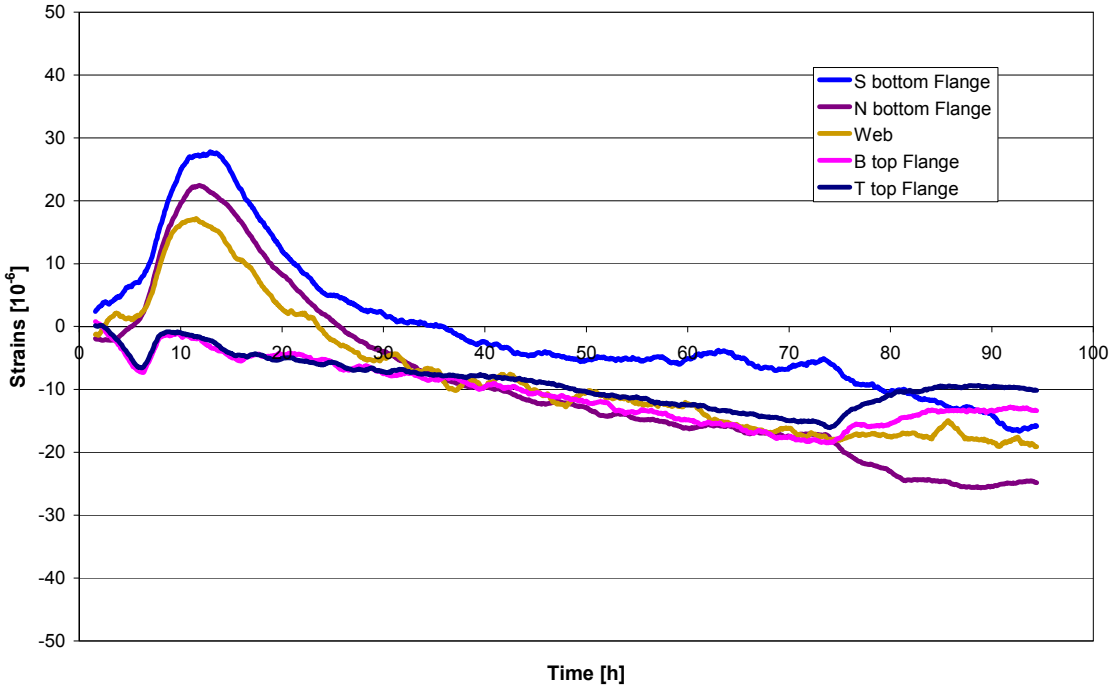

Figure 4-24: Development of strains in the steel girder during the casting of the slab - Section A3

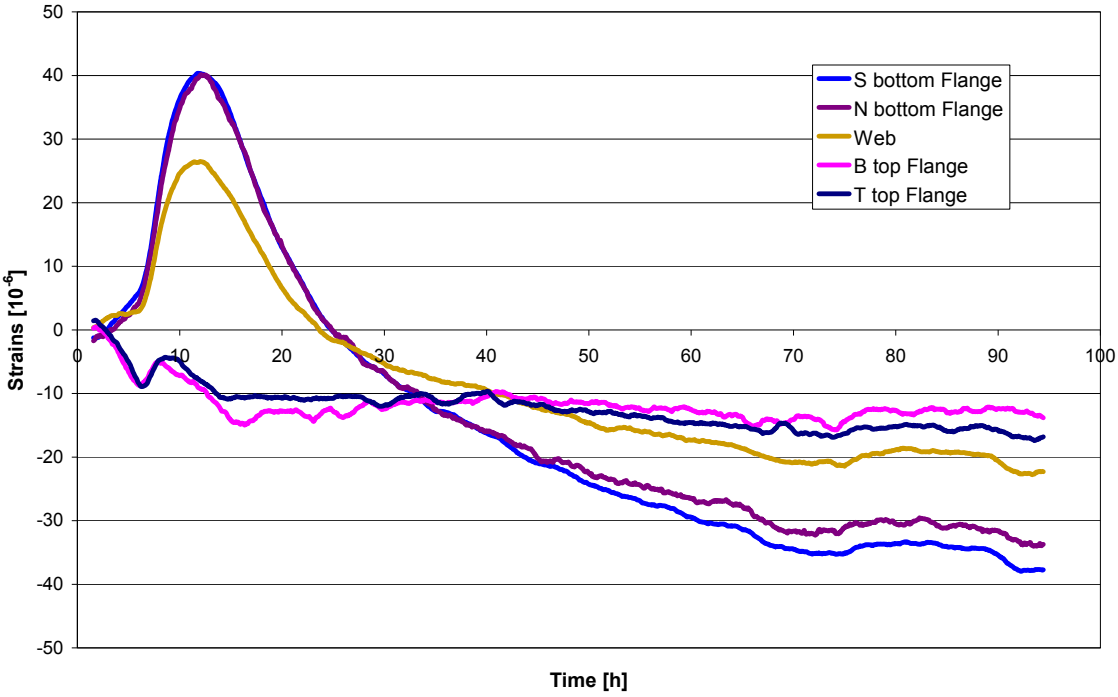

Figure 4-25: Development of strains in the steel girder during the casting of the slab - Section B2

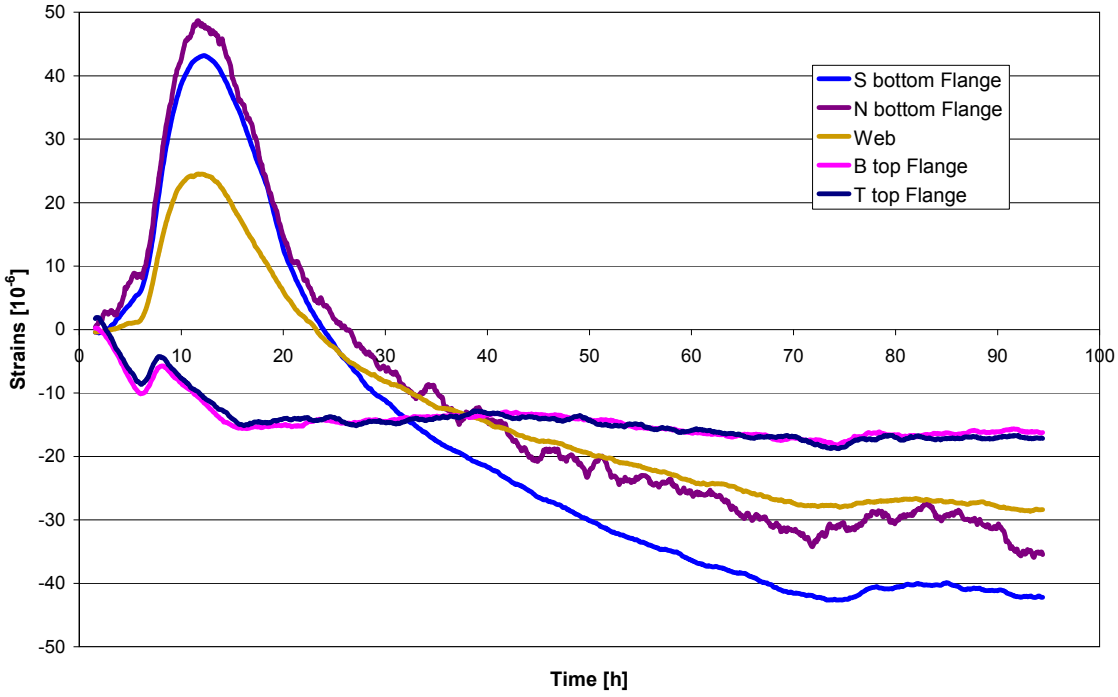

Figure 4-26: Development of strains in the steel girder during the casting of the slab - Section A2

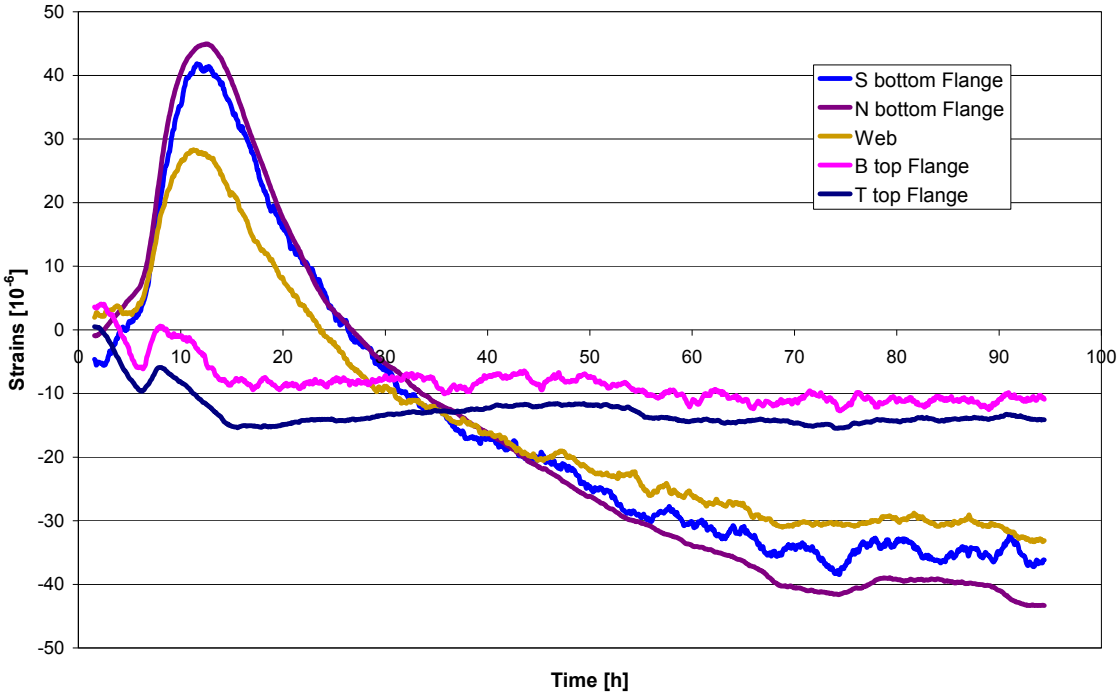

Figure 4-27: Development of strains in the steel girder during the casting of the slab - Section B1

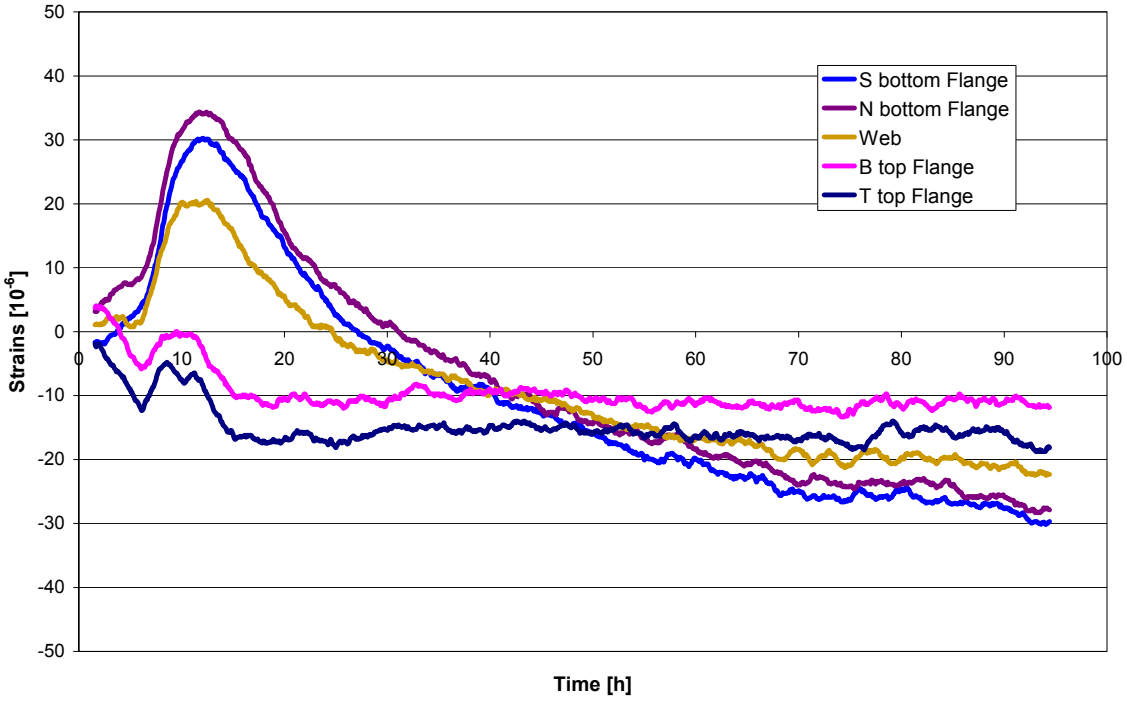

Figure 4-28: Development of strains in the steel girder during the casting of the slab - Section A1

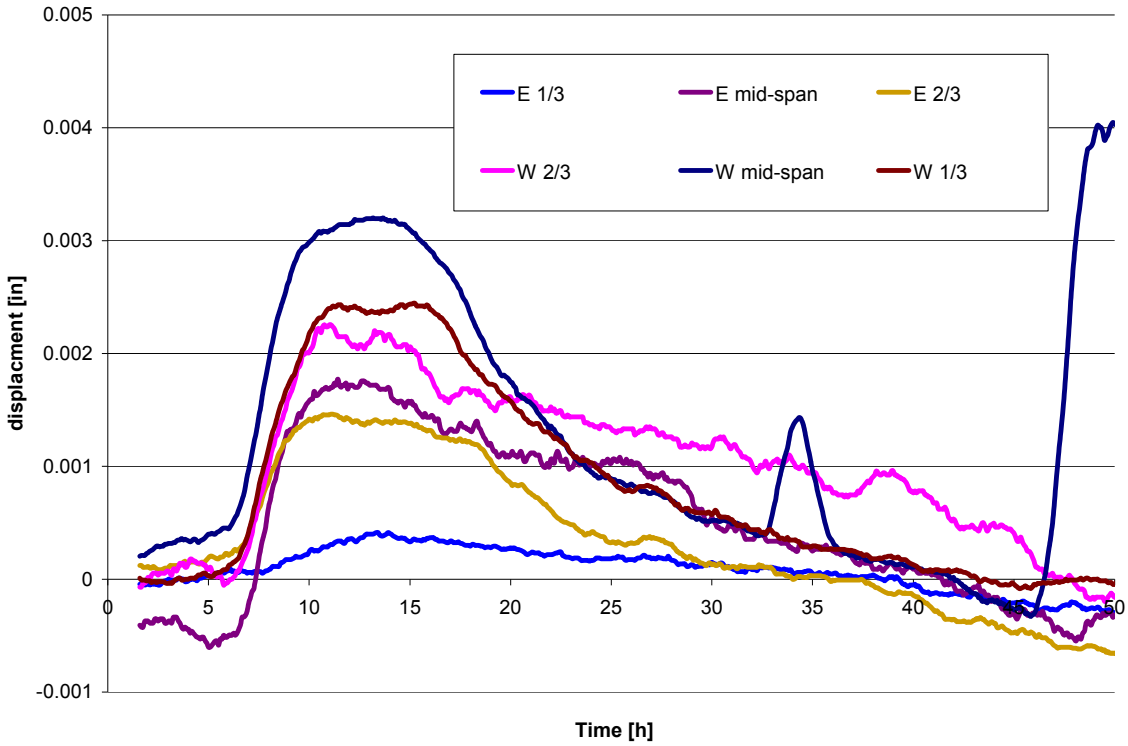

Figure 4-29: Vertical displacement of the steel girder during the casting of the slab - Section A1

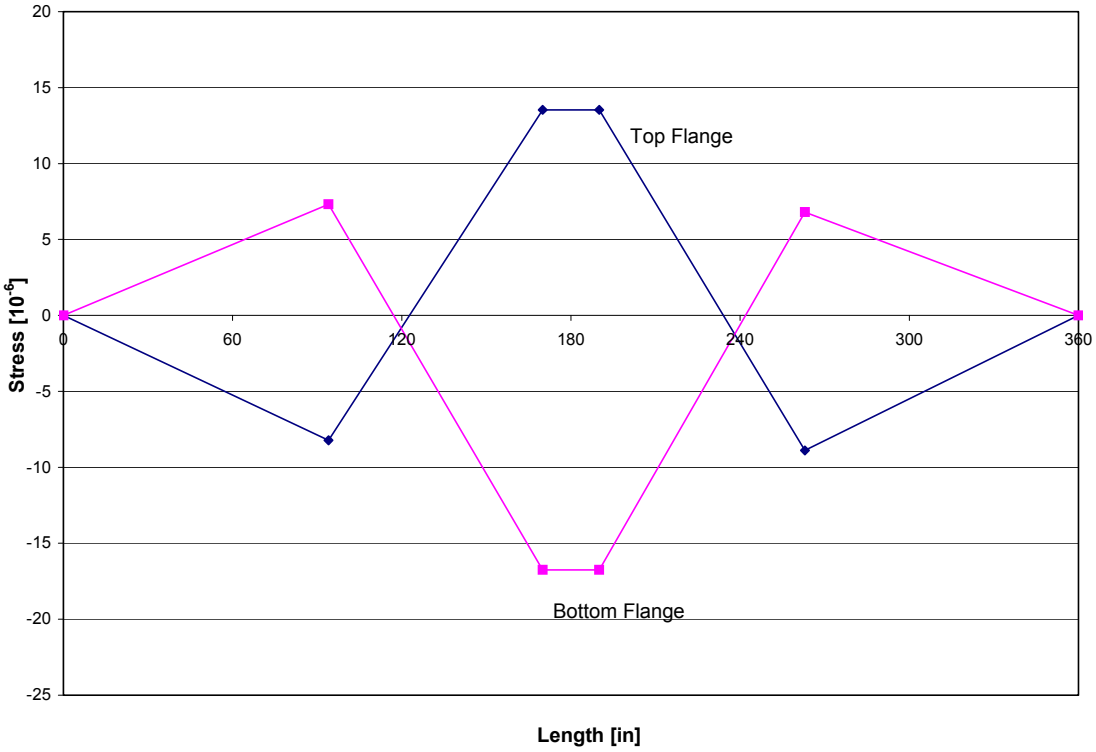

Figure 4-30: Stresses in the girder flanges eight days after casting the slab

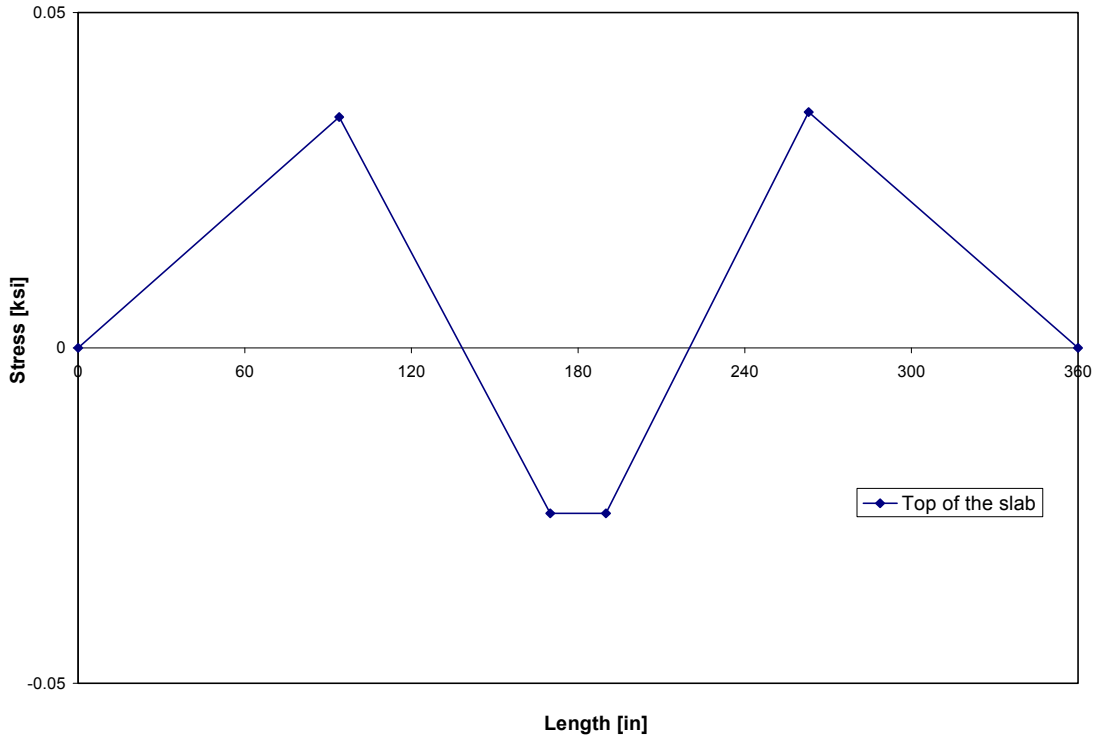

Figure 4-31: Stresses in the top of the concrete slab eight days after the casting of the deck

4.4.3 PHASE III LOADING

The third loading phase was the lowering of the center support, which was equivalent to applying a concentrated load at that point. At this time, the concrete had been allowed to cure for 28 days. The result of applying the displacement at the interior support was a compressive stress in the top of the deck at the pier of 480 psi, very close to the targeted stress of 500 psi.

4-32 shows the stress at the top and bottom of the slab due to the downward displacement of the center support, as shown in Figure 4-33.

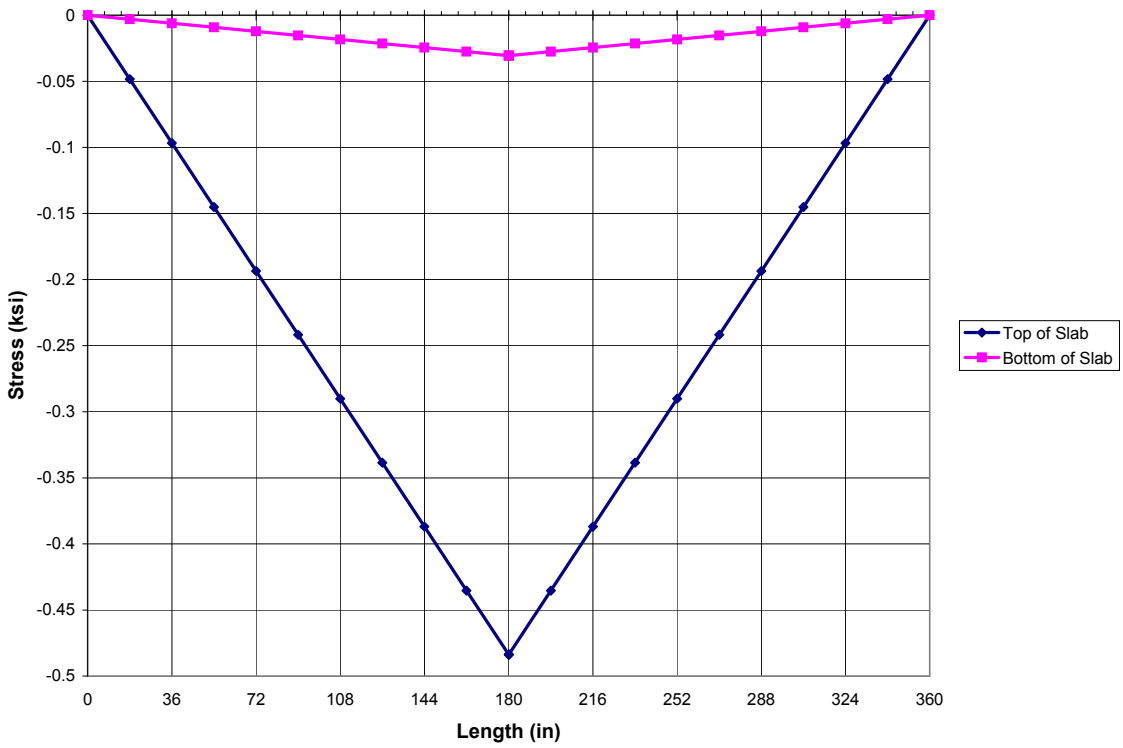

Figure 4-32: Stresses in the top and bottom of the slab after the lowering of the center support

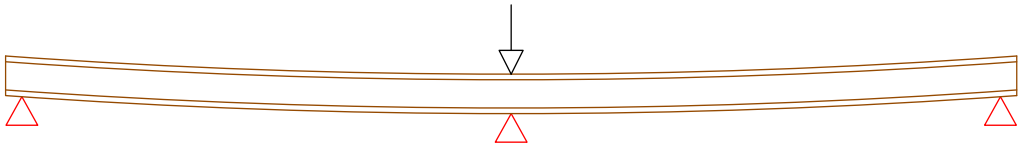

Figure 4-33: Center Support Displacement Load

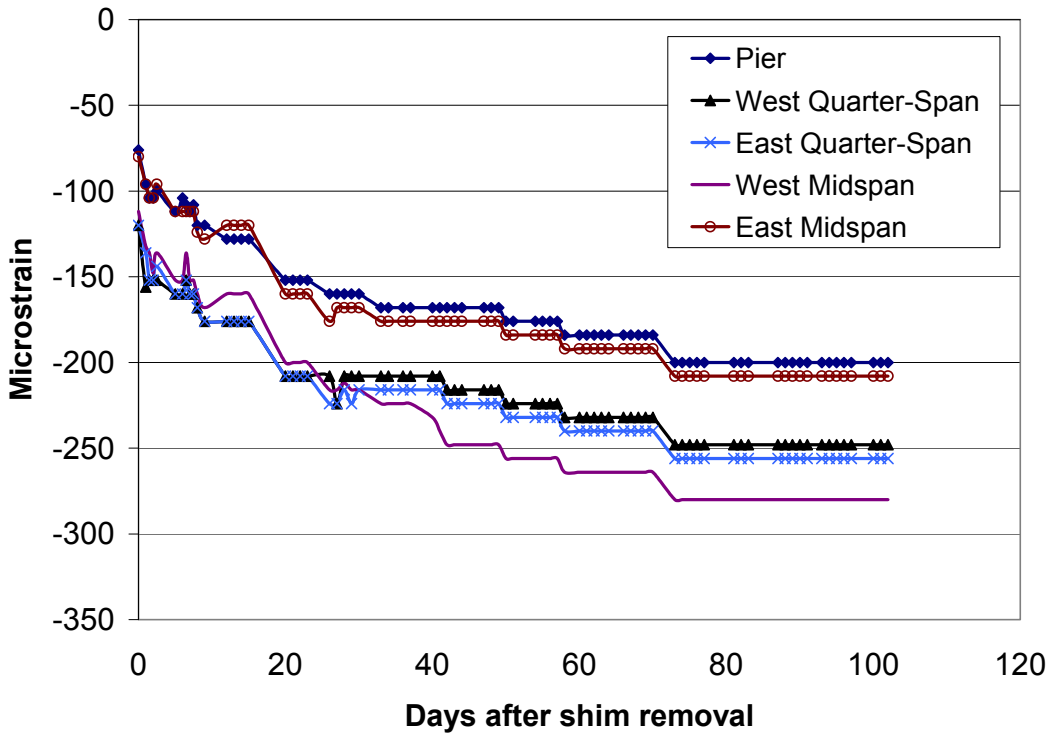

Figure 4-34: Ultimate Load

For approximately 100 days following the lowering of the middle support, strain readings were taken on the surface of the concrete deck. Figure 4-34 shows these strain readings beginning with the strain read immediately following the removal of the shim. It can then be seen that the deck underwent additional compressive strains due to the creep of the concrete. From the shape of the curves, it can be seen that the additional strain due to creep increased by smaller amounts as time passed.

4.4.4 Phase IV Loading

After the center support had been lowered and the concrete had been allowed to cure for 100 days, the Phase IV loading was completed. This phase was the ultimate load test. Point loads were applied at the each mid-

span for the ultimalte load test. Figure 4-35 shows displacement of the specimen due to ultimate load.

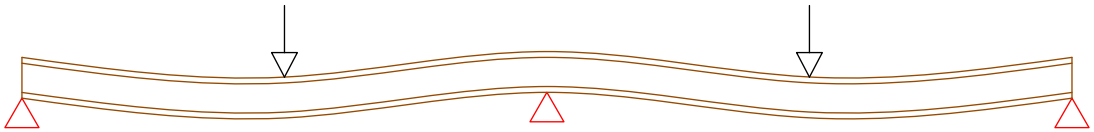

Figure 4-35: Ultimate Load

Figure 4-36 shows the observed load-deflection curve obtained from testing of the beam. The load-deflection response of the system was nearly linear until a deflection of approximately 0.25 inches, which corresponded to an applied load of 55 kips. The unloading of the system seen in Figure 4-36 at about 60 kips was done to correct the loading frame. After correction the loading was resumed. At 72 kips, yielding of the web occured near the pier. This corresponded to a deflection of 1.1 inches at midspan. It can also be seen in Figure 4-36 that the specimen exhibited a sufficient amount of ductility.

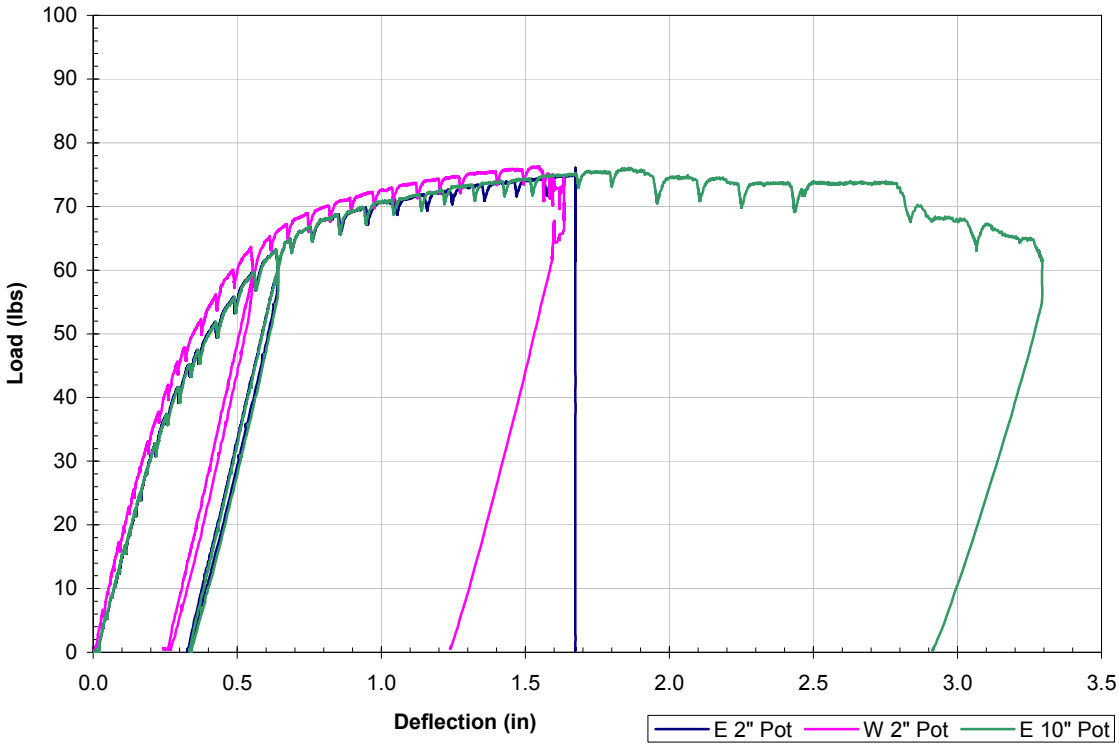

Figure 4-36: Load-Deflection curve during the ultimate load test.

There were very few observable events prior to the reaching of ultimate load. At a load of 65 kips the transverse crack pattern was first observed. The load ceased to increase after reaching 75 kips, at which point the vertical deflection at the middle of the east span was 1.65 inches. The deflection continued to increase with no increase in load until crushing was observed at the top of the deck. Beyond this point, the specimen was able to absorb additional deflection, but at a reduced level of loading. The maximum deflection at the end of the test was approximately 3.25 inches at midspan. The observed ultimate load was slightly lower than the predicted failure load of 81 kips. This can likely be attributed to the fact that design calculations were made assuming a yield strength of 50 ksi. The material testing showed that the actual yield strength of the beam was slightly lower at 47.6 ksi.

Figures 4-37 through 4-41 show the load versus strain relationship during the load test at the five previously discussed instrumented sections. It is important to note that the segment of data observed during the unloading and reloading has been omitted from these plots. The specimen was still in the elastic range at the time of unloading, which can be seen in the load-deflection curve shown in Figure4-36. These data were removed from the figures for clarity.

Figure 4-37 shows the behavior at the midspan section in the east span. The web and bottom flange gauges show the expected behavior, with a distinct linear range followed by quickly increasing strains until the failure of the gauges. The top flange gauge shows periods of both tensile and compressive strains, possibly because of the movement of the neutral axis in this region of the girder. In Figure 4-41, the gauges located on the midspan section of the west span also show the expected behavior with a slightly better result from the concrete gauge. The top flange gauge did not show both tensile and compressive strains as in the west span. Figure 4-43 shows the vertical strain profile at the west midspan section. The profile is shown for varying levels of load up to very near the ultimate load. It can be seen that the neutral axis loacation remained constant and the strain remained linear throughout the entire range of loading.

Interesting behavior was observed from the gauges at sections B1 and B2, as can be seen in Figures 4-38 and 4-40. The bottom flange gauges in Figure 4-40 best show this behavior, initially reading compressive strains and finally reading tensile strains. The explanation for these readings lies in the location of the section instrumented. At the beginning of the ultimate load test, the section was subjected to a negative moment, inducing compression in the bottom flange. As the loading increased, a plastic hinge eventually formed near the pier. After the forming of the hinge, the additional load acted on the now simple-supported span, subjecting the instrumented section to a positive moment, which eventually outweighed the negative

moment applied by the plastic hinge and resulted in a net positive moment effect at high levels of load. Thus, the bottom flange was subjected to tensile strains at the ultimate load. This can be seen in Figure 4-44 which shows the strains in the vertical profile. It can be seen that as the load nears ultimate the magnitudes of the strains begin to decrease, with the exception of the web, which reads increasing tensile strain. This is likely due to out of plane movement, however cannot be confirmed due to the lack of a companion gauge on the other face of the web. It can be seen that the bottom flange strain actually begins to be subjected to tensile strains, although the top flange strain remains positive.

Figure 4-39 shows the load-strain plot for the instrumented section at the pier. The observed behavior was mostly as expected, with the exception of the bottom flange. The south side of the bottom flange showed a linear relation followed by large compressive strains near the ultimate load, but slightly different behavior was demonstrated by the north side of the bottom flange. When the specimen began approaching the ultimate load, this part of the bottom flange was observed to begin twisting. The gauge reflects this behavior, showing that the increase of compressive strains was inhibited by the twisting deformation. The top flange experienced both compressive and tensile strains because of its location in relation to the changing neutral axis. The web gauge showed the expected linear behavior under compressive strains until the loading approached ultimate at which point the gauge failed. Figure 4-42 shows the load-strain relation for the top of the slab at the center of each span. Other gauges attached to the top of the slab existed, but quickly failed during the ultimate testing due to the cracking of the slab.

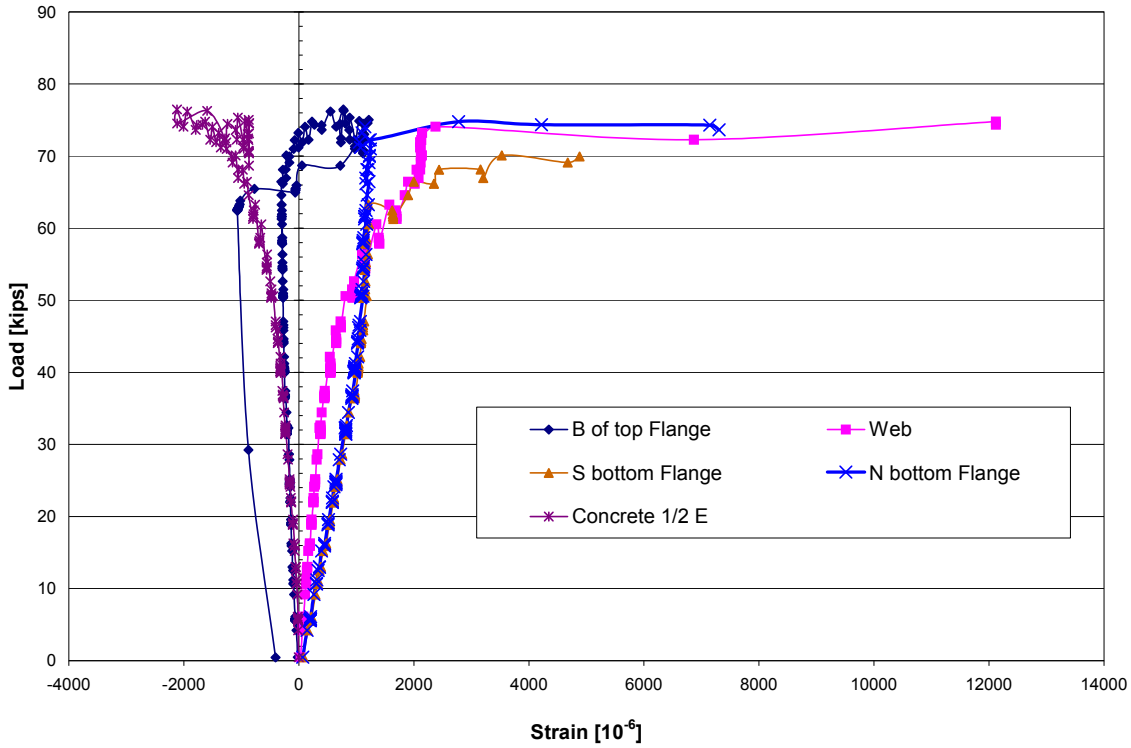

Figure 4-37: Strain development during the ultimate load test - Section A3

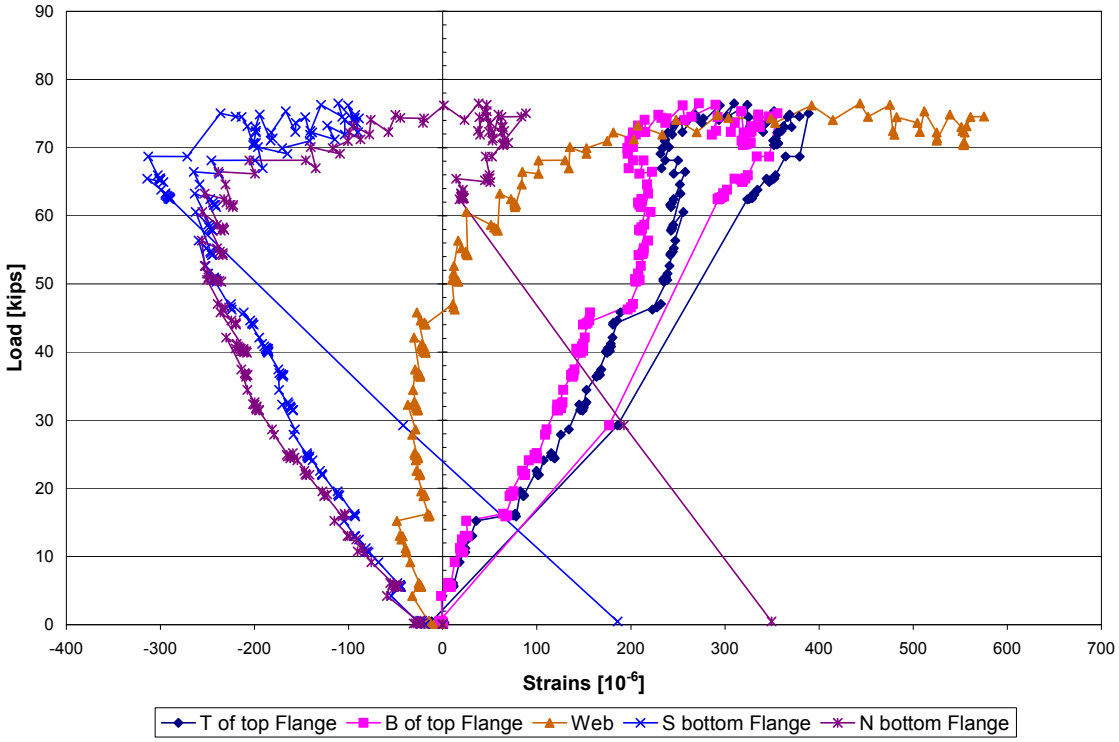

Figure 4-38: Strain development during the ultimate load test - Section B2

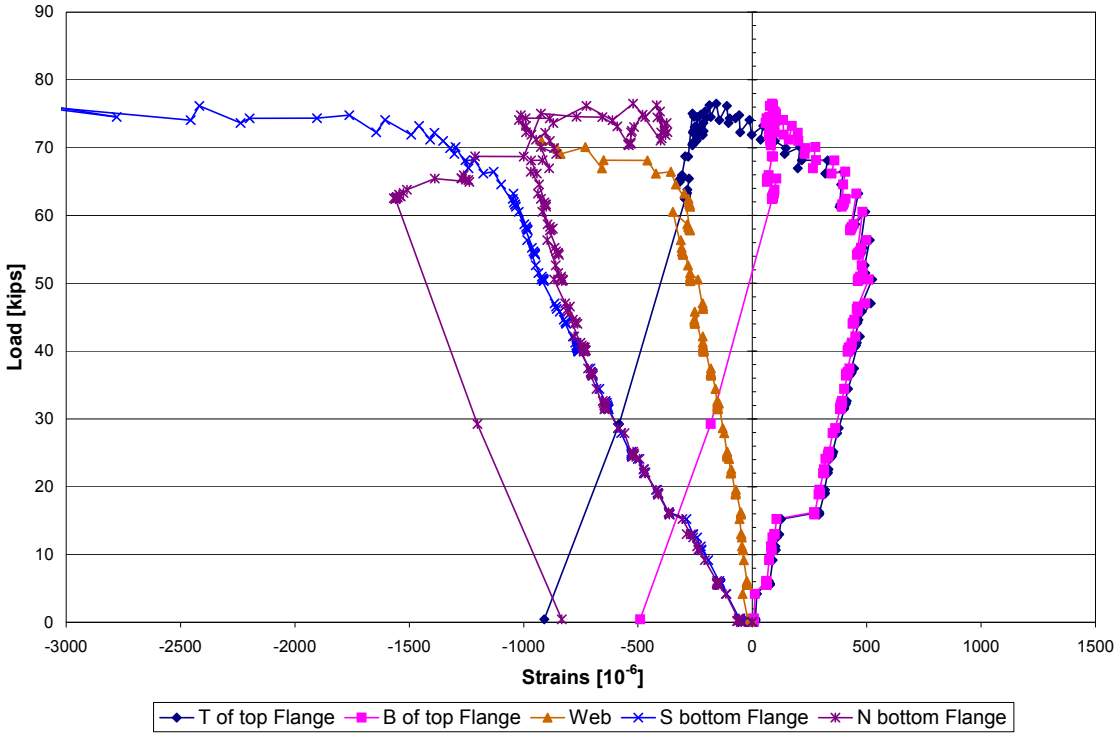

Figure 4-39: Strain development during the ultimate load test - Section A2

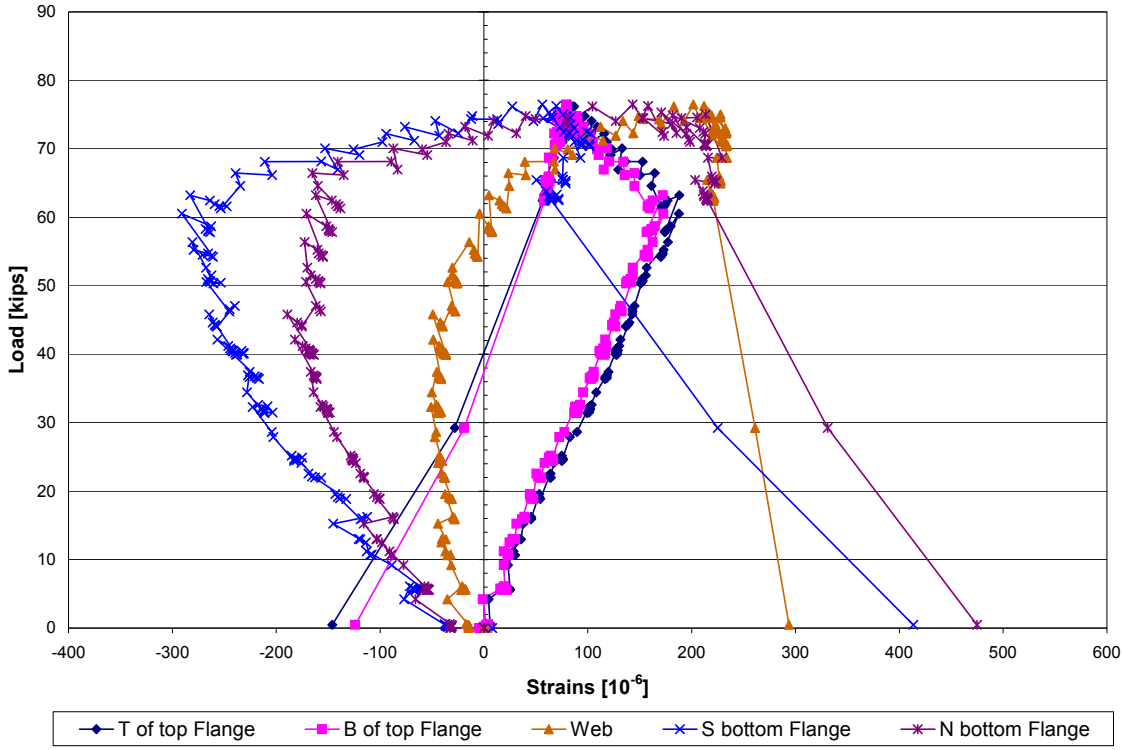

Figure 4-40: Strain development during the ultimate load test - Section B1

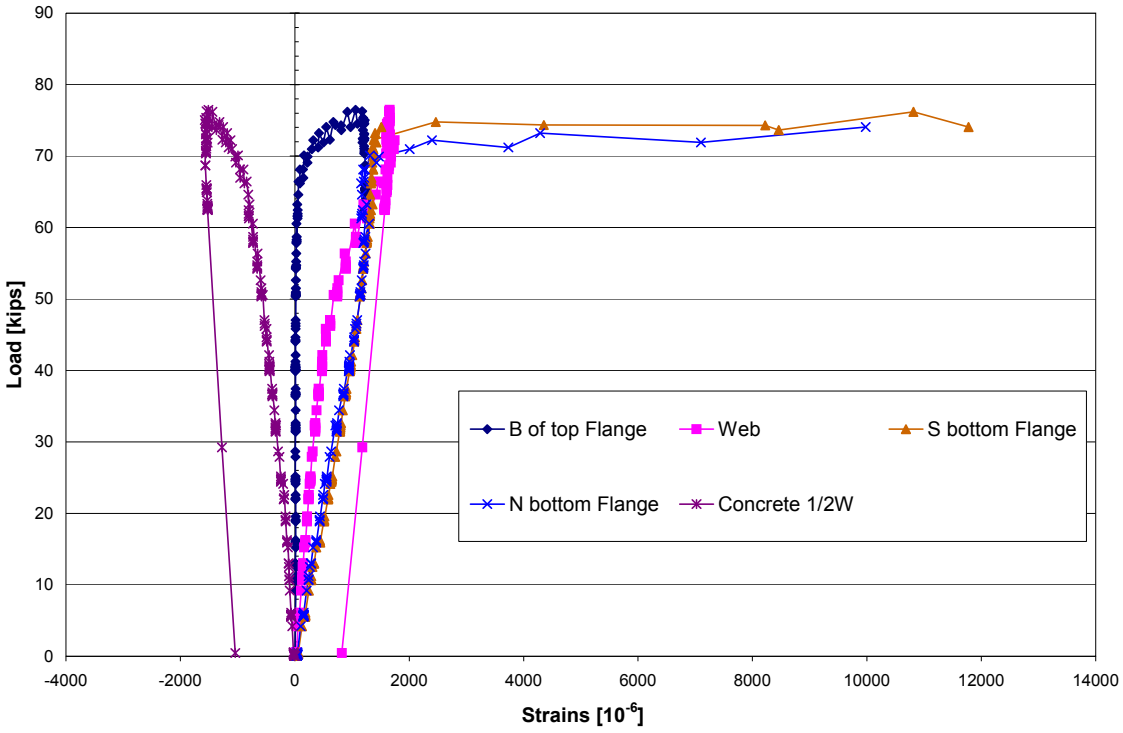

Figure 4-41: Strain development during the ultimate load test - Section A1

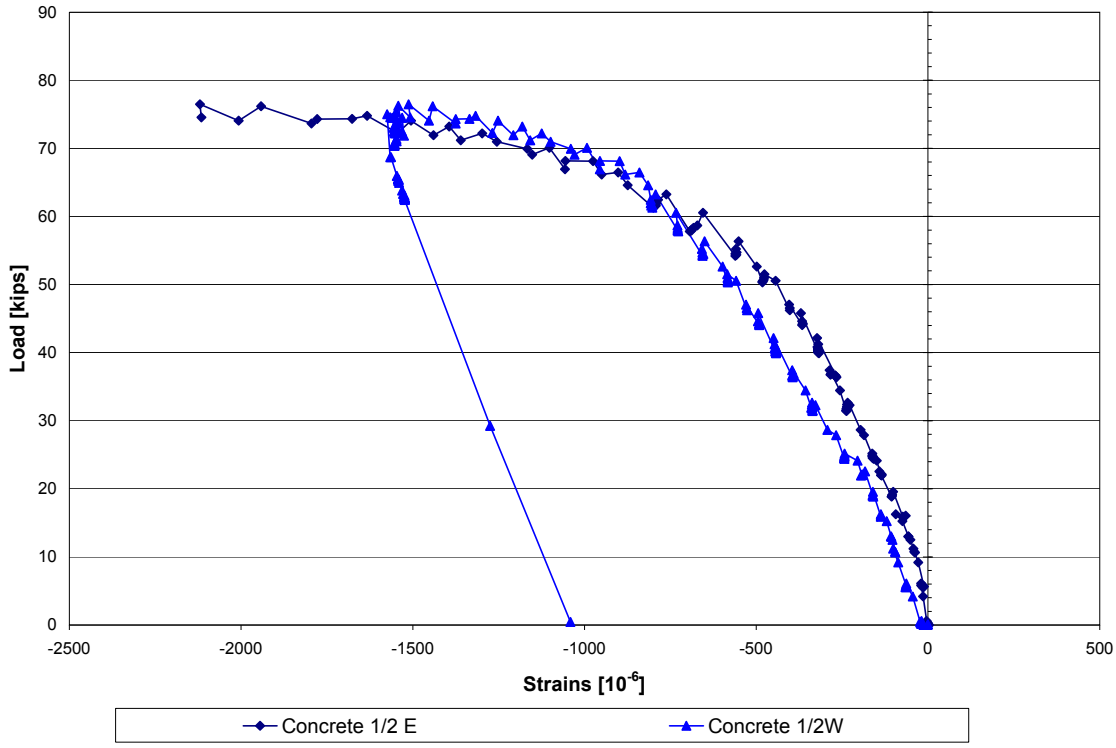

Figure 4-42: Strain development on the top surface of the concrete deck during the ultimate load test

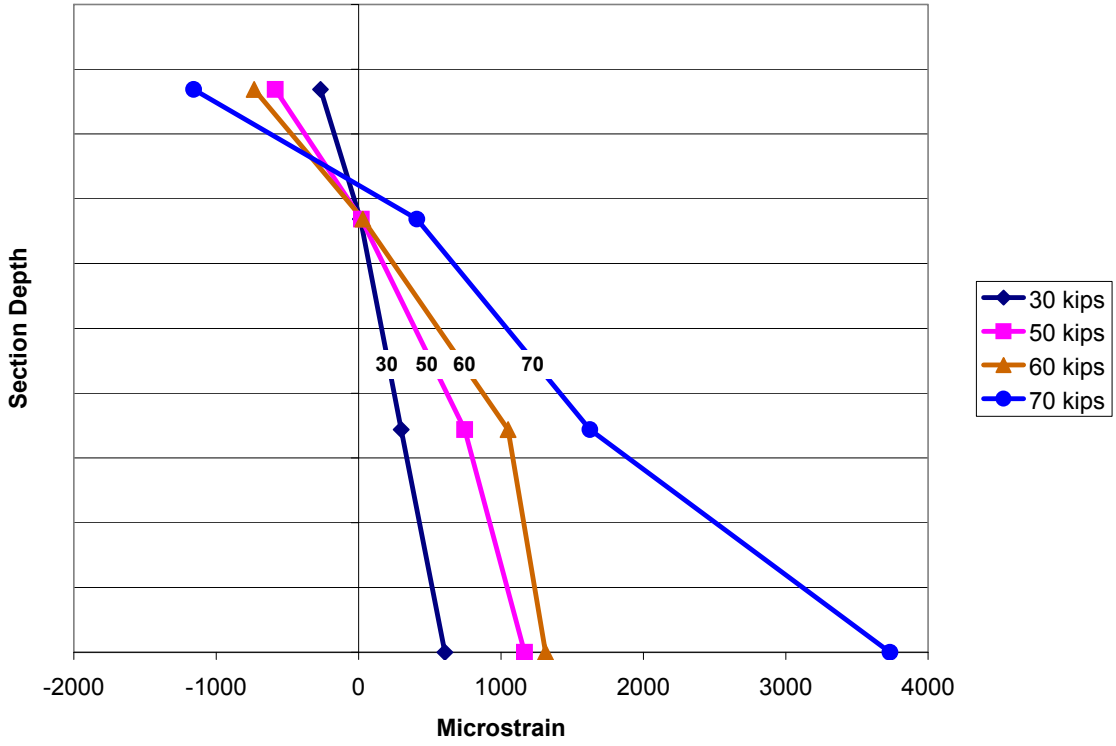

Figure 4-43: Strain profile at section A1 during multiple levels of loading.

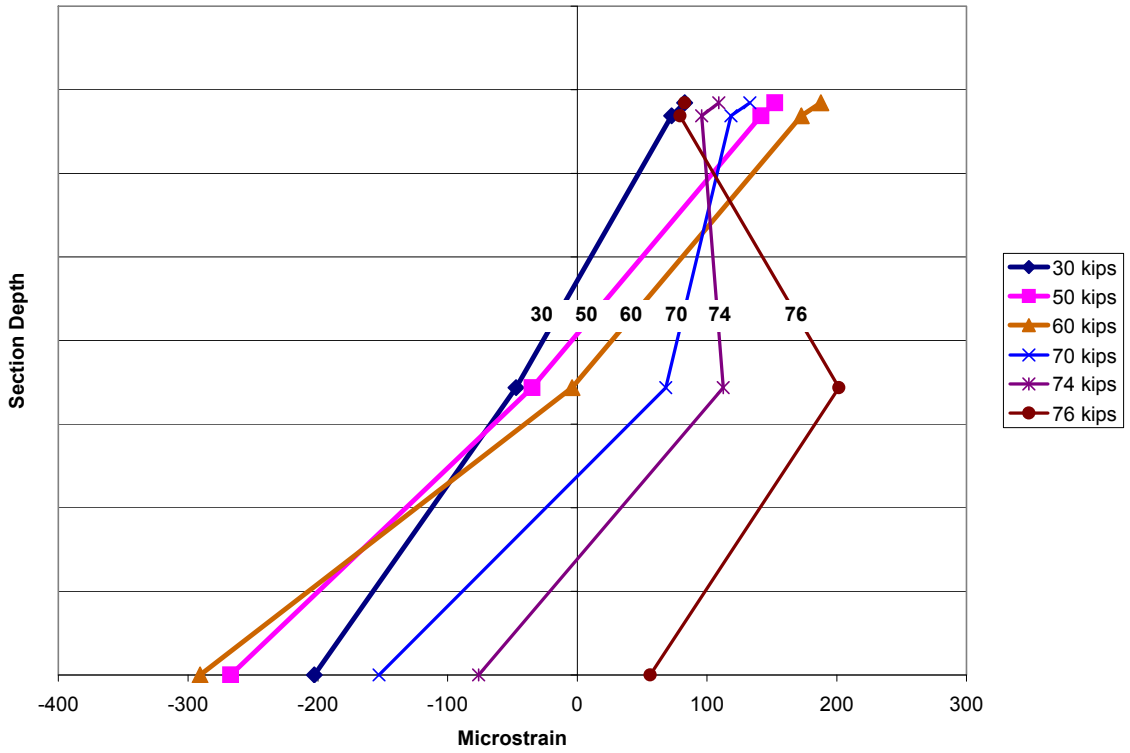

Figure 4-44: Strain profile at section B1 during multiple levels of loading.

Once failure was reached during the load test, crushing of the deck slab occured at the points of loading. Also, cracking was observed on the top of the slab over the middle support. Figures 6-36 through 6-39 show points of interest of the system after failure.

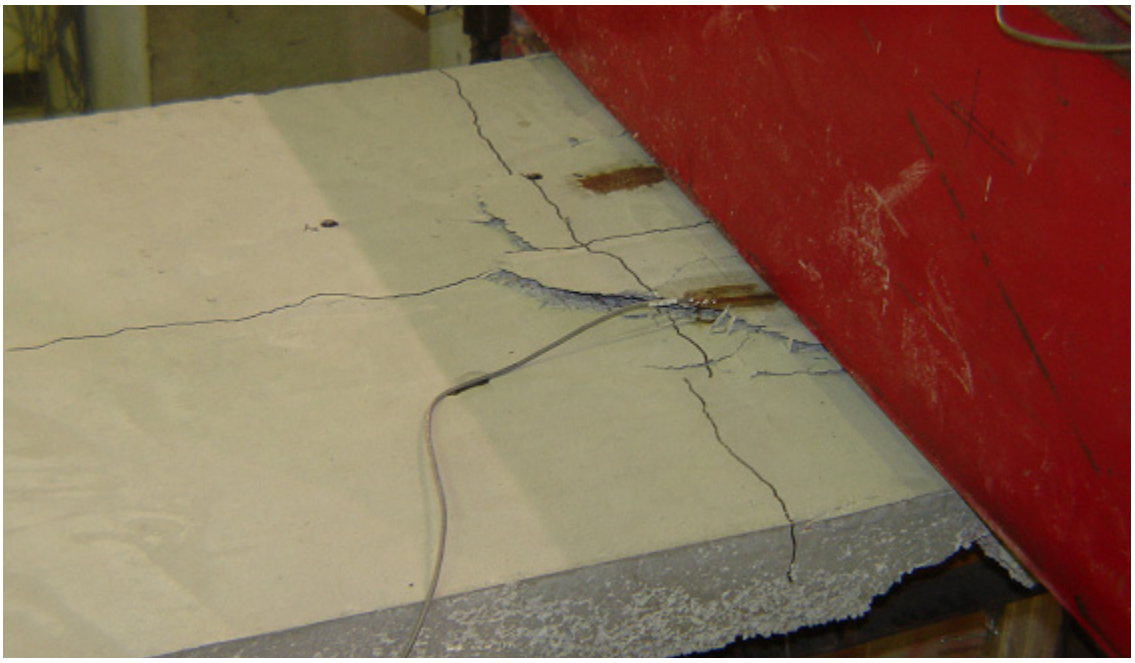

Figure 4-45: Crushing the concrete slab at the point of applied load

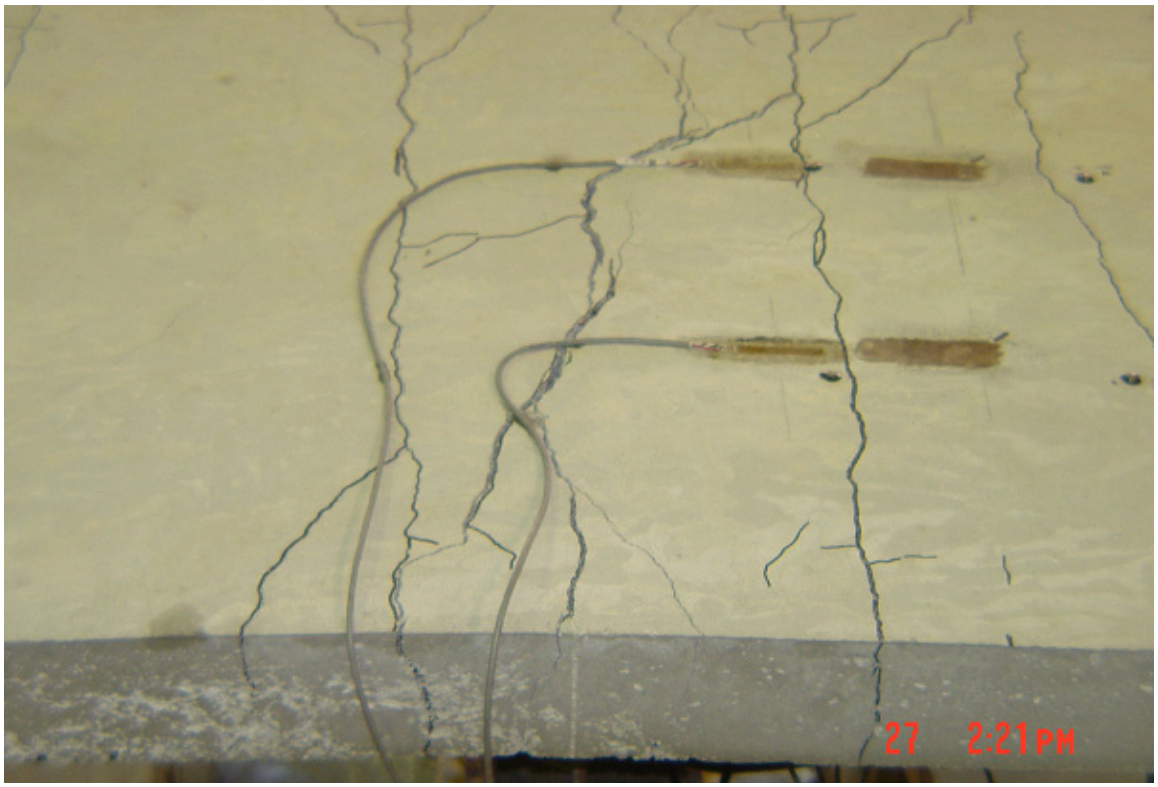

Figure 4-46: Crack pattern over the center support

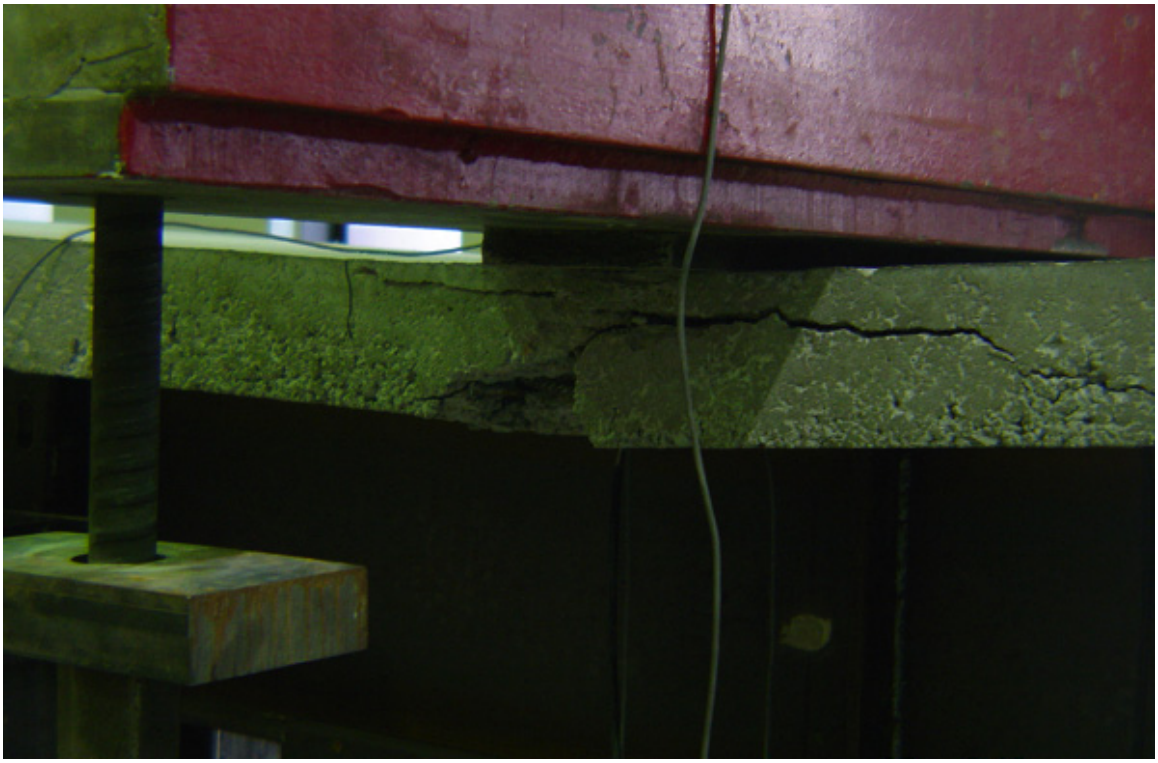

Figure 4-47: Deck crushing failure mode

Figure 4-48: Structure at failure

4.5 CONCLUSIONS

As an alternative to a post-tensioned concrete deck system used for preventing transverse deck cracking, a new method was proposed. The new method involved adding a shim over the middle support to slightly elevate the middle of the girder. Once the concrete had hardened, the shim was removed, puting the slab in compression over the pier.

The failure of the specimen was initiated by the yielding of the steel web close to the pier. It was followed by local buckling of the web and crushing of the concrete deck. This is typical for a continuous steel I-girder, only with this specimen it was observed that the cracking of the concrete deck was reduced. The system performed satisfactorily and as expected, exhibiting good stability, sufficient ductility and a delayed crack occurence over the pier.

Based on this experimental program, the system seems to be a simple and viable method when compared to the more common method, post-tensioning of the deck slab. Precompression of the slab prevented any observable cracks from forming in the negative flexure region over the interior support until well within the ultimate load test.

Chapter

5 Conclusions

5.1 Summary

The current number of deficient bridges in the U.S. and increasing labor costs have necessitated the search for innovative bridge configurations that are effective, durable, and easy to construct. Three such designs were suggested and investigated. The idea behind the designs was to use the advantages that steel and concrete have to offer as materials, while decreasing construction time and minimizing the need for costly elements such as intermediate transverse stiffeners and cross-frames. Combining theory, finite element analysis, and experimentation, the three proposed designs were investigated.

5.2 Inverted Box

One of the objects of the first configuration was to evaluate the effectiveness of the AASHTO-LRFD code for inverted box girders. First and foremost, it was found that the equations governing the design of normal box girders could also be applied for the design of inverted box girders. It was also concluded that the articles concerned with the prediction of the buckling of the compression flange and its effect on the ultimate capacity are conservative. Based on this conclusion, it is suggested that the corresponding equations in the code should be modified to include the post-buckling strength of the box section, pending more research in this area.

Concerning the design of the beam itself, it was first concluded that a longitudinal stiffener is needed on the top flange to prevent buckling during construction loading. Without this stiffener, it is likely that the design would be governed by construction loading, not in-service loading. Also, it was found that using a uniform thickness for either the web plate or the top flange is not economical for span lengths in the longer range of probable applicability. Along these lines, a more in-depth study would need to be completed to find the actual range of applicable span lengths for this bridge configuration. It is estimated that this system would likely be best suited for spans of less than 100 feet for vehicular traffic.

5.3 Tube Girder

One of the main ideas behind the concrete-filled tube design was that local and global stability could be maintained throughout loading. The concrete inside the tube would prevent local buckling while the closed shape of the tube would provide torsional stability. Through testing it was proven that the design was successful on both accounts. Since this level of stability was achieved, the mode of failure became the yielding of the steel tube. Upon

further loading, the inner reinforcement yielded followed by the crushing of the deck slab. This behavior provided a ductile failure similar to that of a concentional steel I-girder.

Throughout all stages of loading, it was shown that the strain distribution within the specimen remained linear. This facilitated the use of moment curvature analysis to predict the specimen capacity, which proved to be accurate when compared to the results of the experimental testing. This means that a moment curvature analysis is an effective method of capacity prediction for designs using the concrete-filled tube configuration.

Much like the inverted box, a more in-depth economic study needs to be completed in order to determine the applicable range of span lengths for this configuration. It is likely that for vehicular traffic short span lengths of less than 100 feet will be those for which this design is best suited. However, it has been suggested that pedestrian bridges might also be an acceptable application of this new girder type.

Although this design performed as expected, more research must be done before it can be implemented. This program was intended to determine the ultimate capacity of the system and investigate the failure mode, but design criteria must now be developed and other limit states, such as fatigue, must be explored. Another area of additional research that could be conducted on this configuration are alternatives such as post-tensioning, which may increase capacity and applicable span length.

5.4 Self-Stressing Girder

The idea behind the self-stressing girder was the prevention of deck cracking in the negative moment region over the pier. By inserting a shim over the pier before the casting of the deck and removing it after the deck hard-

ens, an initial compressive force is created in the deck. The design was deemed a success because the cracking was satisfactorily delayed.

During the load test, the specimen was observed to find the failure modes. The first noticeable mode in this specimen was the yielding of the web near the pier. This was followed by local buckling of the web and finally, crushing of the concrete deck under the point of load application. This was seen as typical behavior for a continuous steel I-girder.

Overall, the specimen performed as expected, exhibiting good stability, delayed cracking, and a sufficient amount of ductility. Based on this experimental program, the system appears to be a simple and viable alternative to the more common method of post-tensioning the deck to obtain an initial compressive force in the deck slab.

Bibliography

[1] AASHTO (1998). AASHTO LRFD Bridge Design Specifications - 1994, American Association of State Highway and Transportation Officials, Inc., Washington D.C.

[2] AASHTO (2004). AASHTO LRFD Bridge Design Specifications - 1994 American Association of State Highway and Transportation Officials, Inc., Washington D.C.

[3] AASHTO; AWS, "Bridge Welding Code: A Joint Publication of AASHTO and American Welding Society." (1996). ANSI/AASHTO/AWS D1.5-96, AASHTO and AWS, Washington D.C.

[4] ACI Committee 209, Subcommittee II, "Prediction of Creep, Shrinkage and Temperature Effect," 2, Draft Report, Detroit, October 1978, 98 pp.

[5] ANSYS, Release 5.7, ANSYS, Inc., Houston, PA

[6] American Society for Testing and Materials (ASTM), Annual Book of ASTM Standards A370. Vol.01.01, 2000.

[7] Azizinamini, A.; Fallaha, S.; Foud, J.; Farimani, R., "Outside the Box," Civil Engineering, ASCE, Vol. 74, No. 9, Sep. 2004, pp. 58-61

[8] Bresler, B., and Selna, L., "Analysis of Time Dependent Behavior of Reinforced Concrete Structures", *Symposium on Creep of Concrete*, *ACI Special Publication SP-9*, No. 5, Mar 1964, pp 115-128.

[9] Elremaily, A., Azizinamini, A., "Design Provisions for Connections Between Steel Beams and Concrete Filled Tube Columns." J. Constructional Steel Research, 2001, 57(9), 971-995.

[10] Elremaily, A.; Azizinamini, A., "Experimental Behavior of Steel Beam to CFT Column Connections." J. Constructional Steel Research, 2001, 57(10), 1099-1119.

[11] Elremaily, A., Azizinamini, A., "Behavior and Strength of Concrete-Filled Tube Columns." J. Constructional Steel Research, 2002, 58(12), 1567-1591.

[12] Faber, O., "Plastic Yield, Shrinkage and Other Problems of Concrete and their Effects on Design," *Minutes of Proc. of the Inst. of Civil Engineers, 225, Part I*, London, 1927, pp 27-73.

[13] Farimani, M.R., "Resistance Mechanism of Simple-Made-Continuous Connections in Steel Girder Bridges", Ph.D. Dissertation, University of Nebraska-Lincoln, 2006

[14] HDR Engineering, "Four LRFD Design Examples of Steel Highway Bridges." Vol.2, Chap. 1B, 1997.

[15] Meyers, B.L., Branson, D.E., Schumann, C.G. and Christiason, M.L., "The Prediction of Creep and Shrinkage Properties of Concrete", Final Report No 70-5, Iowa Highway Commission, August 1970, 140 pp.

[16] Stallings, J.M. and Yoo, C.H. (1993), "Tests and Ratings of Short-Span Steel Bridges," Journal of the Structural Division, ASCE, 119, ST7 (July 1993).

[17] Swendroski, J.P. (2001), "Field Monitoring of a Staged Construction Bridge Project," M.S. thesis, University of Nebraska, Lincoln, NE, 626 pp.

[18] Swett, G.D. (1998), "Constructability issues with widened and stage constructed steel plate Girder Bridges," M.S. thesis, University of Washington, 124 pp.

[19] Thomas Telford Services Ltd., London, for Comité Euro-International du Béton, Laussance, CEB-FIP Model Code 1990. 1993, 437 pp.